

Lars Zenke Hansen

# Unreinforced Masonry Walls

Transversely and Axially Loaded

Lars Zenke Hansen

Unreinforced Masonry Walls  
Transversely and Axially Loaded

Ph.D. Thesis  
BYG · DTU  
2004

## Preface

This report is prepared as a partial fulfilment of the requirements for obtaining the Ph.D. degree at the Technical University of Denmark.

The work has been carried out at the Department of Structural Engineering and Materials, Technical University of Denmark (BYG • DTU) under the supervision of Professor, Dr. techn. M. P. Nielsen.

I would like to thank my supervisor for giving valuable advice and inspiration as well as valuable criticism to the present work.

Thanks are also due to my co-supervisor M.Sc. Ph.D. Bent Steen Andreasen, RAMBØLL, Ph.D.-student Tim Gudmand-Høyer, Ph.D.-student Karsten Findsen, Ph.D.-student Jakob L. Laugesen, Ph.D.-student Thomas Hansen, Ph.D.-student João Domingues Costa, M.Sc. Ph.D. Bent Feddersen, RAMBØLL and Architect MAA Søren Bøgh, MURO, for their engagement and criticism to the present work and my Ph.D. project in general.

The Ph.D. project is financed by MURO and RAMBØLL. This support is hereby gratefully acknowledged.

Finally I would also like to thank my girlfriend, Jane Sofie Pørlov and my family for their encouragement and support.

Lyngby, June 2004

Lars Zenke Hansen



## Summary

The present report concerns calculation of the load carrying capacity of laterally loaded masonry walls with small or without axial loads.

The load carrying capacity will in both cases be calculated using the yield line theory, developed by Å. Ingerslev and K. W. Johansen for concrete slabs.

In both load conditions, equations for the bending yield moments are established. The moments are calculated from an upper bound solution, where it is assumed that failure in most cases takes place in the interface between the mortar and the brick. The failure is a sliding failure, following Coulombs modified failure hypothesis. The tensile strength of the interface is neglected through the entire report.

When using the yield line theory it is assumed that the rotation axes are placed at the face, where the transverse load is applied as compression. This together with the assumption of no tensile strength, lead to the result that the moment capacity in a horizontal yield line is zero.

In the case of laterally loaded masonry walls it has been observed in experiments that initial cracking takes place in the bed joint before failure, indicating that the horizontal yield line has no moment capacity at failure.

To justify the use of the yield line theory, the theory is compared with experiments.

The yield line theory in the case of axial loads has to be adjusted compared to the usual theory by introducing the axial load in the external work. The external work is due to the expansion of masonry walls when they fail and is therefore negative, when the external load is compressive.

In the report examples are produced to illustrate the use of the theory both in the case of no axial load and in cases with axial load.

The yield line theory is in both loading cases compared with experiments on full size walls. The comparisons shows that the theory is in good agreement with reality. The tests used are taken from the literature.

## Resumé

Nærværende rapport omhandler beregning af tværbelastede murede vægge med små eller ingen normalkræfter.

Bæreevnen bestemmes i begge tilfælde ved at anvende brudlinieteorien for ortotrope betonplader udviklet af Å. Ingerslev og K. W. Johansen.

For begge belastningstilfælde er der opstillet udtryk til bestemmelse af momentkapaciteten. Momentkapaciteten er beregnet ud fra øvreværdiløsninger, hvor det er antaget at bruddet sker i skillefladen mellem sten og mørtel. Bruddet antages at være et glidningsbrud der følger Coulombs modificerede brudhypotese. Trækstyrken af skillefladen er sat til nul igennem hele rapporten.

Ved anvendelse af brudlinieteorien antages at rotationsakserne er placeret ved den side af væggen, hvor tværlasten påføres som tryk. Dette betyder, sammen med antagelsen om at trækstyrken er nul, at horisontale brudlinier ikke har nogen momentkapacitet.

I det tilfælde hvor den murede væg alene er belastet med tværlast, har det ved eksperimentelle observationer vist sig, at begyndende revnedannelse finder sted i liggefladens skilleflade før det egentlige brudliniemønster er udviklet. Dette indikerer, at momentkapaciteten i den horisontale brudlinie er udtømt før brud, og at den derfor ikke skal medtages.

Brudlinieteorien er, i tilfældet med små normalkræfter, udvidet så normalkræfterne kan medtages i det ydre arbejde. Murede vægge udviser ved brud dilatation, hvorved en tryknormalkraft giver et negativt ydre arbejde.

I rapporten er der udarbejdet eksempler, som viser brugen af teorien.

Der er også foretaget en sammenligning med forsøg.

Forsøgene er udført på vægge af fuld størrelse. Sammenligningerne viser, at begge belastningstilfælde kan beregnes ved at anvende brudlinieteorien for ortotrope betonplader. Forsøgene er samlet fra litteraturen.

---



---

# Contents

<b>PREFACE</b> .....	<b>I</b>
<b>SUMMARY</b> .....	<b>III</b>
<b>RESUMÉ</b> .....	<b>IV</b>
<b>CONTENTS</b> .....	<b>V</b>
<b>NOTATIONS</b> .....	<b>VII</b>
<b>1 INTRODUCTION</b> .....	<b>1</b>
<b>2 LATERALLY LOADED WALLS</b> .....	<b>5</b>
2.1 MOMENT CAPACITIES FOR LATERALLY LOADED WALLS .....	5
2.1.1 <i>Introduction</i> .....	5
2.1.2 <i>Diagonal yield line</i> .....	6
2.1.2.1 <i>Simplified calculation method</i> .....	8
2.1.3 <i>Yield line theory for laterally loaded masonry walls</i> .....	13
2.2 UPPER BOUND SOLUTIONS .....	14
2.2.1 <i>Introduction</i> .....	14
2.2.2 <i>Calculation of orthotropic walls</i> .....	16
2.2.2.1 <i>Upper bound solution using plane strain solution</i> .....	16
2.2.2.2 <i>Upper bound solution using yield moments</i> .....	17
2.2.2.3 <i>Comparison between calculation methods</i> .....	18
2.2.3 <i>Simple yield line patterns</i> .....	22
2.2.4 <i>Illustrative examples</i> .....	26
2.2.4.1 <i>Example 1. Calculation of a wall</i> .....	27
2.2.4.2 <i>Example 2. Cavity wall</i> .....	29
2.2.4.3 <i>Example 3. Walls with openings</i> .....	33
2.2.4.4 <i>Example 4. Comparison with the calculation method in some codes</i> .....	35
2.3 COMPARISON WITH EXPERIMENTS .....	36
2.3.1 <i>Investigations</i> .....	37
2.3.2 <i>Comparison with experiments for laterally loaded slabs</i> .....	38
2.3.3 <i>Biaxial bending tests</i> .....	48

2.3.4	<i>Comparisons regarding pure bending</i> .....	51
<b>3</b>	<b>LATERALLY LOADED WALLS WITH SMALL IN PLANE (AXIAL) LOADS</b> .....	<b>55</b>
3.1	MOMENT CAPACITIES FOR WALLS WITH SMALL AXIAL LOADS.....	55
3.2	UPPER BOUND SOLUTIONS .....	57
3.2.1	<i>Orthotropic walls</i> .....	57
3.2.2	<i>Illustrative examples</i> .....	59
3.2.2.1	Example 1, Calculation of a wall .....	59
3.2.2.2	Example 2, Simplified calculation of a masonry wall .....	62
3.2.2.3	Example 3, The influence of axial load .....	66
3.3	COMPARISON WITH EXPERIMENTS.....	67
3.3.1	<i>Investigations</i> .....	67
3.3.2	<i>Comparison with experiments</i> .....	69
<b>4</b>	<b>CONCLUSION</b> .....	<b>73</b>
<b>5</b>	<b>LITERATURE</b> .....	<b>74</b>
<b>6</b>	<b>APPENDIX</b> .....	<b>78</b>
6.1	APPENDIX 1, TENSILE STRENGTH AND FLEXURAL MODULUS OF CLAY BRICKS .	78
6.2	APPENDIX 2. DEFLECTION OF LATERALLY LOADED MASONRY WALLS .....	83
6.3	APPENDIX 3. INCLINATION OF A DIAGONAL YIELD LINE .....	96
<b>7</b>	<b>SUPPLEMENTS</b> .....	<b>98</b>
7.1	LATERALLY LOADED WALLS .....	98
7.1.1	<i>Kheir, A. M. A. 1975</i> .....	98
7.1.2	<i>West, H. W.H et. al. 1977</i> .....	100
7.1.3	<i>Cajdert, A. 1980</i> .....	103
7.1.4	<i>Lawrence, S. J. 1983</i> .....	105
7.1.5	<i>Buhelt, M. 1984</i> .....	109
7.2	LATERALLY LOADED WALLS WITH SMALL AXIAL LOADS .....	110
7.2.1	<i>Hendry, A. W., Sinha, B. P. and Maurenbrecher, A. H. P. 1973</i> .....	110

## Notations

The most commonly used symbols are listed below. Exceptions from the list may appear, and they will be explained in the text.

### Geometry

$x, y, z$	Cartesian co-ordinate system
$h$	Height
$b$	Width
$t$	Thickness
$l$	Length
$h_b$	Height of brick
$l_b$	Length of brick
$b_b$	Width of brick
$h_j$	Height of joint
$x_0$	Length of a periodic yield line in the $x$ direction
$y_0$	Length of a periodic yield line in the $y$ direction
$\delta$	Initial displacement
$u$	Displacement
$\alpha$	Angle of the displacement vector to the yield line
$\theta_x, \theta_y$	Rotation angle about the $x$ and $y$ axis, respectively
$\omega$	Rotation
$\omega_x, \omega_y$	Rotation about the $x$ and $y$ axis, respectively
$\theta$	Angle

### Physics

$\sigma$	Stress
$\sigma_x, \sigma_y$	Stresses in the $x$ and $y$ direction respectively
$f_c$	Compressive strength
$f_{cb}$	Compressive strength of the brick

$f_{cm}$	Compressive strength of the mortar
$f_{ci}$	Formal compressive strength of the interface
$f_t$	Tensile strength
$f_{tb}$	Tensile strength of the brick
$f_{tm}$	Tensile strength of the mortar
$\tau$	Shear stress
$\tau_{xy}$	Shear stress in the $x, y$ co-ordinate system
$c$	Cohesion
$\mu$	Friction coefficient
$\mu$	ratio between the bending yield moments
$\varphi$	Friction angle
$k$	Factor
$k$	Factor dependent on the friction angle
$m_x, m_y$	Bending moment per unit length in a section perpendicular to the $x$ and $y$ direction, respectively
$m_b$	Sectional bending moment per unit length
$m_{px}, m_{py}$	Yield moment per unit length in the $x$ and $y$ direction, respectively
$m_\theta$	Moment per unit length at an angle of $\theta$ to the bed joint
$n_x, n_y$	Axial loads per unit area in the $x$ and $y$ direction, respectively
$p^+$	Load carrying capacity by upper bound method
$p_x^+, p_y^+$	Tensile strength by an upper bound solution in the $x$ and $y$ direction. respectively
$W$	Dissipation
$W_l$	Dissipation per unit length
$W_I$	Internal work
$W_E$	External work
$IRA$	Initial rate of absorption
$\rho$	Specific weight
$w/l$	Water/lime ratio
$w/c$	Water/cement ratio

# 1 Introduction

The present report concerns calculations of the load carrying capacity of laterally loaded masonry walls with small or without axial load.

The load carrying capacity of walls with small axial loads or without axial loads is calculated using the yield line theory developed for reinforced concrete slabs by Å. Ingerslev and K. W. Johansen. For a general description the reader is referred to [2] and [7]. The walls considered are assumed to behave according to the theory of rigid plastic materials, which means that prior to failure the wall is without deformations.

Numerous investigations have been carried out in connection with laterally loaded masonry walls. Only few have included the effect of small axial loads. In the literature different calculation methods have been used when estimating the load carrying capacity of masonry walls. In the literature the yield line theory has achieved a general acceptance as the method to be used when calculating the load carrying capacity, see [14], [27], [29], [31], [33], [37] and [39], which are only a few of the investigations where the yield line theory is preferred as the calculation method.

Using the yield line theory for orthotropic concrete slabs ([5]) and simple methods for calculating the bending yield moments, a theory for unreinforced masonry walls will be developed. The bending yield moments will be determined by considering failure in the interface between the bricks and the mortar. The interface is often the weak part of masonry and its strength is influenced by a large number of factors. The interface between brick and mortar is believed to be a crystalline structure growing from the mortar into the rough surface of the brick making an interlock. The strength of the interface is believed to be the strength of the interlock. A thorough description of the properties may be found in [44] and [45].

Failure in the interface will be assumed to be governed by a sliding failure condition similar to the modified Coulomb failure hypothesis, see Figure 1.1.

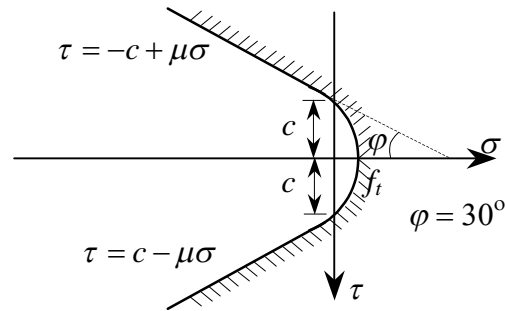


**Figure 1.1 Modified Coulomb failure hypothesis**

In the calculations the tensile strength of the interface will be neglected. This is done because the tensile strength will be encumbered by great uncertainties and many factors influence its value. Only a few are mentioned here: Micro-cracking due to shrinkage, crack growth due to small variations in loading and workmanship.

In this report the theory of plasticity especially the upper bound theorem is used in all calculations. An upper bound solution is produced by considering a geometrical possible yield line pattern. Using the work equation to calculate the load carrying capacity a value higher than or equal to the actual load carrying capacity is achieved.

The bending yield moments will be calculated by the work equation as an upper bound solution. Fixed yield line patterns are assumed when calculating the tensile strength obtained from sliding in the interface. The strain state in the interface is assumed to be plane, because the thickness of the interface is small compared with the length and width (equal to the length and width of the brick) and therefore the strains perpendicular to the bed joint can be neglected.

Using the plastic theory for Coulomb materials, the dissipation per unit length may in the case of plane stress as well of plane strain for  $f_t = 0$  be calculated according to (1.1).

$$W = \frac{1}{2} f_c b u (1 - \sin \alpha) \quad (1.1)$$

where  $\alpha$  is the angle between the displacement vector, with length  $u$ , and the yield line. In plane strain  $\alpha$  is bound to the interval  $\varphi \leq \alpha \leq \pi - \varphi$ . Thus the angle  $\beta$  shown in Figure 1.2 is bound to the interval  $\varphi \leq \beta \leq \frac{\pi}{2} - \varphi$ , because the yield lines considered are stair formed, as shown in Figure 1.2.

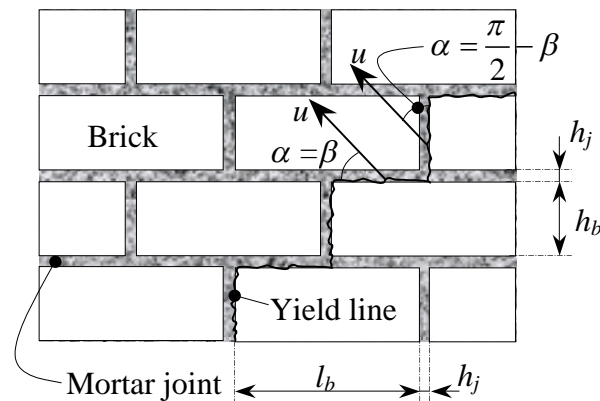


Figure 1.2 Boundaries for  $\beta$

The dissipation formula is achieved by considering v. Mises assumption of maximum work at failure and Coulomb failure hypothesis.

Regarding a general description of Coulomb materials the reader is referred to [10] or [7], where also a complete description of the theory of plasticity may be found.

Sectional forces will be referred to a coordinate system as shown in Figure 1.3. The  $x$ -axis will be parallel to the bed joints and the  $y$ -axis perpendicular to the  $x$ -axis.

The sign convention for bending moments per unit length  $m_x$  and  $m_y$  is also shown in the figure. Bending moments are positive when they give tensile stresses in the bottom face, which for a vertical wall must be defined beforehand. For a wall simply supported on all four sides the bottom face is opposite to the surface where the lateral load is applied as pressure.

The normal forces per unit length  $n_x$  and  $n_y$  are positive as compression. In Figure 1.3 the rotations  $\omega_x$  and  $\omega_y$  are defined.

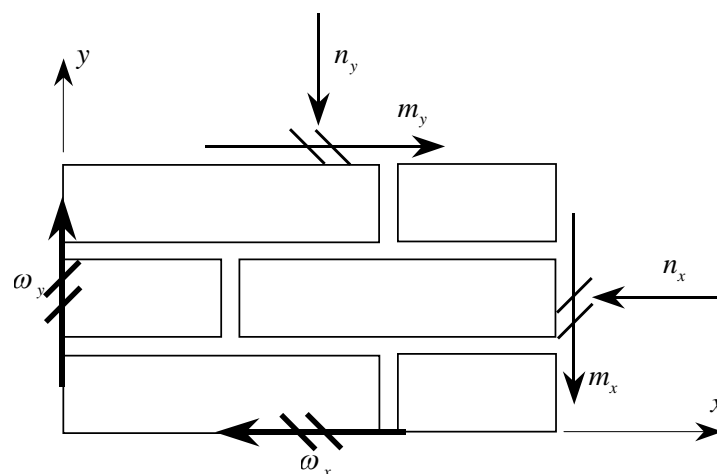


Figure 1.3 Definition of co-ordinate system, bending moments and axial loads

Furthermore, it is in most cases assumed that the bricks are laid in running bond, where the bricks overlap with half of their total length. This is also illustrated in Figure 1.3.

In appendix 3 a survey of some standard bonds is shown together with the maximum inclination of a yield line only running in the interface. Regarding a general description of bonds and workmanship the reader is referred to [11].

---

## 2 Laterally loaded walls

### 2.1 Moment capacities for laterally loaded walls

#### 2.1.1 Introduction

Masonry walls are orthotropic because the bending yield moment about the bed joint is different from the bending yield moment about the head joint.

The general failure pattern of a masonry wall, simply supported on four sides, consists of stair-formed diagonal yield lines, together with horizontal yield lines as illustrated in Figure 2.1.

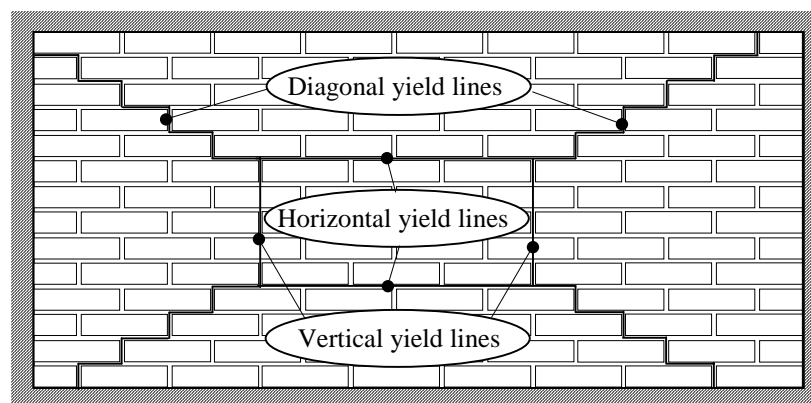


**Figure 2.1 Yield lines in a simply supported transversely loaded masonry wall**

In the horizontal yield line the bending moment capacity is set to zero in agreement with the assumption that the tensile strength of the interface is set equal to zero. That the bending moment capacity must be set to zero is supported by the fact that numerous investigators have reported initial cracking in the bed joint during loading, even long before the failure load is reached. The reason is that the bed joint has a substantially

lower ductility than the diagonal yield lines. This has clearly been demonstrated by Caidert in [27] and Feilberg in [37]. In section 6.2 the deformations of masonry walls are analysed. It turns out that the rotation capacity about the bed joint is about two times smaller than the rotation capacity about the head joint. The ductility of the bed joint may be improved if there are compressive normal forces in the joints. In this chapter compressive normal forces are not taken into account. Normal forces are introduced in Chapter 3.

In the diagonal yield lines sliding will occur in the head and bed joints. This is far more ductile than pure separation failure.

### 2.1.2 Diagonal yield line

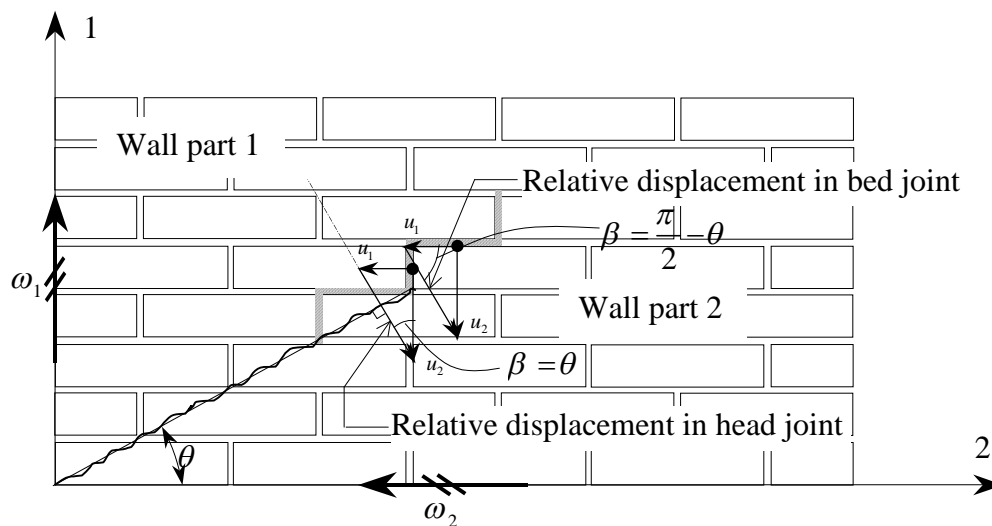


**Figure 2.2 Relative displacements in a diagonal yield line**

The reason why it may be justified to take into account the moment capacity of diagonal yield lines even when the tensile strength is neglected is demonstrated in Figure 2.2. Here a part of a diagonal yield line separating two wall parts 1 and 2 and emerging from a corner is shown. The rotations are  $\omega_1$  and  $\omega_2$ , respectively, and the rotation axes are 1 and 2, respectively. They intersect at the corner and are assumed to be placed in the top face of the wall. The figure shows the displacements in the plane of the wall along the yield line considered and in an arbitrary point along the wall depth.

The displacements from the rotations are marked  $u_1$  and  $u_2$ ,  $u_1$  coming from the rotation about the axis 1 and  $u_2$  coming from the rotation about the axis 2. On the basis of these displacements the relative displacements in the head joint and in the bed joint are constructed. Notice that the displacements perpendicular to the wall plane do not contribute to the relative displacement.

The figure illustrates clearly that in a stair-formed diagonal yield line the relative displacements are not perpendicular to the joints. This means that a sliding failure with dilatation takes place and not a separation failure (with a relative displacement perpendicular to the joint).

This fact has important consequences regarding ductility since a sliding failure in the interface (or in the mortar) has an order of magnitude higher ductility than a pure separation failure. This is the reason why diagonal yield lines may be active until the final failure.

A detailed analysis of the dissipation in a diagonal yield line is extremely complicated. It has been carried out by Hagsten in [43].

In this report a strongly simplified analysis is suggested based on estimated yield line mechanisms. The justification of the assumptions will be carried out by comparing with the results of Hagstens work and with experiments.

The internal work in a yield line emerging from a right angled corner, may be calculated using the dissipation formula assuming plane strain, see Chapter 1. A stair-formed yield line, as the one shown in Figure 1.2, is considered. The internal work for a stair with lengths  $\frac{1}{2}(l_b + h_j)$  and  $h_b + h_j$ , of Figure 1.2, becomes,  $t$  being the wall thickness,

$$W_I = \int_0^t \frac{1}{2} f_{ci} u (1 - \sin \beta) \frac{1}{2} (l_b + h_j) dz + \int_0^t \frac{1}{2} f_{ci} u \left( 1 - \sin \left( \frac{\pi}{2} - \beta \right) \right) (h_b + h_j) dz \quad (2.1)$$

If the angle of the yield line to the bed joint is named  $\theta$ , see Figure 2.2, the angle  $\beta$  is equal to  $\pi/2 - \theta$ .

If the rotation axes are placed at the surface of the wall where the lateral load is applied as pressure, the displacements  $u_1$ ,  $u_2$  and  $u$ , may be calculated as:

$$\begin{aligned} u_1 &= \omega_1 z \\ u_2 &= \omega_2 z \\ u &= \frac{\omega_1 z}{\cos \beta} = \frac{\omega_2 z}{\sin \beta} \end{aligned} \quad (2.2)$$

where  $z$  is the distance from the surface to the point considered and  $u$  is the relative displacement in the yield line, which varies linearly over the thickness of the wall. Only displacements parallel to the plane of the wall have to be considered as stated above.

If the relative displacement  $u$  is inserted into the expression for the internal work, equation (2.1) may be written as:

$$W_I = \frac{1}{4} f_{ci} \frac{1 - \sin \beta}{\cos \beta} \frac{1}{2} (l_b + h_j) \omega_1 t^2 + \frac{1}{4} f_{ci} \frac{1 - \cos \beta}{\sin \beta} (h_b + h_j) \omega_2 t^2 \quad (2.3)$$

Introducing

$$m_{p1} = \frac{1}{4} f_{ci} \frac{1 - \sin \beta}{\cos \beta} \frac{\frac{1}{2}(l_b + h_j)}{h_b + h_j} t^2$$

$$m_{p2} = \frac{1}{4} f_{ci} \frac{1 - \cos \beta}{\sin \beta} \frac{h_b + h_j}{\frac{1}{2}(l_b + h_j)} t^2$$
(2.4)

(2.3) may be written as

$$W_I = m_{p1} (h_b + h_j) \omega_1 + m_{p2} \frac{1}{2} (l_b + h_j) \omega_2$$
(2.5)

The factors  $m_{p1}$  and  $m_{p2}$  can be interpreted as the bending yield moments per unit length in the head and bed joint, respectively.

It should be noted that the bending yield moments given by equation (2.4) are dependent of the geometry of the bricks and the bond of which the wall is built.

Assuming plane strain in the interface, the angle  $\beta$  is as mentioned before, restricted to the interval given as:

$$\varphi \leq \beta \leq \frac{\pi}{2} - \varphi$$
(2.6)

Which means that the angle  $\theta$  is restricted to the interval given as:

$$\varphi \leq \theta \leq \frac{\pi}{2} - \varphi$$
(2.7)

A stair-formed yield line in a masonry wall built in running bond with half a brick overlap, corresponds to an inclination  $\theta$  equal to  $29.5^\circ$ , which is almost equal to the friction angle usually assumed to be  $\varphi = 30^\circ$ . This and other inclinations are described in Appendix 3.

In situations where the angle  $\theta$  is smaller than  $\varphi$  or larger than  $\frac{\pi}{2} - \varphi$ , the axes of rotations cannot be at the same level when a yield line in the interface has to be a geometrically possible yield line.

When the rotation axes are not at the same level the displacements perpendicular to the wall make a contribution to the relative displacements, and the analysis becomes much more complicated. We shall not deal with it here.

### 2.1.2.1 Simplified calculation method

In this section, an alternative method to calculate the moment capacities in a diagonal yield line will be outlined. It turns out that this method is equivalent to the method used above when sliding failure in the interface governs the strength.

The procedure is to calculate the tensile strength in the two directions by means of an upper bound solution. The tensile strength is calculated considering sliding failure in the

bed and head joint, respectively, or tensile failure in the bricks. The bending yield moments are calculated assuming masonry to have infinite compressive strength. The situation where the moment capacities are determined by sliding in the interface is referred to as failure mode 1. Tension failure in the bricks will be referred to as failure mode 2. The latter value furnishes an upper limit for the bending yield moments.

Failure mode 1 is illustrated in Figure 2.3.

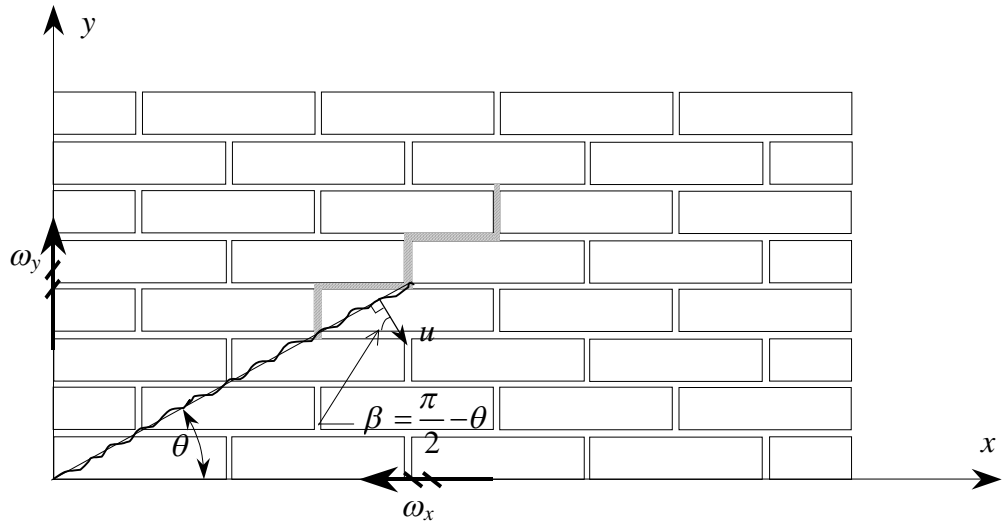


**Figure 2.3 Failure mode 1**

The tensile strengths in the horizontal and vertical direction are determined by the failure mechanisms shown in Figure 2.4. We only need to consider a part of the yield line, since it reproduces itself.

The tensile strength,  $p_x^+$ , is determined considering only the contribution from sliding in the bed joint. The tensile strength,  $p_y^+$ , is determined considering only the contribution from sliding in the head joint.

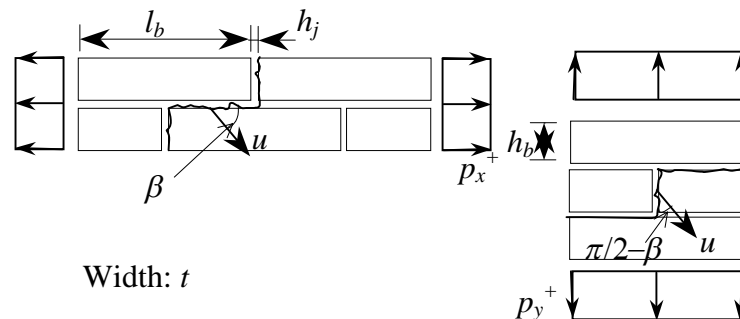


**Figure 2.4 Failure mode 1 for the horizontal and vertical tensile strength**

The strengths in the two cases are calculated using the upper bound theorem. For the horizontal tensile strength, the internal work, when only the yield line in the bed joint is considered, becomes

$$W_I = \frac{1}{2} f_{ci} (1 - \sin \beta) \frac{1}{2} (l_b + h_j) t \cdot u \quad (2.8)$$

The external work becomes

$$W_E = p_x^+ \cos \beta (h_b + h_j) t \cdot u \quad (2.9)$$

From the work equation the tensile strength parallel to the bed joint is obtained:

$$p_x^+ = \frac{1}{2} f_{ci} \frac{1 - \sin \beta}{\cos \beta} \frac{\frac{1}{2} (l_b + h_j)}{h_b + h_j} \quad (2.10)$$

The procedure to find the vertical tensile strength is the same. The contribution to the internal work is only the work dissipated in the head joint. The vertical tensile strength becomes:

$$p_y^+ = \frac{h_b + h_j}{\frac{1}{2} (l_b + h_j)} \frac{1}{2} f_{ci} \frac{1 - \sin \left( \frac{\pi}{2} - \beta \right)}{\cos \left( \frac{\pi}{2} - \beta \right)} \quad (2.11)$$

For  $\beta = 45^\circ$  the ratio between the tensile strengths is:

$$\mu = \frac{p_y^+}{p_x^+} = \left( \frac{h_b + h_j}{\frac{1}{2} (l_b + h_j)} \right)^2 \quad (2.12)$$

The bending yield moment  $m_{px}$  is determined from the stress distribution illustrated in Figure 2.5, where the tensile strength  $p_x^+$  is determined by (2.10).

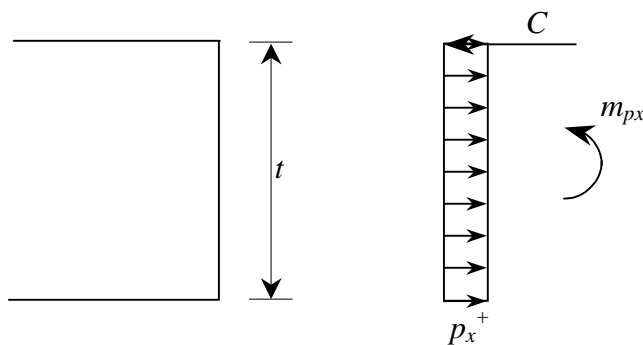


**Figure 2.5 Stresses in the case of pure bending, failure mode 1**

The horizontal bending yield moment,  $m_{px}$ , becomes.

$$m_{px} = \frac{1}{2} t^2 p_x^+ \quad (2.13)$$


---

A similar equation is valid for  $m_{py}$ .

The ratio between the moments is seen to be equal to the ratios between the tensile strengths. The ratio is given by formula (2.12) for  $\beta = 45^\circ$ .

It must be remembered that  $m_{py}$  is only taken into account in a diagonal yield line. Thus in the case of wall strips bent about the bed joint  $m_{py}$  is equal to zero.

It may be seen that  $m_{px} = m_{p1}$  and  $m_{py} = m_{p2}$  for any allowable  $\beta$ -value where  $m_{p1}$  and  $m_{p2}$  are given by equations (2.4). Therefore the two methods are seen to be equivalent.

Now we investigate the effect of the angle  $\beta$  on the internal work per unit length in a stair-formed yield line.

The internal work for a repeated section of a diagonal yield line can for both methods be determined as

$$W_I = m_{px}y_0 \cdot \omega_y + m_{py}x_0 \cdot \omega_x \quad (2.14)$$

where  $\omega_x = \omega_1$ ,  $\omega_y = \omega_2$ ,  $m_{px} = m_{p1}$  and  $m_{py} = m_{p2}$ ,  $x_0$  and  $y_0$  are a repeated section of the interface given an actual value in Table 2.1.

The internal work has been calculated for  $\omega_1 = \omega_x = 1$ . Since  $\omega_1/\omega_2 = \tan\theta$ , we have  $\omega_y = \omega_2 = \omega_1 \cot\theta = \omega_x \cot\theta$

Figure 2.6 shows the internal work for two different values of  $\beta$ , as well as for  $\beta$  determined to make the displacement vector  $u$  a normal to the overall yield line, i.e.  $\beta = \frac{\pi}{2} - \theta$ . In this case  $\omega_y = \omega_x \tan\beta$ . Only situations where the rotation axes are placed in the faces of the wall is considered.

The data used in the calculations are shown in Table 2.1.

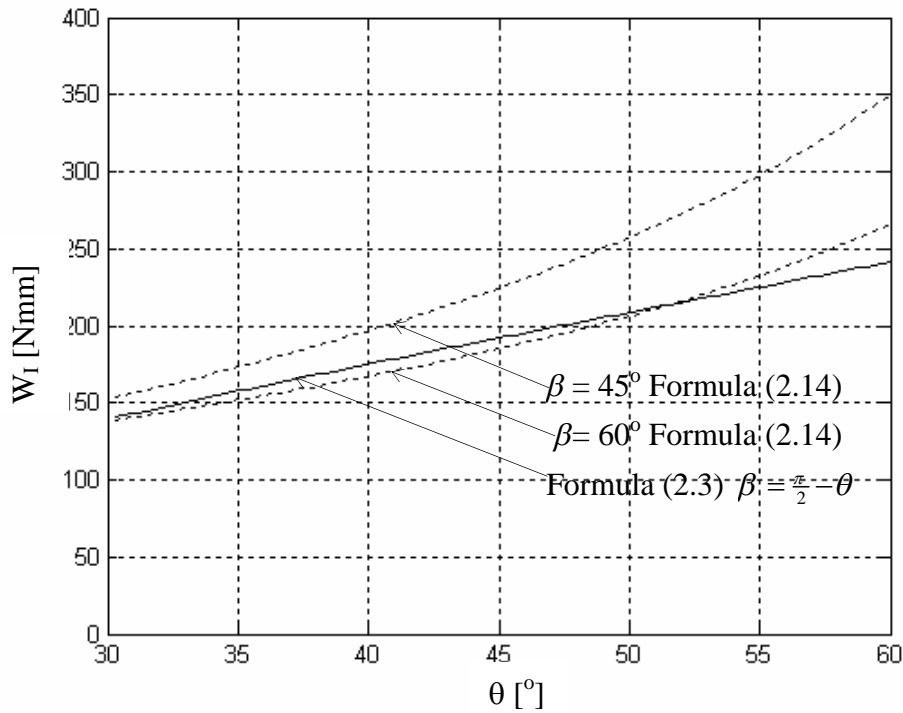


**Figure 2.6 Internal work of a section calculated by the two methods described**

It appears that for practical calculations  $\beta = 45^\circ$  may be used, whereby the equations for  $\mu$  and  $m_{px}$  become very simple.

$t$	108.0[mm]
$h_b$	55.0[mm]
$l_b$	228.0[mm]
$h_j$	12.0[mm]
$y_0$	67[mm]
$x_0$	$y_0/\tan(\theta)$ [mm]
$\varphi$	30.0
$f_{ci}$	5.3[MPa]

**Table 2.1 Data used in the calculations**

Now we must consider failure mode 2 where the bricks fail in tension. This mode will be decisive when the shear resistance in the interface of failure mode 1 exceeds the tensile strength of the bricks. Thus the bending yield moment calculated considering failure mode 2 provides an upper limit for the bending yield moment.

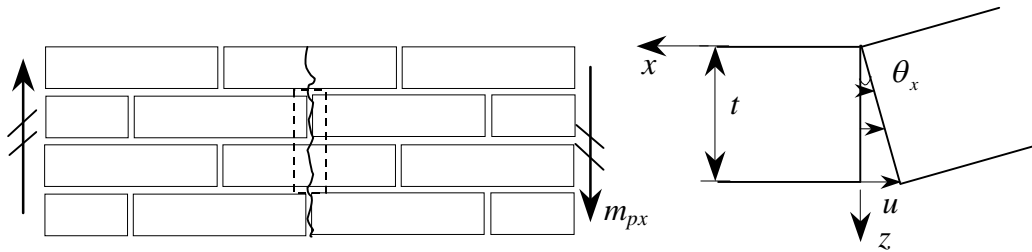


**Figure 2.7 Failure mode 2**

The dissipation becomes, see Figure 2.7,

$$W_I = \int_0^t u(z) \cdot z \cdot h_b f_t dz \quad (2.15)$$

The relative displacement field is illustrated in Figure 2.7 and is easily calculated as

$$u(z) = z \cdot \theta_x \quad (2.16)$$

The dissipation thus becomes.

$$W_I = \frac{1}{2} t^2 h_b \theta_x f_{tb} \quad (2.17)$$

Here one may set  $f_{tb} = \frac{1}{20} f_{cb}$ , see Appendix 1.

The external work becomes.

$$W_E = m_{px} \theta_x \cdot 2(h_b + h_j) \quad (2.18)$$

The work equation gives the following moment capacity for failure mode 2

$$m_{px} = \frac{1}{4} t^2 f_{tb} \frac{h_b}{h_b + h_j} \quad (2.19)$$

Thus  $p_x^+$  attains a maximum value  $p_{x,\max}^+$  due to the tensile strength of the bricks,  $p_{x,\max}^+$  is given as:

$$p_{x,\max}^+ = f_{tb} \frac{h_b}{2(h_b + h_j)} \quad (2.20)$$

### 2.1.3 Yield line theory for laterally loaded masonry walls

A simplified method for calculating laterally loaded masonry walls may now be formulated using the results from section 2.1.2.1 combined with the traditional upper bound method for orthotropic reinforced concrete slabs.

In the latter method the bending moments are usually calculated by considering a stair-formed yield line with stairs perpendicular to the reinforcement bars. In these sections

the bending moments at yielding are considered equal to the bending yield moments in the reinforcement directions.

A calculation method for laterally loaded masonry walls now suggests itself. In the stair-formed diagonal yield lines the bending yield moments are calculated using the results from section 2.1.2.1 and then an upper bound solution may be obtained in the same way as for reinforced concrete slabs.

In [2] and [7] it has been demonstrated that the procedure used for reinforced concrete slabs is in agreement with a proper set of yield conditions.

Since the yield conditions for masonry walls in bending and torsion are not yet developed, no attempt will be made here to justify the procedure suggested by means of yield conditions.

## 2.2 Upper bound solutions

### 2.2.1 Introduction

When comparing the theoretical values of the load carrying capacity with the load carrying capacities obtained experimentally it is very important to have a detailed knowledge about what happens during loading of a wall.

In the literature only uniform transverse load has been considered.

Several investigators have reported that in the case of simply supported rectangular walls, initial cracking in the bed joint in the middle of the wall takes place long before the yield line pattern is fully developed. The general belief is that cracking in the bed joint before failure is observed because the rotation capacity of masonry bent about the bed joint is much less than that of masonry bent about the head joint.

This phenomenon has been reported by A. Cajdert, [27], Å. Hallquist, [11] and S. J. Lawrence, [29].

Lawrence [29] carefully investigates the load deflection curve for different support conditions. The load of initial cracking is dependent on the support conditions, which influence the mode of failure. These problems have been described thoroughly in [29].

Lawrence reports that a masonry wall undergoes three stages before the load carrying capacity is reached:

1. Initial cracking
2. Fully developed failure pattern
3. Ultimate load

In [29] five different walls with different support conditions marked category 1 to 5 are used in the investigation. These are shown in Figure 2.8, where also the course of the bricks is illustrated. All walls are loaded with a transverse uniform load.

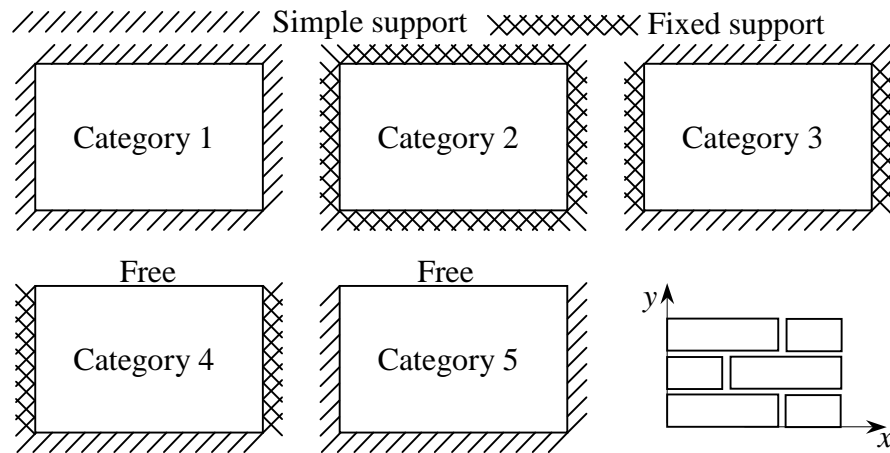


Figure 2.8 Different support conditions used in [29]

Lawrence found four different failure modes each corresponding to a particular load deflection curve, see Figure 2.9, where  $p$  is the uniform transverse load and  $u$  is the maximum deflection measured at the middle of the wall in the case of category 1-3 walls and at the middle of the free edge in the case of category 4-5 walls. The curves in Figure 2.9 are sketches based on the curves reported in [29].

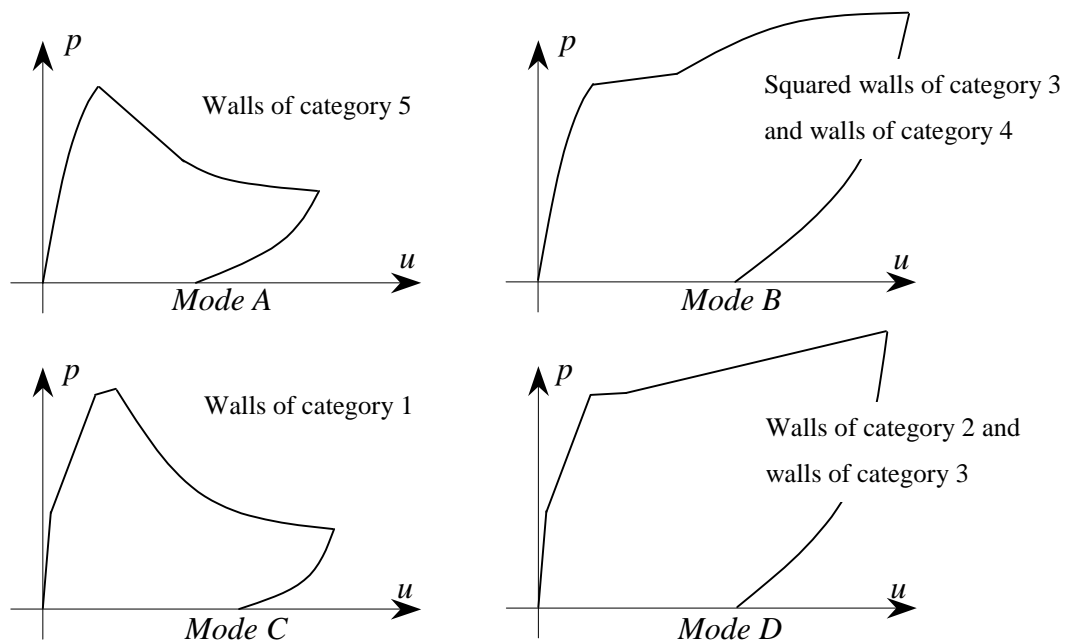


Figure 2.9 Load deflection curves, based on observations made in [29]

The different stages of the curves may be reviewed by looking at Table 2.2. Here a “yes” means that this stage exists and the load carrying capacity is higher than the stage before. A “=1” means that no increase in the load and no change in failure pattern are observed prior to the stage before.

Failure Mode	Stage 1	Stage 2	Stage 3
A	Yes	=1	=1
B	Yes	=1	Yes
C	Yes	Yes	=1
D	Yes	Yes	Yes

**Table 2.2 Failure modes and observed stages of cracking**

The failure pattern observed in the case of a category 1 wall is mainly failure mode C. Category 2 walls failed by failure mode D. Category 3 walls failed in the case of squared slabs by failure mode B, otherwise by failure mode D. Category 4 walls all failed in mode B. Category 5 walls all failed in mode A.

From the observations made by Lawrence it may be seen that category 2 and 3 walls behaves similar. This is in agreement with the observations of the lower rotation capacity of the bed joint, which means that horizontal restraints only have little influence on the load deflection curve and no influence on the load carrying capacity.

In the case of mode B and D the yield line theory will predict the load at the first plateau. The increase in load after the yield line pattern has been developed is due to membrane action, which is not taken into consideration here, Figure 2.9 shows that mode B and D walls have a large deformation capacity and the behaviour is very ductile.

The observations made by Lawrence, Cajdert and Hallquist justify that a horizontal yield line has no moment capacity when the yield line pattern is fully developed.

## **2.2.2 Calculation of orthotropic walls**

Calculations of orthotropic walls may be made in two different ways, both being upper bound solutions. One method was used by Hagsten, L. G in [43]. The method assumes that the yield line is fixed to run in the interface in a way, determined by the bond in which the bricks are laid.

Another method is the yield line theory for orthotropic walls described in section 2.1.

### **2.2.2.1 Upper bound solution using plane strain solution**

An upper bound solution for masonry walls may be derived under the assumption that yield lines are formed in the interface between the brick and the mortar. In the interface,

the state of strain is plane meaning that the dissipation per unit area may be calculated as

$$W_A = \frac{1}{2} f_{ct} u (l - m \sin \alpha) \quad (2.21)$$

Here  $l = 1$  and  $m = 1$  when the tensile strength is set to zero, which is assumed in the calculations, see [2] for more details. The dissipation depends on the displacements in an extremely complicated way.

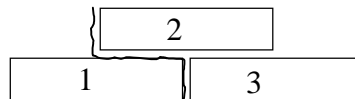


**Figure 2.10 A yield line formed in the interface**

Roughly, the displacement field may be described by means of Figure 2.10. In both a horizontal section and a vertical section, the displacement will be a translation combined with a rotation. The problem becomes three-dimensional. The calculations have been carried through by L. G. Hagsten in [43]. They are difficult and lengthy. The method has been compared with experiments and the correlation is very good. However, the method is difficult to use for practical purposes.

### 2.2.2.2 Upper bound solution using yield moments

Upper bound solutions may be found in a similar way as for orthotropic concrete slabs by means of simple yield line patterns, see section 2.1.3. The bending yield moments in two perpendicular directions are used to calculate the bending moment in the yield line by means of the formula:

$$m_b = m_{px} \sin^2 \theta + m_{py} \cos^2 \theta \quad (2.22)$$

where  $\theta$  is the angle between the  $x$ -axis and the yield line. The dissipation becomes

$$W_l = m_b \omega \quad (2.23)$$

Here  $\omega$  is the relative rotation in the yield line. Formula (2.22) determines  $m_b$  as if  $m_{px}$  and  $m_{py}$  were principal moments, which is of course not the case.

When the bending yield moments  $m_{px}$  and  $m_{py}$  may be calculated by the procedure described in section 2.1.2.1 the method of orthotropic concrete slabs is completely equivalent to the method described in section 2.1.2.1. Notice that when using the method of section 2.1.2.1 we have left the strict requirements in section 2.1.2 to the correspondence between relative displacements in the interface and the running bond.

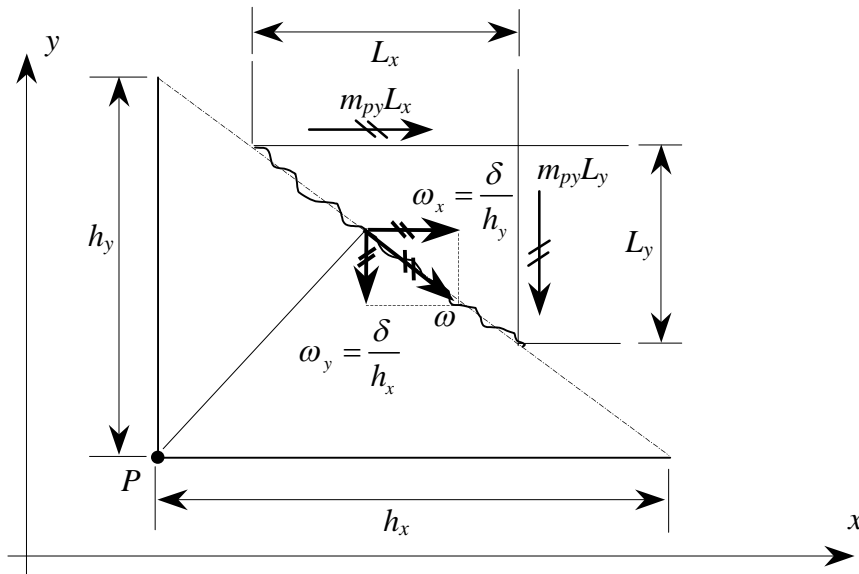


Figure 2.11 Moments and rotations in the case of orthotropic slabs

The dissipation in the case of an orthotropic wall becomes, when the point  $P$ , see Figure 2.11, is displaced  $\delta$  downwards:

$$W_I = m_{px}L_y \frac{\delta}{h_x} + m_{py}L_x \frac{\delta}{h_y} \quad (2.24)$$

### 2.2.2.3 Comparison between calculation methods

In this section, the calculation method developed by Hagsten, L. G. in [43] and the method for orthotropic walls described in section 2.2.2.2 will be compared. The main difference between the methods is that Hagsten's method is strictly related to the bond of the masonry, while the method outlined in this report assumes a homogeneous wall. The comparison may be made for a small repeated section as shown in Figure 2.12. The angle  $\theta$  is changed by changing  $x_0$ .

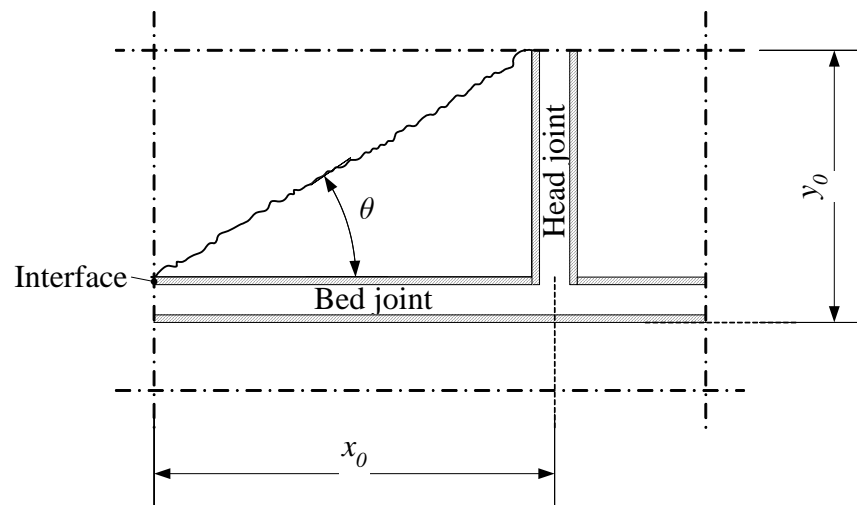


**Figure 2.12 Repeated section**

In the following the internal work  $W_i$  in a diagonal yield line will be shown for different angles  $\theta$ . Comparisons are only made for right-angled corners. The comparison between the two methods may be seen in Figure 2.13.

The internal work is calculated based on the compressive strength or the cohesion of the interface. The cohesion is influenced by the properties of the brick and the mortar and may be calculated by

$$c = \left( -0.11 \frac{w}{l} + 0.03 \right) IRA - 0.5 \frac{w}{c} + 3.6 \quad [\text{MPa}] \quad (2.25)$$

where  $w/l$  is the water/lime ratio,  $w/c$  the water/cement ration and  $IRA$  is the one minute suction of the brick also called the initial rate of absorption.

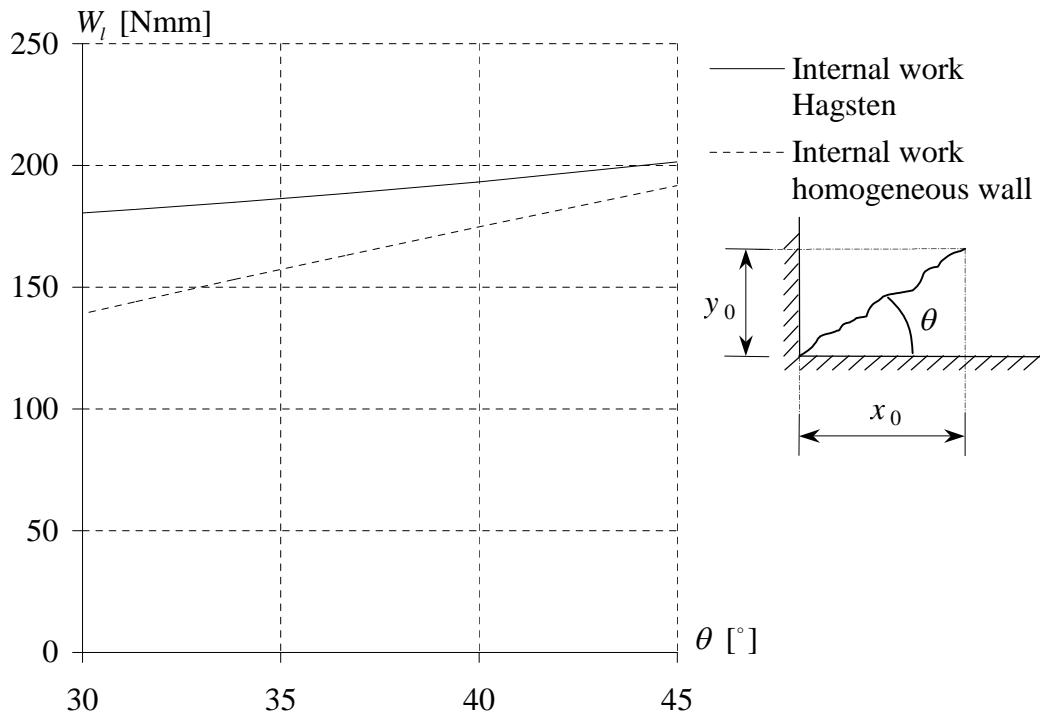


Figure 2.13 The internal work per unit length  $W_l$  as a function of  $\theta$

The calculations are performed by use of the data listed in Table 2.3.

$b_b$	108.0[mm]
$h_b$	55.0[mm]
$l_b$	228.0[mm]
$h_j$	12.0[mm]
$y_0$	67[mm]
$x_0$	$y_0/\tan(\theta)$ [mm]
$f_{cb}$	60.0[MPa]
$IRA$	2.5[ $\text{kg}/\text{m}^2/\text{min}$ ]
$w/k$	2.8
$w/c$	2.8
$c$	1.5[MPa]
$\varphi$	30.0 [°]
$f_{ci}$	5.3[MPa]

Table 2.3 The data used in the calculations

The contributions from the head and bed joint are compared in Figure 2.14. The work in the head joint is what provides the moment  $m_{py}$  in the method proposed in section 2.2.2.2 of this report.

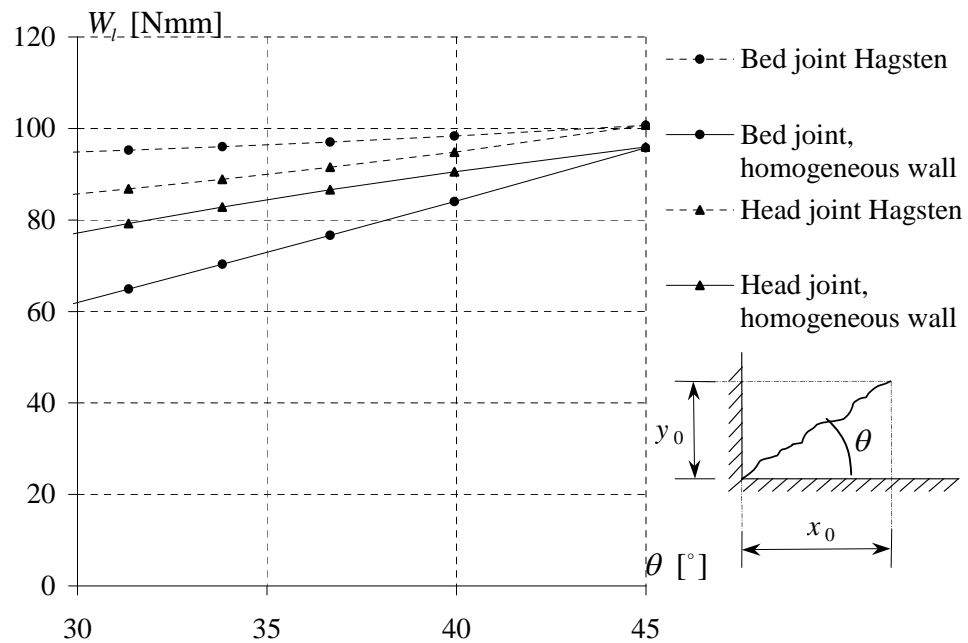


**Figure 2.14** The different calculation methods as a function of  $\theta$

If the total internal work, calculated by Hagsten, is divided by the internal work calculated according to the theory of homogeneous walls, the variation with respect to  $\theta$  becomes as shown in Figure 2.15. It appears that the method of homogeneous masonry walls is on the safe side compared with the method developed by Hagsten for the data used in the comparison.

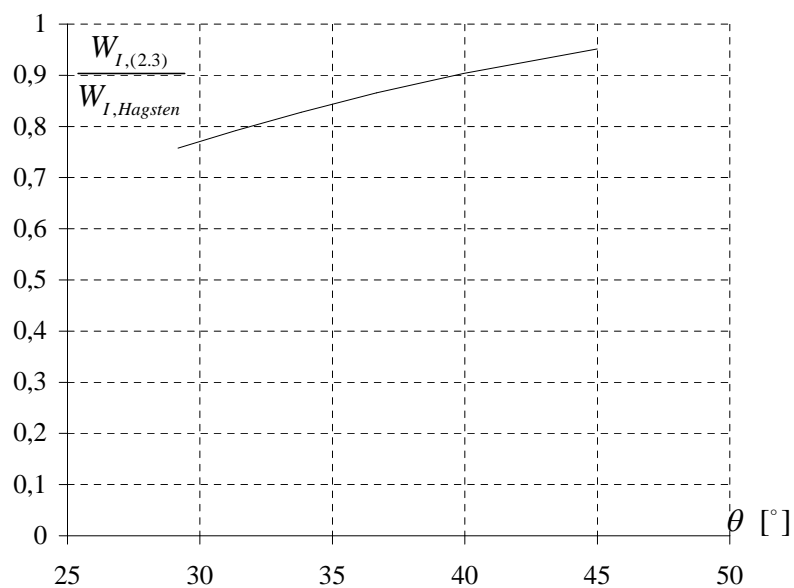


**Figure 2.15** Comparison of the calculation method developed by Hagsten and the one presented in section 2.2.2.2 of this report

### 2.2.3 Simple yield line patterns

In this section, the theory of orthotropic walls developed is used to calculate different yield line patterns, considering different walls all loaded with an uniform transverse load.

The method assumes that the dissipation in a diagonal yield line may be calculated according to section 2.1.2.1, i.e,  $m_{py} = \mu m_{px}$ . The moment capacity of a horizontal yield line in the bed joint is zero. Otherwise, the calculations are made as traditional calculations for orthotropic walls.

Notation for support conditions:

//////////////////// Simple support    xxxxxxxxxxxx Fixed support

Drawing	Work equation
	$W_I = 2m_{px}\delta \left( 4\mu \frac{x}{h} + \frac{h}{x} \right)$ $W_E = p^+\delta \left( \frac{1}{2}bh - \frac{1}{3}hx \right)$ $W_E = W_I : p^+ = \frac{2m_{px} \left( 4\mu \frac{x}{h} + \frac{h}{x} \right)}{\frac{1}{2}bh - \frac{1}{3}hx}$ $\frac{dp^+}{dx} = 0 \Rightarrow x = \frac{1}{12} \frac{(-2h \pm 2\sqrt{h^2 + 9\mu b^2})h}{\mu b}$
	$W_I = 2m_{px}\delta \left( \mu \frac{b}{y} + 2\frac{h}{b} \right)$ $W_E = p^+\delta \left( \frac{1}{2}bh - \frac{1}{3}by \right)$ $W_E = W_I : p^+ = \frac{2m_{px} \left( \mu \frac{y}{h} + 2\frac{h}{b} \right)}{\frac{1}{2}bh - \frac{1}{3}by}$ $\frac{dp^+}{dy} = 0 \Rightarrow y = \frac{1}{4} \frac{(-2b\mu \pm 2\sqrt{\mu^2 b^2 + 3\mu h^2})b}{h}$



	$W_I = 2m_{px} \delta \left( \frac{1}{2} \mu \frac{b}{y} + 4 \frac{h}{b} \right)$ $W_E = p^+ \delta \left( \frac{1}{2} bh - \frac{1}{6} by \right)$ $W_E = W_I : p^+ = \frac{2m_{px} \left( \frac{1}{2} \mu \frac{b}{y} + 4 \frac{h}{b} \right)}{\frac{1}{2} bh - \frac{1}{6} by}$ $\frac{dp^+}{dy} = 0 \Rightarrow y = \frac{1}{8} \frac{(-\mu b \pm 2\sqrt{\mu^2 b^2 + 24\mu h^2}) b}{h}$
	$W_I = m_{px} \delta \left( \mu \frac{b}{y} + \frac{y}{b} \right)$ $W_E = p^+ \delta \left( \frac{1}{2} bh - \frac{1}{6} by \right)$ $W_E = W_I : p^+ = \frac{m_{px} \left( \mu \frac{b}{y} + \frac{y}{b} \right)}{\frac{1}{2} bh - \frac{1}{6} by}$ $\frac{dp^+}{dy} = 0 \Rightarrow y = \frac{1}{6} \frac{(-2\mu b \pm 2\sqrt{\mu^2 b^2 + 9\mu h^2}) b}{h}$
	$W_I = m_{px} \delta \left( \mu \frac{x}{h} + \frac{h}{x} \right)$ $W_E = p^+ \delta \left( \frac{1}{2} bh - \frac{1}{6} hx \right)$ $W_E = W_I : p^+ = \frac{m_{px} \left( \mu \frac{x}{h} + \frac{h}{x} \right)}{\frac{1}{2} bh - \frac{1}{6} hx}$ $\frac{dp^+}{dx} = 0 \Rightarrow x = \frac{1}{6} \frac{(-2h \pm 2\sqrt{h^2 + 9\mu b^2}) h}{\mu b}$

	$W_I = 2m_{px}\delta \left( \frac{y}{b} + \mu \frac{b}{y} \right)$ $W_E = p^+\delta \left( \frac{1}{2}bh - \frac{1}{3}by \right)$ $W_E = W_I : p^+ = \frac{2m_{px} \left( \frac{y}{b} + \mu \frac{b}{y} \right)}{\frac{1}{2}bh - \frac{1}{3}by}$ $\frac{dp^+}{dy} = 0 \Rightarrow y = \frac{1}{6} \left( \frac{-4\mu b \pm 2\sqrt{4\mu^2 b^2 + 9\mu h^2}}{h} \right) b$
	$W_I = m_{px}\delta \left( \frac{h}{x} + 4\mu \frac{x}{h} \right)$ $W_E = p^+\delta \left( \frac{1}{2}bh - \frac{1}{6}hx \right)$ $W_E = W_I : p^+ = \frac{m_{px} \left( \frac{h}{x} + 4\mu \frac{x}{h} \right)}{\frac{1}{2}bh - \frac{1}{6}hx}$ $\frac{dp^+}{dx} = 0 \Rightarrow x = \frac{1}{12} \left( \frac{-h \pm \sqrt{h^2 + 36\mu b^2}}{\mu b} \right) h$

Table 2.4 Some yield line patterns for masonry walls

In the case of category 2 and 3 walls, a yield line pattern as the one in Figure 2.16 provides a lower load carrying capacity than the ones calculated in Table 2.4. However, an analytical minimum solution by using the work equation is difficult.

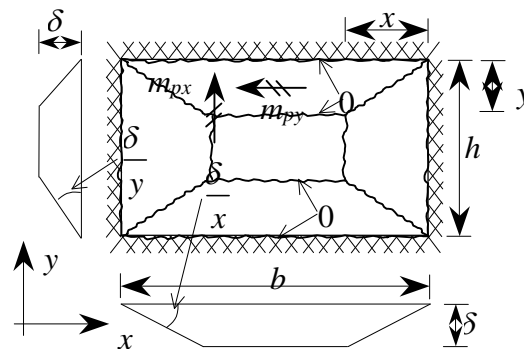


Figure 2.16 Optimal yield line pattern in the case of category 2 and 3 walls

The work equation provides the following load carrying capacity:

$$p^+ = \frac{2m_{px} \left( (1+i) \frac{h}{x} + 2\mu \frac{x}{y} \right)}{bh - hx - by + \frac{8}{6} xy} \quad (2.26)$$

where  $i$  is the degree of fixing along the vertical fixed supports.

Similarly in the case of simply supported walls ( $i = 0$ ), the yield line pattern in Table 2.4 provides a higher load carrying capacity than the yield line pattern in Figure 2.16. However, the error by using the simple yield line pattern given in Table 2.4, is small, see Figure 2.17

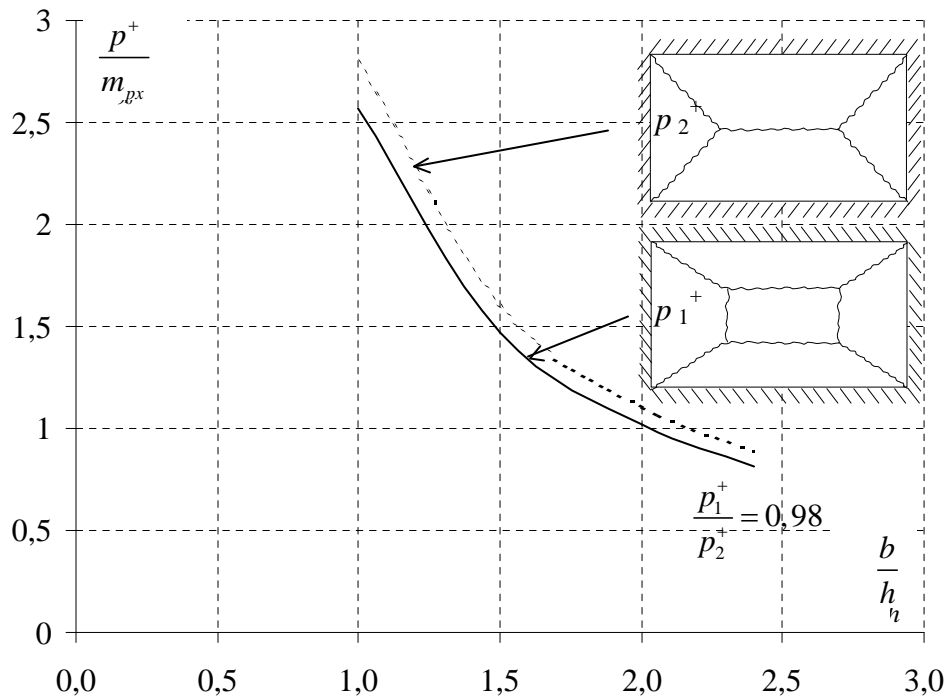


**Figure 2.17 Comparison of two yield line patterns for a simply supported wall**

Figure 2.17 shows that the ratio between the two calculated load carrying capacities is about 0.98. In these calculations  $\mu$  has been calculated by formula (2.12) using the data in Table 2.1.

### 2.2.4 Illustrative examples

In order to further illustrate the yield line theory of masonry walls a few examples are outlined in this section. Among other issues, the calculations demonstrate the influence of the horizontal yield line.

### 2.2.4.1 Example 1. Calculation of a wall

In this example a masonry wall simply supported on four sides loaded with a transverse pressure  $p$  (kN/m<sup>2</sup>) will be considered. This example illustrates the correlation between the simplified calculation procedure and the more general procedure. Furthermore the results of the example may be compared with results from an example in chapter 3 whereby the influence of axial loads may be seen. The properties of the wall are listed in Figure 3.9.

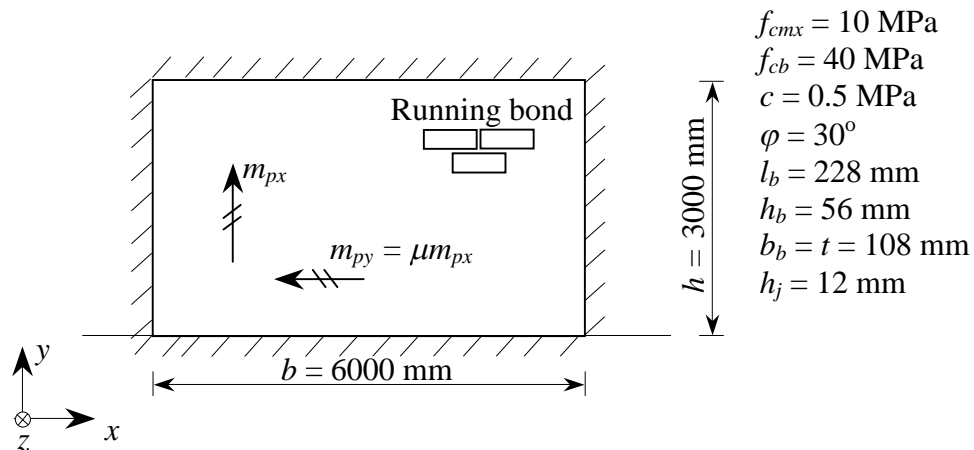


Figure 2.18 Data for wall

Equation (2.10) provides the tensile strength,  $p_x^+$ . For  $\beta = 45^\circ$  we find that

$$p_x^+ = \frac{\frac{1}{2}(l_b + h_j)}{h_b + h_j} \frac{1}{2} f_{ci} \frac{1 - \sin 45^\circ}{\cos 45^\circ} \Rightarrow$$

$$p_x^+ = \frac{\frac{1}{2}(228 + 12)}{56 + 12} 0.5 \frac{\cos 30^\circ}{\cos 45^\circ} \frac{1 - \sin 45^\circ}{1 - \sin 30^\circ} = 0.63 \text{ MPa}$$

where  $f_{ci} = 2c \cdot \cos \varphi / (1 - \sin \varphi)$  has been introduced. This relation is obtained by calculating the tangent point between Coulomb friction hypothesis and Mohr's circle for  $\sigma_1 = 0$  and  $\sigma_3 = -f_{ci}$

The maximum tensile strength is calculated by equation (2.20)

$$p_{x,\max}^+ = \frac{h_b}{2(h_b + h_j)} f_{tb} \Rightarrow$$

$$p_{x,\max}^+ = \frac{56}{2(56 + 12)} \frac{1}{20} 40 = 0.82 \text{ MPa}$$

The tensile strength of the bricks is assumed to be equal to  $1/20 f_{cb}$ , see Appendix 1. The yield moment  $m_{px}$  is determined from equation (2.13).

$$m_{px} = \frac{1}{2} t^2 p_x^+ \Rightarrow$$

$$m_{px} = \frac{1}{2} 108^2 \cdot 0.63 = 3.69 \frac{\text{kNm}}{\text{m}}$$

The yield moment in the bed joint is determined in the same way.

$$p_y^+ = \frac{h_b + h_j}{\frac{1}{2}(l_b + h_j)} c \frac{\cos \varphi}{\cos 45^\circ} \frac{1 - \sin 45^\circ}{1 - \sin \varphi} \Rightarrow p_y^+ = 0.2 \text{ MPa}$$

$$m_{py} = \frac{1}{2} t^2 p_y^+ \Rightarrow m_{py} = 1.19 \frac{\text{kNm}}{\text{m}}$$

The load carrying capacity is calculated for the yield line pattern shown in Figure 2.19. The moment capacity in the horizontal yield line is zero because of the rotation axis being at the top face of the wall and because the tensile strength of the bed joint is assumed equal to zero.

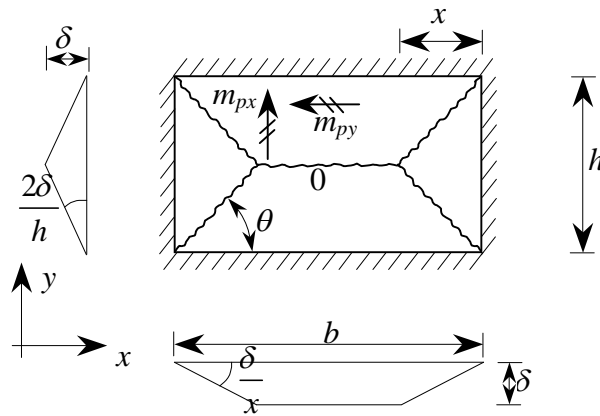


Figure 2.19 Yield line pattern

The internal work becomes:

$$W_I = 2m_{px} \left( 4 \frac{m_{py}}{m_{px}} \frac{x}{h} + \frac{h}{x} \right) \delta$$

The external work becomes:

$$W_E = p^+ \delta \left( \frac{1}{2} bh - \frac{1}{3} hx \right)$$

The work equation provides the load carrying capacity by minimizing with respect to  $x$ . The results of the calculations are shown in Figure 2.20. In Figure 2.20 the load carrying capacity obtained using the general approach of section 2.1.2 ( $\beta = \pi/2 - \theta$ ) is shown as well. It may be seen that the two methods are nearly identical around the minimum of the load carrying capacity.

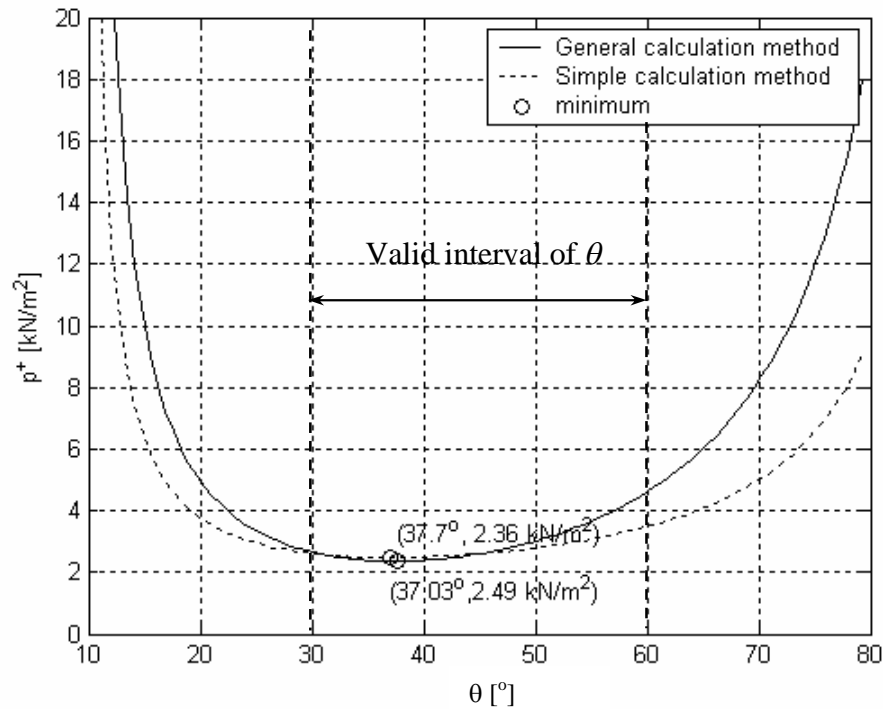


Figure 2.20 Calculated load carrying capacity as a function of  $\theta$

#### 2.2.4.2 Example 2. Cavity wall

This example is bound on an experiment carried out at NBI [12] (Building Institute of Norway). The wall considered is shown in Figure 2.21. The vertical edges were fixed since metal ties were anchored in the surrounding concrete by use of expansion bolts. The wall consists of two halves held together by metal ties placed with a centre distance of 500 mm. The metal ties transfer half of the load to the other half. The load applied is uniform distributed. The moment capacity in the head joint was measured to 4.54 kNm/m. No attempts are made here to calculate the moment capacity, since lack of information makes it impossible to estimate the cohesion.

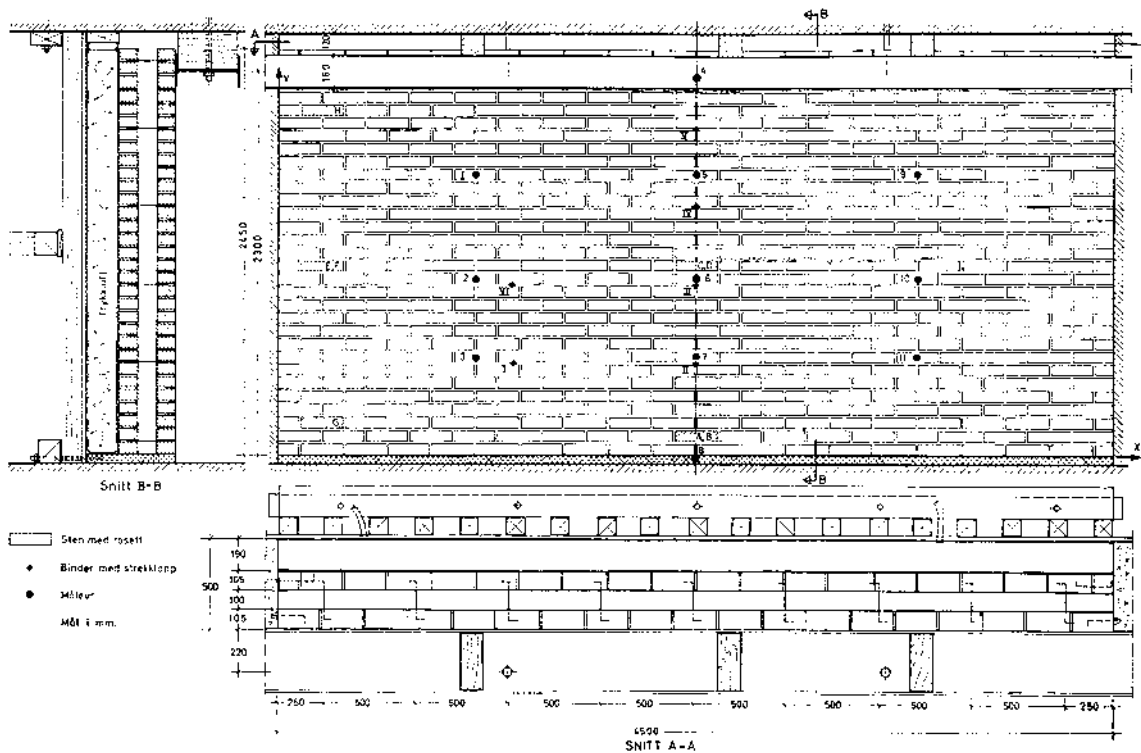


Figure 2.21 The geometrical properties of the wall, taken from [12]

The bricks used had 19 holes. The length was 240 mm, the height 63 mm and the width 105 mm. This provides a ratio between  $m_{px}$  and  $m_{py}$  for  $\beta = 45^\circ$  cf. formula (2.12).

$$\mu = \frac{m_{py}}{m_{px}} = \left( \frac{h_b + h_j}{\frac{1}{2}(l_b + h_j)} \right)^2 = \left( \frac{75}{\frac{1}{2}(240 + 12)} \right)^2 = 0.35 \quad (2.27)$$

when the joint thickness is assumed equal to 12 mm. The bricks are laid in running bond with half a brick overlap.

The load carrying capacity of the wall is calculated for the two yield line patterns shown in Figure 2.22. The load carrying capacity calculated is valid for one half of the wall, which means that the load carrying capacity measured should be twice the calculated value if the two halves work fully together. In the calculations  $i$  is the ratio of fixing along the fixed support at the vertical edges relative to the bending yield moment  $m_{px}$ . It is set equal to one in the calculations.



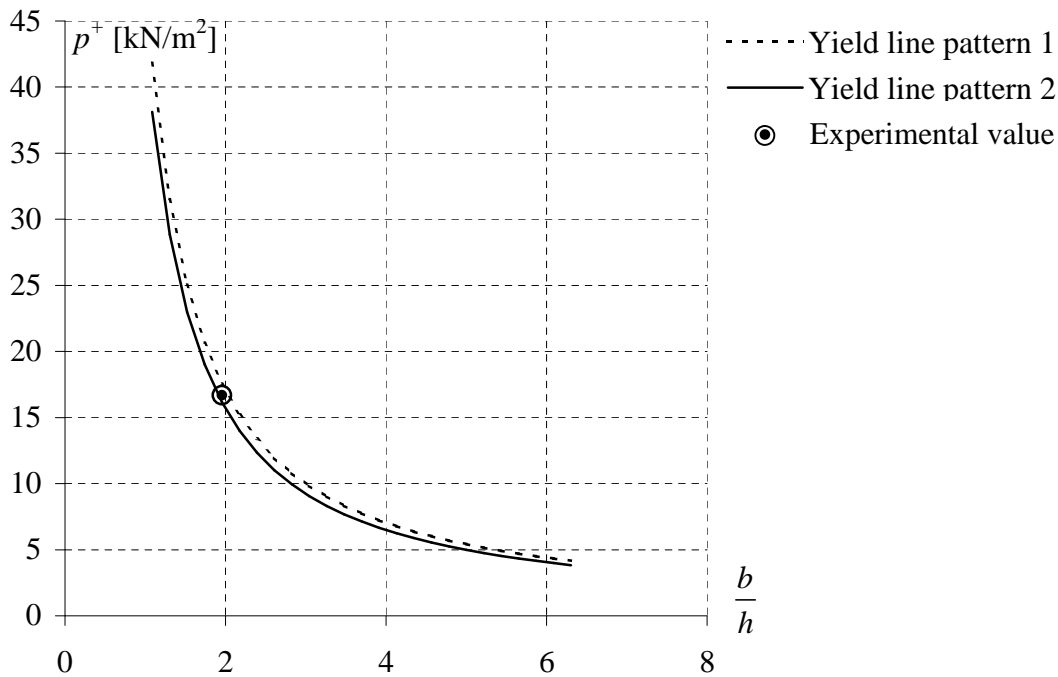


**Figure 2.23 The variation of the load carrying capacity with  $b/h$  for the two yield line patterns and the measured value**

	$b$	$h$	$m_{px}$	$\mu$	$x$	$y$	$p^+$	$p_{exp}$	$\frac{p_{exp}}{p^+}$
	[mm]	[mm]	[kNm/m]		[mm]	[mm]	[kN/m <sup>2</sup> ]	[kN/m <sup>2</sup> ]	$p^+$
Yield line pattern 1	4500	2300	4.54	0.35	1741	1150	17.52	16.68	0.95
Yield line pattern 2	4500	2300	4.54	0.35	1357	656	16.09	16.68	1.04

**Table 2.5 The result from the calculations compared with experiments**

The theoretical load carrying capacity is compared with the load, for which the yield line pattern is fully developed, the flat plateau in Figure 2.9, curve D. From Table 2.5 it appears that there is a very good agreement between theoretical and measured load carrying capacity. The maximum load measured is 24.9 kN/m<sup>2</sup>. The higher load is due to membrane action, which is also illustrated in Figure 2.9 curve D where an additional load carrying capacity is achieved for very large deflections..

In the tests the yield line pattern was monitored during loading as illustrated in Figure 2.24. The numbers refer to load steps, which are given in Table 2.6. It may be seen that the horizontal yield line develops earlier than the remaining yield line pattern. The load for which the horizontal yield line is developed is 33% lower than the load corresponding to the fully developed yield line pattern, which confirms that the contribution to the internal work is zero as assumed in the calculations. This supports the observations made by Lawrence ([26]) regarding the load deflection curve of masonry walls.

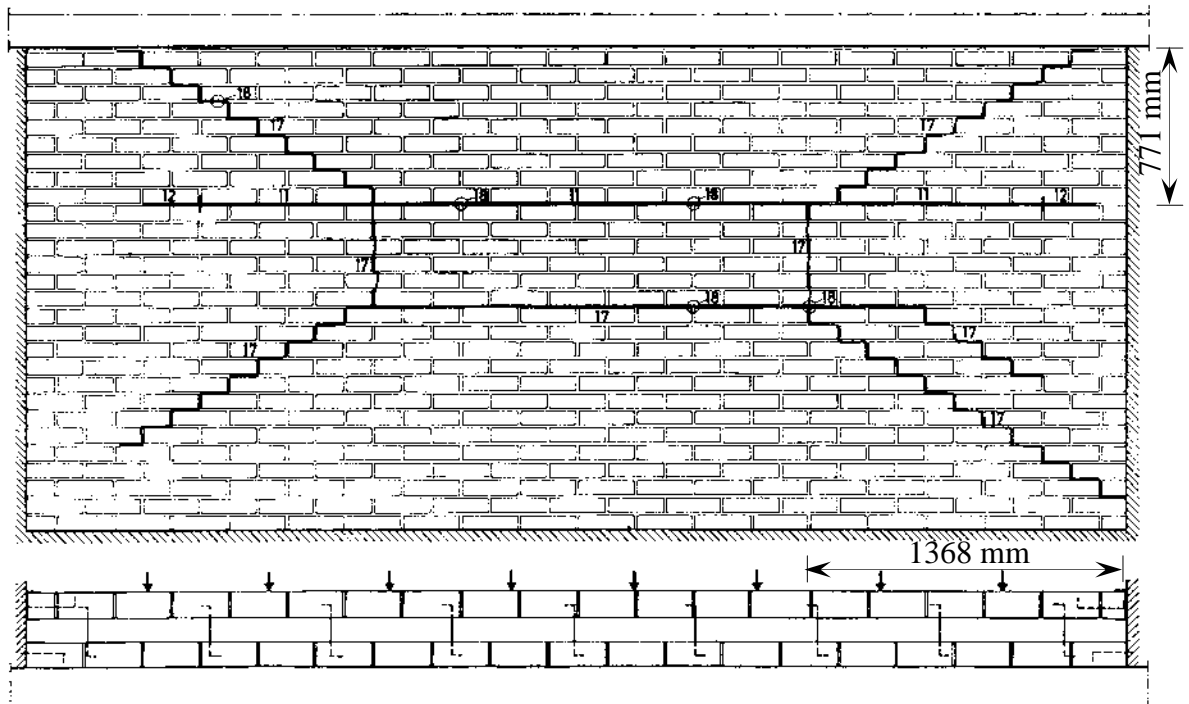


Figure 2.24 Observed yield line pattern taken from [11]

In Figure 2.24 the observed lengths of  $x$  and  $y$  are illustrated. Compared with the calculated values the agreement is seen to be very good (yield line pattern 2 ( $x_{calc}$ ,  $y_{calc}$ ) = (1357 mm, 656 mm).

Load step	Load [ $\text{kg}/\text{m}^2$ ]	
10	1000	
11	1100	Horizontal yield line is developed
12	1200	
13	1300	
14	1400	
15	1500	
16	1600	
17	1700	Yield line pattern fully developed
18	1800	

Table 2.6 Load step with numbers referring to the observed yield line pattern as they are given in [12]

### 2.2.4.3 Example 3. Walls with openings

In [14] different walls have been tested. Three of them are with openings as illustrated in Figure 2.25. In this example the walls will be calculated by using the yield line theory

of section 2.2.2.2 in this report. The bricks are laid in running bond with half a brick overlap.

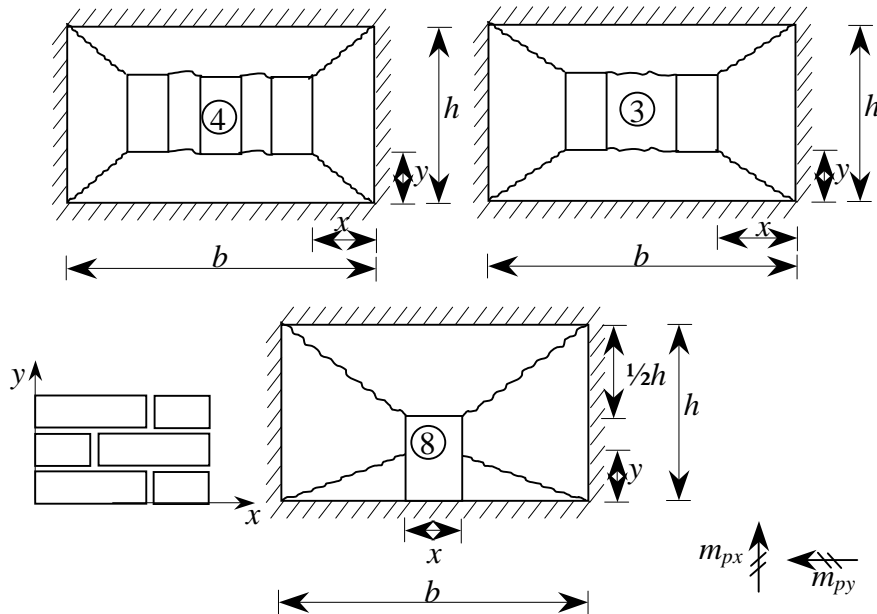


Figure 2.25 The walls with openings

The calculations are carried out by calculating the internal and external work using the work equation and minimizing the load with respect to the free geometrical parameters. The yield line patterns are illustrated in Figure 2.25. For the walls at the top in Figure 2.25 the parameters  $x$  and  $y$  are not free, they are bound by the openings. In the wall below the parameter  $y$  is free and  $x$  is fixed to be the width of the door opening. The moment  $m_{px}$  is once again taken as the measured value.

No.	Comments	$b$	$h$	$m_{px}$	$\mu$	$X$	$y$	$p^+$	$p_{exp}$	$\frac{p_{exp}}{p^+}$
		[mm]	[mm]	[kNm/m]		[mm]	[mm]	[kN/m <sup>2</sup> ]	[kN/m <sup>2</sup> ]	
3	2 windows	3500.00	2000.00	3.73	0.28	1030.00	510.00	5.01	7.06	1.41
4	3 windows	3500.00	2000.00	4.32	0.28	766.00	510.00	5.09	6.72	1.32
8	1 door	3500.00	2000.00	3.73	0.28	492.00	464.16	5.53	5.74	1.04

Table 2.7 Calculations compared with experiments

The results show that the load carrying capacity obtained in the experiments are higher than the calculated values. This may be due to the fact, that the load for which the yield line pattern was fully developed is not recorded and therefore the load carrying capacity compared with may be influenced by membrane action, which is not considered.

#### 2.2.4.4 Example 4. Comparison with the calculation method in some codes

In the Danish code DS414 and in the European code EC6 the yield line theory is used to calculate the load carrying capacity of masonry walls. However the modification of disregarding the horizontal yield line is not taken into account. In the present example a rectangular wall simply supported on four sides is considered. The wall is shown in Figure 2.26.

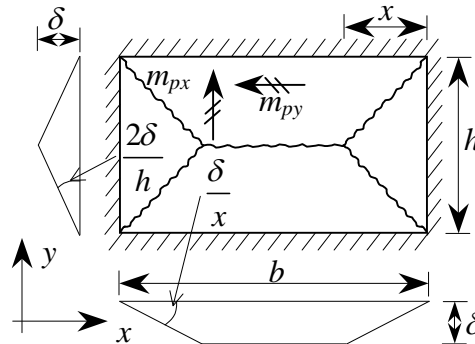


Figure 2.26 Wall considered

The data used in the calculation are listed in Table 2.8. These are the same as the data reported by Lawrence in [29].

$h$	2500	mm
$\mu$	0.46	
$m_{px}$	3.98	kNm/m

Table 2.8 Data used in the calculation

Taking into account the horizontal yield line when calculating the internal work we get:

$$W_I = 2m_{py}b\frac{2\delta}{h} + 2m_{px}h\frac{\delta}{x} \quad (2.33)$$

Inserting  $m_{py} = \mu m_{px}$ , the internal work becomes

$$W_I = 2m_{px}\left(2\mu\frac{b}{h} + \frac{h}{x}\right)\delta \quad (2.34)$$

The external work becomes

$$W_E = p^+\delta\left(\frac{1}{2}bh - \frac{1}{3}hx\right) \quad (2.35)$$

From the work equation the optimal solution for  $x$  is obtained:

$$x = \frac{1}{4} \frac{(-2h \pm 2\sqrt{h^2 + 3\mu b^2})h}{\mu b} \quad (2.36)$$

Inserting  $x$  into the work equation provides the load carrying capacity of the wall.

In Figure 2.27a results from the calculations using equation (2.34) to (2.36) ( $p_2^+$ ) and from the equations given in Table 2.4 ( $p_1^+$ ) are shown. Furthermore, results from tests carried out by Lawrence are plotted. In Figure 2.27b the ratio between the two calculated load carrying capacities is plotted. The calculations show that by including the horizontal yield line follows an overestimation of the load carrying capacity and the error increases with increasing  $b/h$  ratio. Thus an essential reduction in safety is suffered when taking the yield line along the bed joint into account.

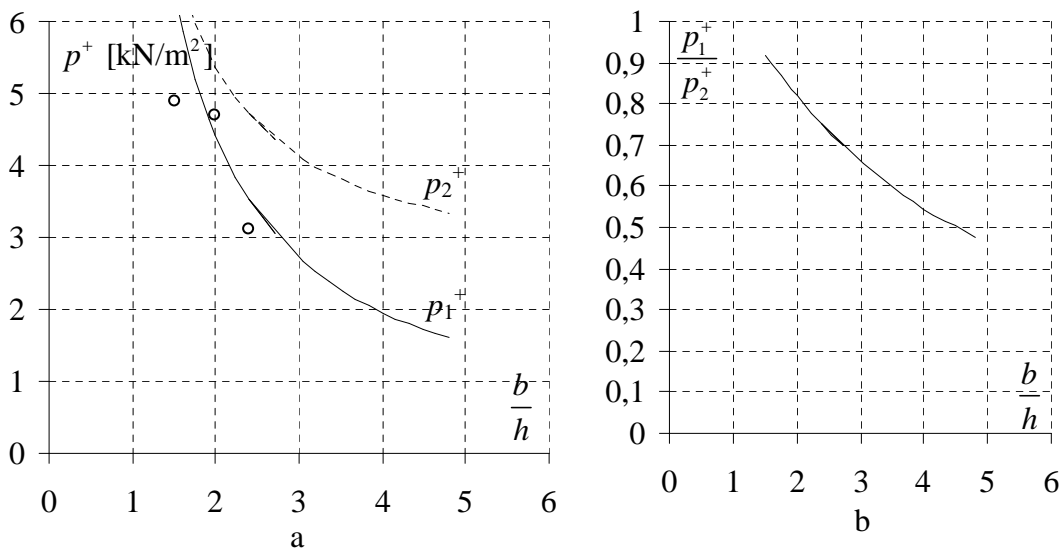


Figure 2.27 Results from calculations comparing the effect of taking the horizontal yield line into account

### 2.3 Comparison with experiments

In this section comparison between a number of further experiments and the calculation method presented in section 2.2.2.2 will be carried out.

Each investigation used will be described, and then plots comparing experiments with the theory will be shown. The previous calculations seem to indicate that the simplified method provides similar results as the more general method around the optimal solution. In the comparisons the simplified method is used to calculate the ratio between the moments (equation (2.12)). For the bending yield moment in the head joint the measured value of  $m_{px}$  is used. We are only able to calculate  $m_{px}$  by estimating the cohesion which is not reported. Estimating the cohesion on the basis of  $m_{px}$  will be the same as using  $m_{px}$ . All investigations provide measurements of the bending yield moment in the head joint.

The lateral load was in all cases applied by an air bag. All experiments are on rectangular walls with bricks in running bond with half a brick overlap.

### **2.3.1 Investigations**

#### ***Kheir, A. M. A. 1975 [18]***

The investigation made by Kheir consists of 19 test panels, 11 simply supported on three sides and 8 panels simply supported on all 4 sides. The bricks used were 1/6<sup>th</sup> scale bricks with a compressive strength of 26.5 MPa. The mortar used was a 1:¼:3 (lime:cement:sand) mortar with a compressive strength after 21 days at 31 MPa. The compressive strength of the brickwork were measured to be 20.3 MPa. The bending moments in the head and bed joint were measured in connection with the tests of the wall panels. The relevant data are listed in section 7.1.1.

#### ***West, H. W. H et. al. 1977 [21]***

The investigation made by West, H. W. H. consists of 71 experiments on full size wall panels simply supported on three sides. In the investigation three different mortars were used, X= 1:¼:3, Y=1:1:6 and Z=1:2:9. These mortars were used with various types of bricks with different IRA's. Further, a large investigation on the bending capacity in the head and bed joint was reported. The relevant data are listed in section 7.1.2

#### ***Cajdert, A 1983 [27]***

The investigation made by Cajdert, A. consists of 6 experiments on full size walls, 3 simply supported on 3 sides and 3 simply supported on 4 sides. In the investigation, six different perforated bricks were used with an IRA varying from 0.59-1.89 kg/m<sup>2</sup>/min. These were combined with two different mortars, a 1:6 mortar (A) and a 1:3.5 mortar (B). The strengths of the mortars were 15 and 30 MPa, respectively. Furthermore, tests on the bending moment capacity at an angle to the bed joint were carried out. The relevant data are listed in section 7.1.3.

#### ***Lawrence, S. J. 1983 [29]***

The investigation made by Lawrence, S. J. consists of 32 experiments. These were divided into five categories dependent on the support conditions. The five support conditions are illustrated in Figure 2.28. The ratio between the width and the height varied from 1 to 2.4.

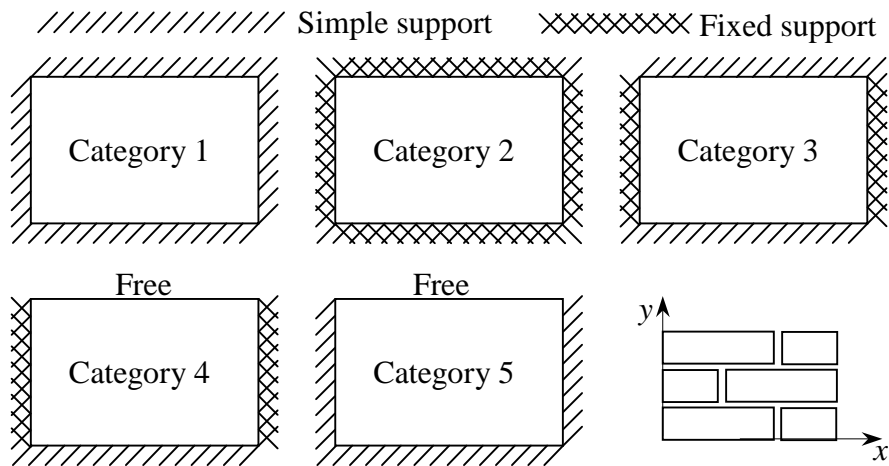


Figure 2.28 Walls tested by Lawrence, S. J.

In the investigation seven different 10-holed bricks were used together with one 1:1:6 mortar. The IRA varied from 0.2 – 0.51 kg/m<sup>2</sup>/min. For the different walls, the crack development was monitored together with the load deflection curve, which enabled the investigator to report four different types of load deflection curves. The relevant data are listed in section 7.1.4.

***Buhelt, M. 1984 [31]***

The investigation made by Buhelt, M. consists of 6 walls simply supported on two perpendicular edges. The bricks are laid in running bond with ¼ brick overlap. In the investigation one type of brick and mortar was used. The brick had an IRA of 3.1 kg/m<sup>2</sup>/min and a compressive strength of 35 MPa. The mortar was a KC 50/50/750 mortar. Further, an investigation of the bending moment capacities about the head and bed joint has carried out. The relevant data are listed in section 7.1.5.

**2.3.2 Comparison with experiments for laterally loaded slabs**

In this section, the load carrying capacity found by the yield line theory is compared with the experimental load at fully developed yield line pattern. Six different support conditions are used in the comparison. All experiments are on full size walls except the walls tested by Kheir, A. M. A. where the walls (bricks), as mentioned above, were scaled to 1/6<sup>th</sup>.

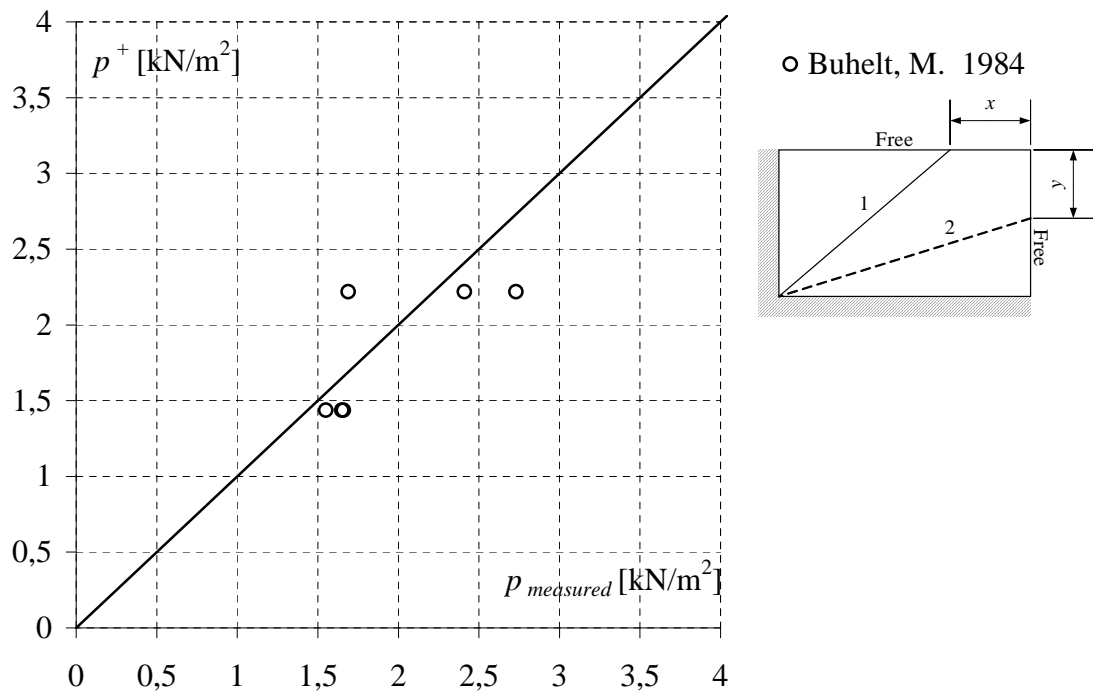


**Figure 2.29 Comparison with experiments on walls simply supported on two perpendicular sides**

In Figure 2.29 two different yield line patterns are used in the calculations of the load carrying capacity of the wall, which is supported on two perpendicular edges intersecting in the lower left corner of the wall. The yield line patterns used in the calculations consist of a yield line emerging from the corner where the supports intersect and ending on either side of the diagonal corner. A yield line pattern where the free corner breaks off has been considered. However, calculation showed that the load carrying capacity was larger than the load carrying capacities calculated by Figure 2.29.

Figure 2.29 compares theoretical and measured load carrying capacity.

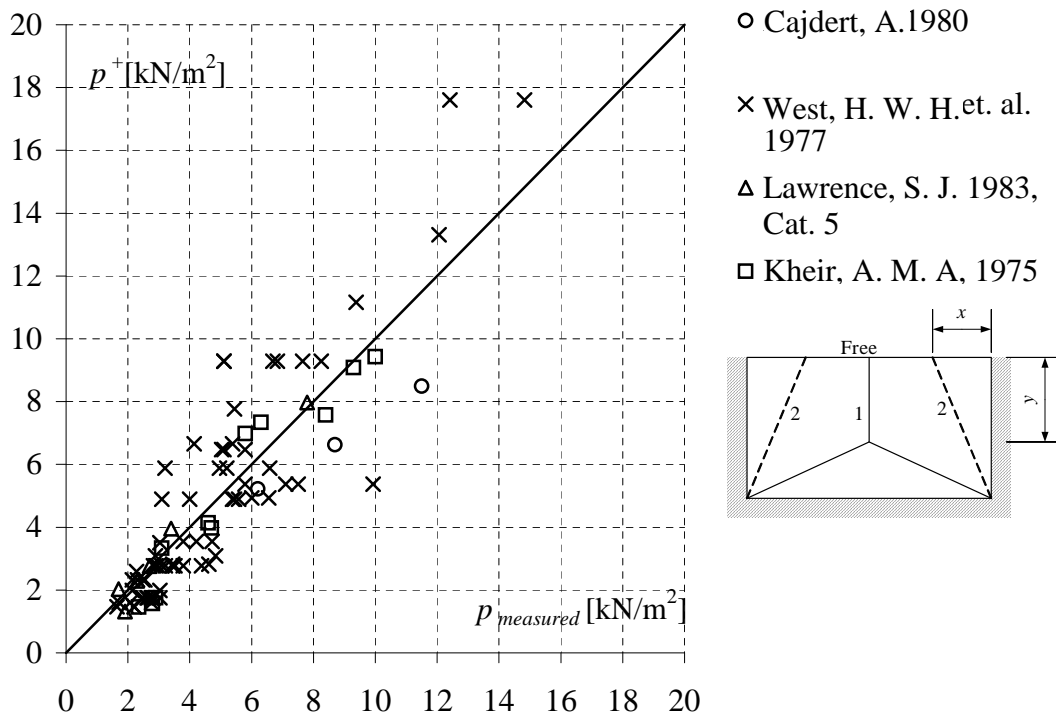
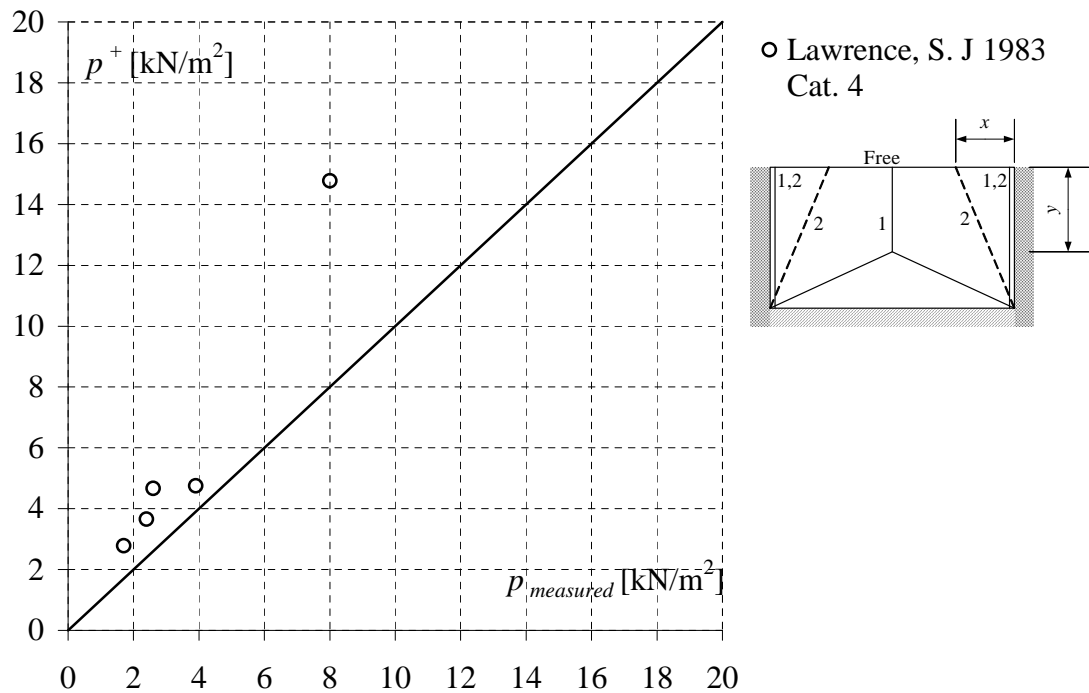


Figure 2.30 Comparison with experiments on walls simply supported on three sides

In Figure 2.30 and Figure 2.31 measured load carrying capacities of walls supported on three edges are compared with the theoretically calculated load carrying capacities. The yield line patterns used are those shown in Figure 2.30. The walls in Figure 2.31 have fixed supports along the vertical edges. Thus a vertical yield line along the support has to be taken into account.

Vertical yield lines are assumed to have the moment capacity  $m_{px}$ . In the tests failure in the bricks is often observed. However, this is taken into account by using the measured value of  $m_{px}$ .



**Figure 2.31 Comparison with experiments on walls simply supported on one side and fixed along two sides**

Figure 2.32 and Figure 2.33 show the comparison between experiments and theory for walls supported along all four edges. In general two different yield line patterns are used, as shown in Figure 2.32. In Figure 2.33 walls with fixed edges are considered. Horizontal yield lines along the supports are disregarded as are the horizontal yield lines in the middle of the walls.

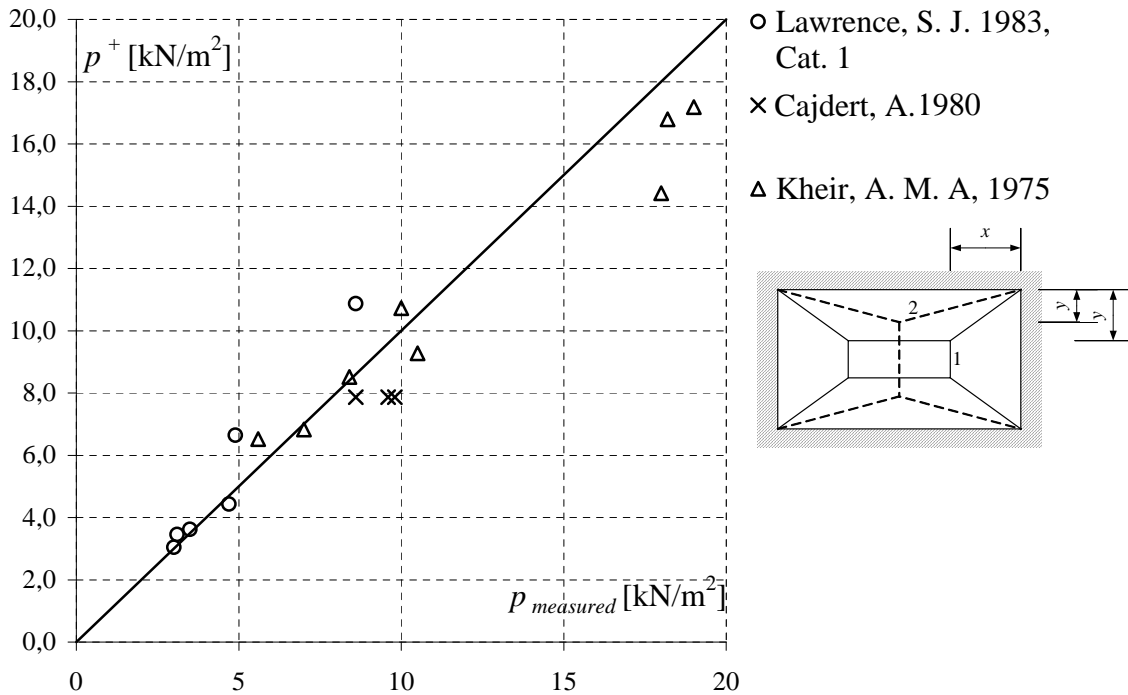


Figure 2.32 Comparison with experiments on walls simply supported on four sides

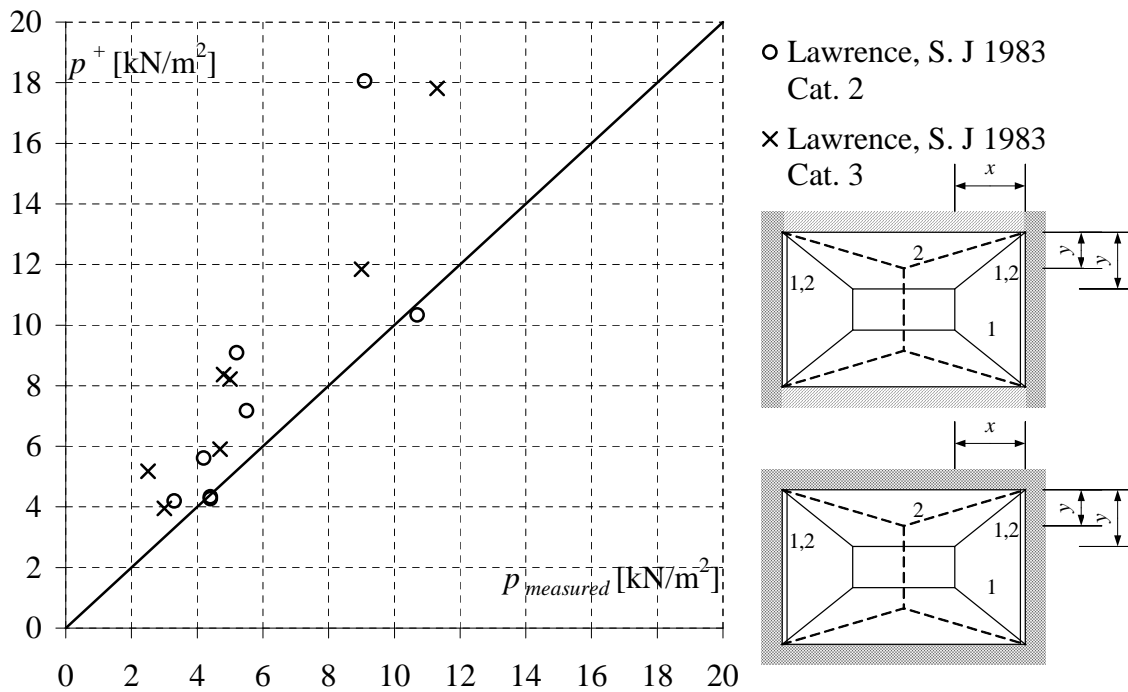


Figure 2.33 Comparison with experiments on walls fixed along four sides, or fixed along two sides and simply supported along the other two sides

From Figure 2.29 to Figure 2.33 it is seen that the agreement with experiments is good in all cases except in the case where two or four sides are fixed, where the load carrying capacity is overestimated.

The overestimation of the load carrying capacity may be explained by the action of the supports. It is very difficult to establish a fixed support; a rotation usually is present. Lawrence did not report whether yield lines along the boundaries were observed or not. If the moment at the vertical boundaries is set to zero the results become as shown in Figure 2.34. The restraints along the vertical fixed edges were also disregarded in the comparison made by Hagsten in [43].

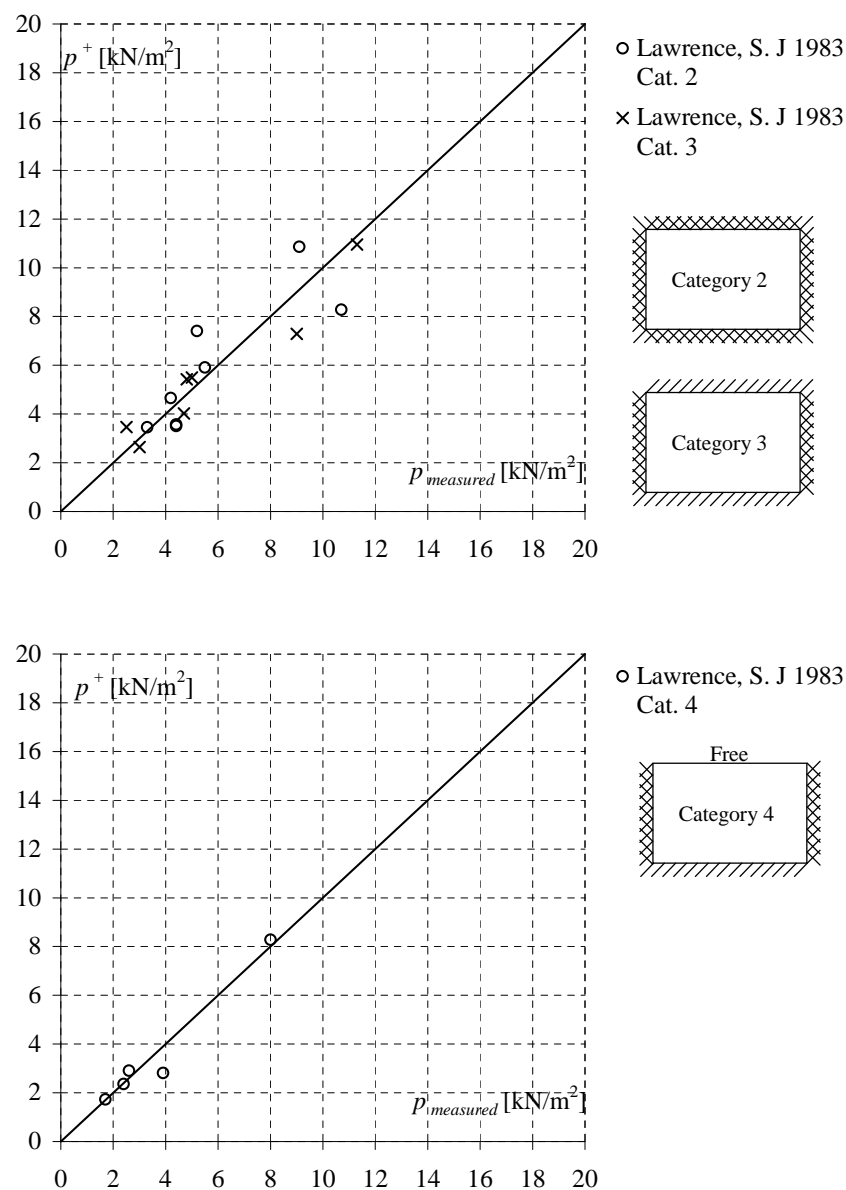


Figure 2.34 Walls with fixed edges, moment at the vertical fixed edges are set equal to zero

The above results provide the mean values and standard deviations listed in Table 2.9. The values are given for the ratio: failure load / calculated upper bound.

Yield lines along vertical edges have been disregarded.

Investigation	$\mu$	$s$
Kheir, A. M. A., 1975	1.1	0.27
West, H. M. H. et. Al., 1977	1.1	0.31
Cajdert, A. 1983	1.2	0.09
Lawrence, S. J. 1983	1.0	0.18
Buhelt, M. 1984	1.1	0.16

**Table 2.9 Mean value and standard deviation**

It is seen that the method used gives very good results.

In the comparison above, the self weight of the walls is not considered. However, since all walls are tested in a vertical position, the walls may only have been able to expand vertically in one direction because of the laboratory floor. This means that the self weight of the wall may influence the load carrying capacity, since the wall has to be lifted from the laboratory floor, when the yield line pattern is developed.

The effect of the self weight is studied by calculating a category 1 and a category 5 wall in some selected experiments. The calculations are carried out for a wall with  $h = 3000$  and  $b = 6000$  mm. These walls are similar to the ones tested by Lawrence.

It may be remembered that a category 1 wall is a rectangular wall simply supported along all four edges and a category 5 wall is a rectangular wall simply supported along three of the edges as shown in Figure 2.35.

In the case of category 5 walls two different yield line patterns have to be considered as shown in Figure 2.35.

The data used in the calculations are shown in Figure 2.35. The walls considered are loaded with a uniformly distributed transverse load.

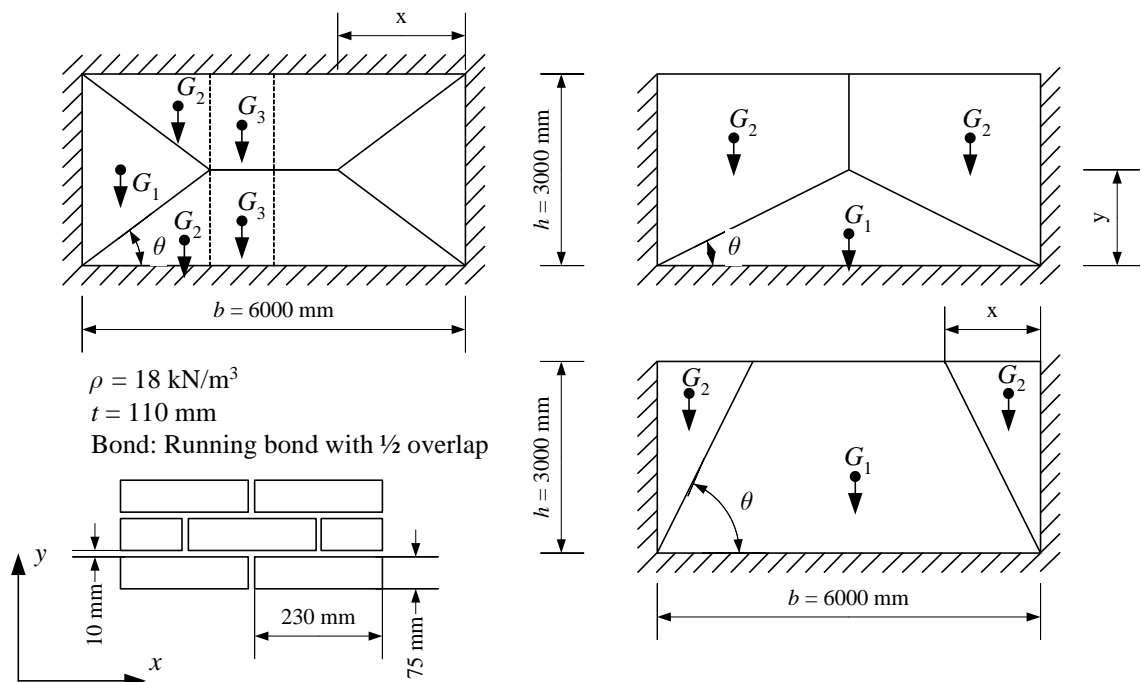


**Figure 2.35 Yield line patterns in walls with self weight**

The load carrying capacity is now considered only to be determined by the self weight of the wall. Thus the internal work in the yield lines is zero and the load carrying capacity is determined from the external work only. The in-plane deformation for a category 1 wall may be seen in Figure 2.36.

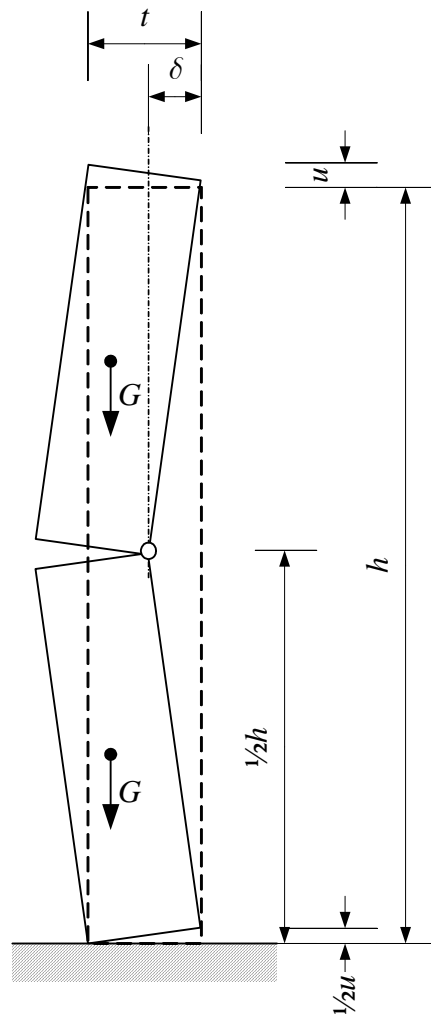


Figure 2.36 In-plane deformations

The external work in the case of a category 1 wall, see Figure 2.35, becomes:

$$W_E = p^+ \delta \left( \frac{1}{2}bh - \frac{1}{3}hx \right) - 2 \left( G_1 \frac{1}{2}u + G_2 u \left( \frac{1}{4} + \frac{3}{4} \right) + G_3 u \left( \frac{1}{4} + \frac{3}{4} \right) \right) \quad (2.37)$$

where  $u$  is the vertical displacement. The displacement  $u$  becomes:

$$u = 4 \frac{t}{h} \delta \quad (2.38)$$

It is assumed that the vertical displacement may take place without any resistance from the supports. The supports are assumed frictionless for vertical displacements.

The weights of the wall parts are,  $\rho$  being the specific weight ( $\text{kN/m}^3$ ),

$$\begin{aligned}
 G_1 &= \frac{1}{2}hx\rho t \\
 G_2 &= \frac{1}{4}hx\rho t \\
 G_3 &= \frac{1}{4}(b-2x)h\rho t
 \end{aligned}
 \tag{2.39}$$

The load carrying capacity of the wall will be:

$$p^+ = \frac{2bh\rho \frac{t^2}{h}}{\frac{1}{2}bh - \frac{1}{3}hx}
 \tag{2.40}$$

In a similar way the load carrying capacity for category 5 walls is obtained. The load carrying capacity, in case of a yield line pattern shown right next to the category 1 wall in Figure 2.35, becomes:

$$p^+ = \frac{\left(bh - \frac{1}{4}by\right)\rho \frac{t^2}{y}}{\frac{1}{2}bh - \frac{1}{6}by}
 \tag{2.41}$$

In the case of the yield line pattern shown below in Figure 2.35, the load carrying capacity becomes:

$$p^+ = \frac{\frac{1}{2}(bh + hx)\rho \frac{t^2}{h}}{\frac{1}{2}bh - \frac{1}{3}hx}
 \tag{2.42}$$

In Figure 2.37 the results of the calculation are plotted together with the experimental results obtained by Lawrence ( $\rho$  is assumed equal to 18 kN/m<sup>3</sup>).

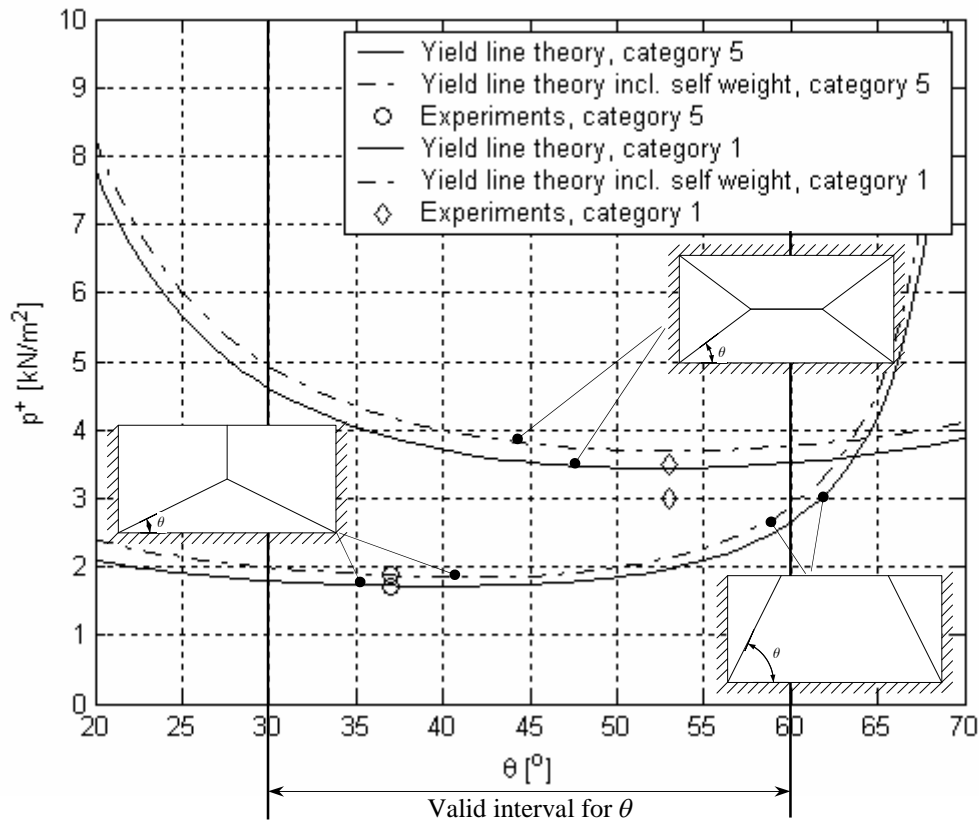


Figure 2.37 Results of calculations for walls with self weight

In the case of category 1 walls the minimum solution becomes the solution for a one way wall, see [46], when only the self weight is considered.

Figure 2.37 shows that the influence of the self weight is small and therefore it is reasonable to disregard it in the comparison with experiments.

### 2.3.3 Biaxial bending tests

In [36], biaxial bending of masonry is investigated. The aim of the investigation was to establish a yield condition for masonry in biaxial bending. The results of the investigation will be shown here because they may indicate whether a yield condition as the one developed for reinforced concrete slabs may be adopted for unreinforced masonry walls as well.

A number of 36 wallettes were tested. 18 in bending about the bed joint and 18 about the head joint. From these tests the bending yield moments  $m_{py}$  and  $m_{px}$  are obtained, see Table 2.10.

Bending about the head joint	Bending about the bed joint
$m_{px}$	$m_{py}$
[Nmm/mm]	[Nmm/mm]
9.74	2.82

Table 2.10 Bending yield moment

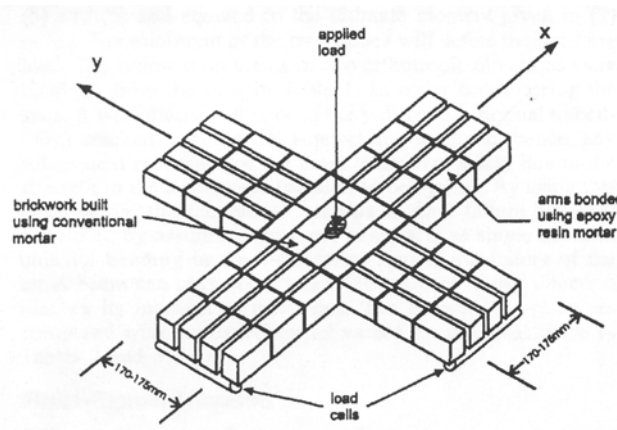


Figure 2.38 Layout of a crossbeam

Furthermore 33 crossbeams were tested. The test set-up used is shown in Figure 2.38. One type of bricks was used together with one mortar. The mortar was a 1:3 cement:sand mortar, the amounts measured by volume. Since masonry is orthotropic, the weak direction will fail before the strong direction. In [36] the load at cracking and the load at failure is reported. The results are listed in Table 2.11.

		Cracking		Failure	
$L_x$	$L_y$	$P_x$	$P_y$	$P_x$	$P_y$
[mm]	[mm]	[N]	[N]	[N]	[N]
300	585	3124	260	4805	169
445	585	1811	473	2792	304
585	585	936	754	2022	129
690	585	613	671	1684	241
860	585	318	669	1379	156
1140	585	165	676	1109	184
585	300	489	1327	1839	280
585	445	392	999	1818	220
585	690	1467	557	1814	236
585	860	1595	471	2058	25
585	1140	1812	328	1968	298

**Table 2.11 Results from tests,  $P_x$  and  $P_y$  denote the load at the supports**

If the moment in each direction is calculated as for a beam, the plot shown in Figure 2.39 is obtained.

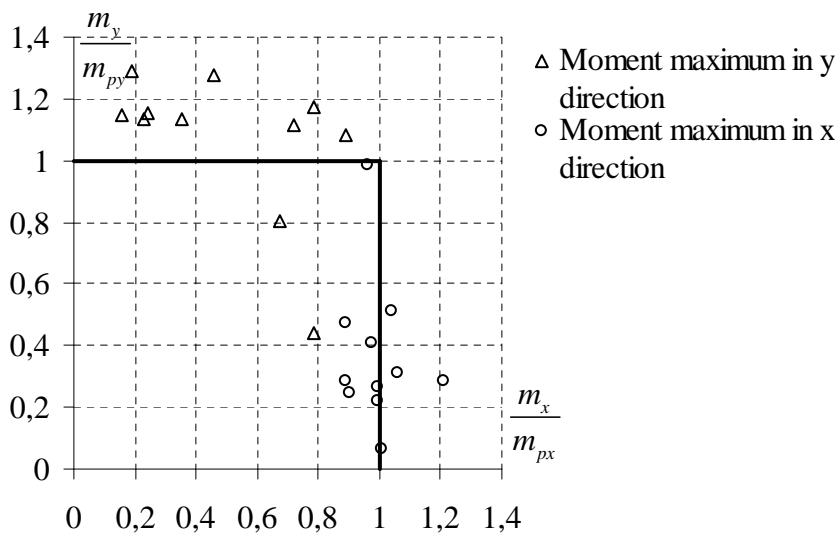


**Figure 2.39 Failure condition for masonry in biaxial bending**

The tests agree reasonably with a simple square yield condition as that used for reinforced concrete. Although the scatter is considerable, generally the square yield condition is conservative.

### 2.3.4 Comparisons regarding pure bending

In this section the calculation procedure outlined in section 2.1.2.1 will be compared with experiments. The reason for making this comparison is that a wallette test, as shown in Figure 2.40, is the standard test for obtaining the bending yield moment,  $m_{px}$ . Section 2.3.2 showed that using the value of the bending yield moment obtained from the wallette test in the yield line theory gave good results compared with actual wall tests.

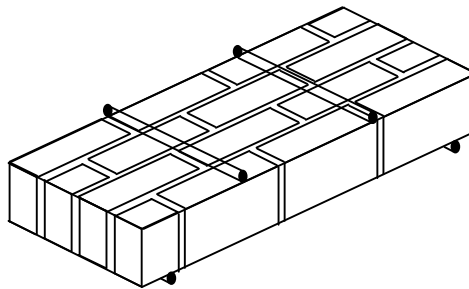


Figure 2.40 Principal sketch of the wallette test

The calculation of the bending yield moment  $m_{px}$  is carried out using the model described in section 2.1.2. The formal compressive strength of the interface is calculated using the cohesion, which is obtained according to the following empirical equation taken from [45].

$$c = \left( -0.11 \frac{w}{l} + 0.03 \right) IRA - 0.5 \frac{w}{c} + 3.6 \text{ [MPa]} \quad (2.43)$$

Here  $w/l$  is the water/lime ratio and  $w/c$  is the water/cement ratio and  $IRA$  is the initial rate of absorption. Based on these assumptions, the moment capacity in the head joint may be calculated. Since masonry is not a rigid plastic material as assumed when using the formulas for the dissipation, see (1.1) an effectiveness factor has to be introduced, see Figure 2.41.

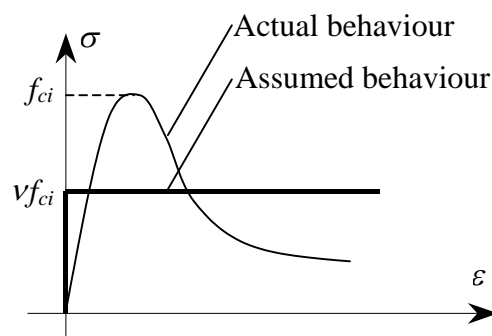


Figure 2.41 Definition of  $v$

In Figure 2.42 the effectiveness factor for the tensile strength is determined for solid and perforated bricks in running bond with half a brick overlap. The solid bricks are used with three different types of mortars (KC50/50/700, KC60/40/850 and KC35/65/650) and the perforated bricks with one mortar (KC60/40/850).

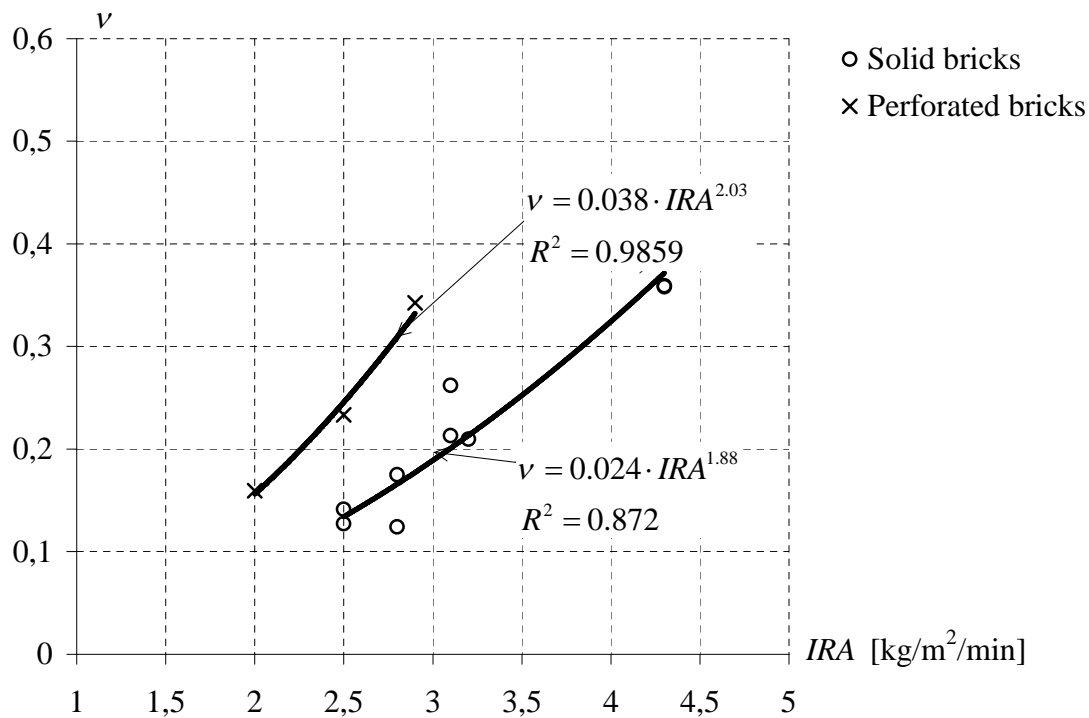


Figure 2.42 The effectiveness factor as a function of IRA

The effectiveness factors are found as:

$$\begin{aligned} v_t &= 0.038IRA^{2.03} \quad (\text{solid bricks}) \\ v_t &= 0.024IRA^{1.88} \quad (\text{perforated bricks}) \end{aligned} \quad (2.44)$$

The effectiveness factor is bound to vary with *IRA* since a stronger interface provides a more brittle failure because of the possibility of brick failure.

Using the effectiveness factors from equation (2.44), the bending yield moment in the head joint may be calculated and compared with experiments. The results are shown in Figure 2.43.

Figure 2.43 shows that the effectiveness factors obtained from (2.44) provide good results when the calculation procedure from section 2.1.2.1 is compared with experiments.

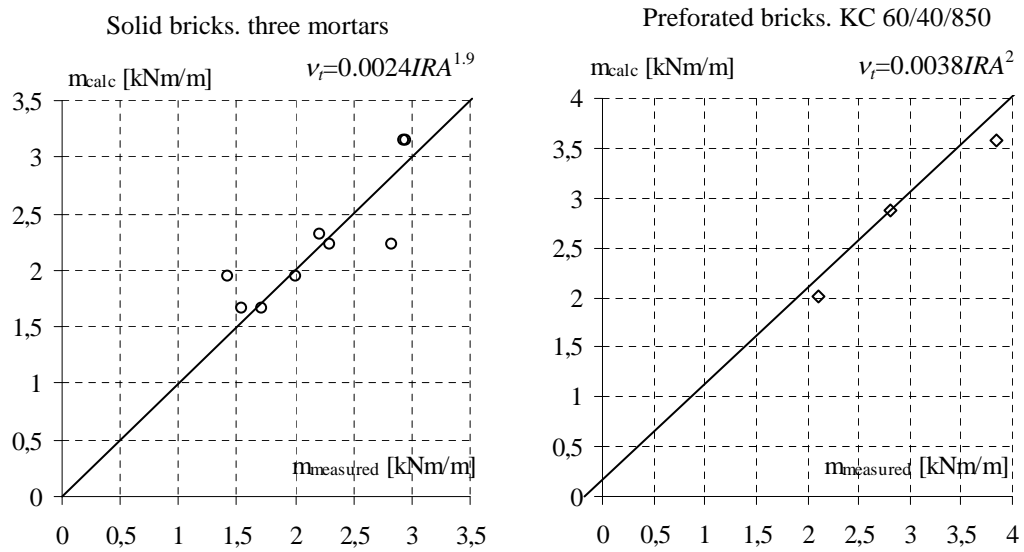


**Figure 2.43** The bending yield moment  $m_{px}$  compared with experiments taken from [31] and [37]

In the investigation made by Cajdert, [27], the moment capacity at an angle to the bed joint is examined. In Figure 2.44 the results from [27] are plotted together with results taken from [44] (referred to as LGH, but they were originally taken from [14]). The results indicate that the moment capacity in the bed joint ( $m_{py}$ ) has to be set to zero if a relation (2.45) is adopted, cf. formula (2.22).

$$m_{\theta} = m_{px} \sin^2 \theta + m_{py} \cos^2 \theta \quad (2.45)$$

However this conclusion should not be taken too seriously, because a test of the type used by Cajdert can not properly reproduce the contribution from the bed joint in a diagonal yield line, cf. section 2.1.2.

The results in Figure 2.44 also confirms that a yield condition as the one used for reinforced concrete slabs may be adopted.

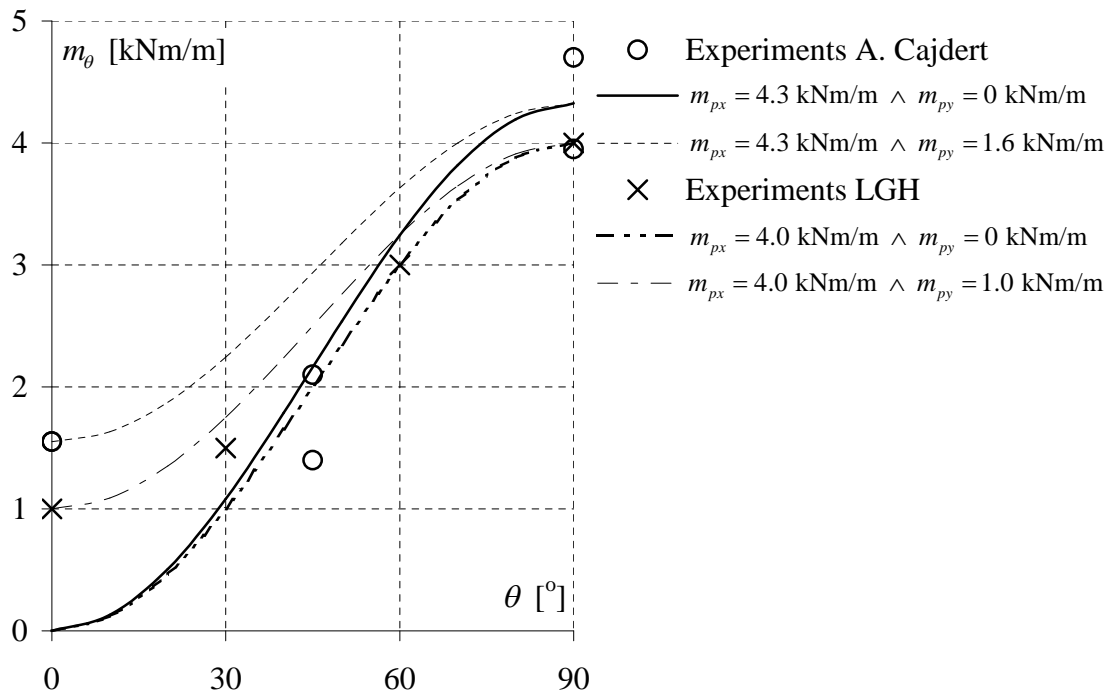


Figure 2.44 Justification of equation (2.45),  $\phi = 30^\circ$

## **3 Laterally loaded walls with small in plane (axial) loads**

### **3.1 Moment capacities for walls with small axial loads**

In this chapter the load carrying capacity of transversely loaded masonry walls with small axial loads parallel and/or perpendicular to the bed joint will be analysed. As in the former chapter dealing with the load carrying capacity of transversely loaded masonry walls, the yield line theory for orthotropic concrete slabs will be used to develop a yield line theory including axial loads.

As in the case of transversely loaded masonry walls the internal work is determined on the basis of a sliding failure in the interface (unless of course if the bricks fail).

It is assumed that the displacement  $u$  is perpendicular to the average yield line as in Chapter 2. This assumption is not quite correct because the axial load will influence the orientation of the displacement. However for small axial loads it may be justified.

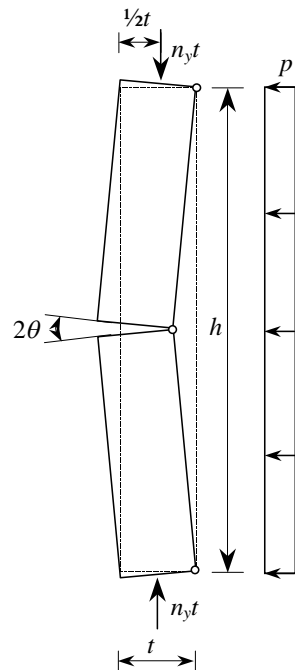


**Figure 3.1 Strip parallel to the bed joint**

The internal work in the diagonal yield lines is, as in Chapter 2, calculated considering an equivalent tensile strength parallel to the bed joint and an equivalent tensile strength perpendicular to the bed joint. This means that the internal work may be calculated considering a strip parallel and perpendicular to the bed joint, respectively. The moment capacities of each strip may be determined from a cross-section analysis. A strip parallel to the bed joint determines the bending yield moment  $m_{py}$  and a strip perpendicular to the bed joint determines the bending yield moment  $m_{px}$ .

A strip perpendicular to the bed joint is shown in Figure 3.1. The rotation axis is placed at the face of the wall where the transverse load,  $p$ , is applied as pressure. The axial load is assumed to be acting in the middle-plane of the wall.

If the relative rotation in the hinge is placed at the edge of the section (infinite compressive strength) it is seen that the dissipation in the hinge may be calculated as before. This further means that the normal force only has to be taken into account in the external work.

Thus, in the following the internal work is calculated considering only the tensile strength from sliding in the interface (unless the bricks fail). The external work is calculated considering the transverse load and the axial load.

### 3.2 Upper bound solutions

Since masonry expands when the yield line pattern is developed the axial load enters the external work. In this section, the work of the axial load is examined and thereby the use of the yield line theory.

#### 3.2.1 Orthotropic walls

The displacements of the boundaries of the wall may be calculated from the rotation of the boundary in question, see Figure 3.2, where the axes of rotation are placed at a face where the transverse load is applied as pressure.

In the case of a uniformly distributed normal stress along a boundary we have a situation as shown in Figure 3.2. Notice that in what follows  $n_x$  and  $n_y$  are stresses, not forces per unit length. They are positive as compression.

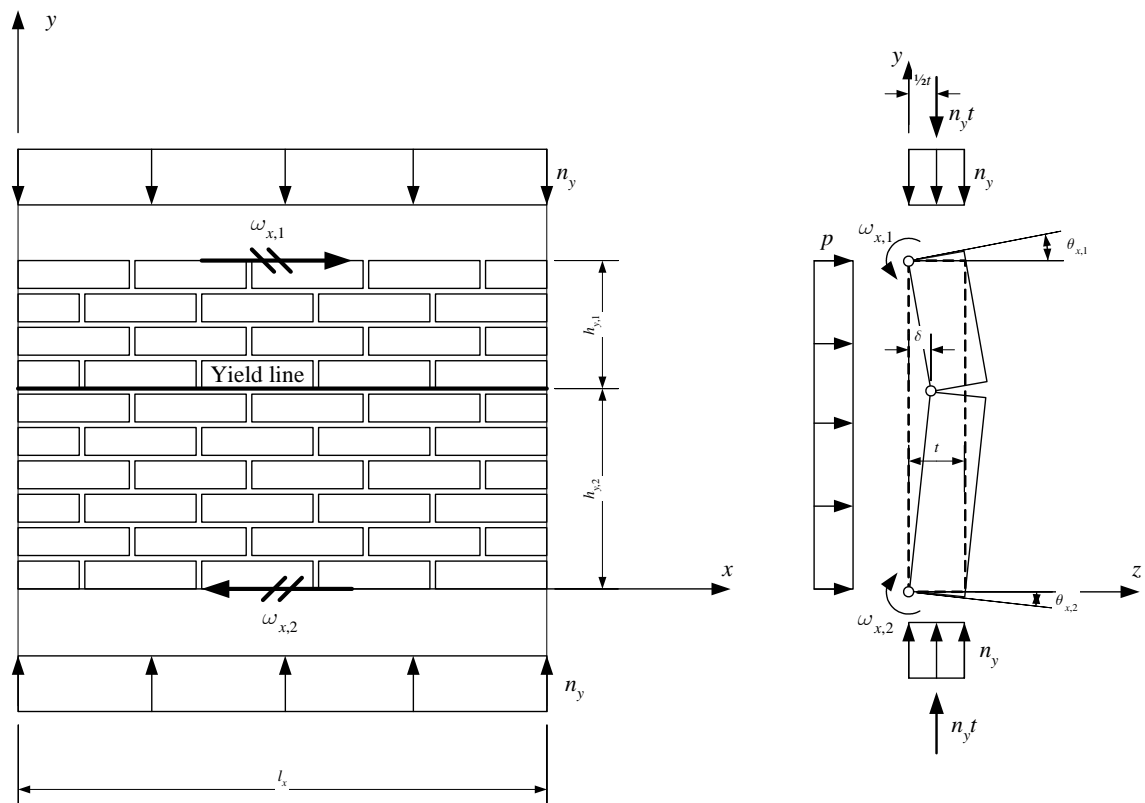


Figure 3.2 Displacements at the boundary

The contribution to the external work from the axial load is then easily calculated as:

$$\Delta W_{E,n_y} = -\frac{1}{2} n_y t^2 l_x (\theta_{x,1} + \theta_{x,2}) = -\frac{1}{2} n_y t^2 l_x \left( \frac{\delta}{h_{y,1}} + \frac{\delta}{h_{y,2}} \right) \quad (3.1)$$

Thus when  $n_y$  is a compressive normal stress  $\Delta W_{E,n_y}$  is negative.

Other distributions of the axial load than the one in Figure 3.2 may be treated in the same way.

Two different cases are shown in Figure 3.3, where only the contribution for one edge is given.

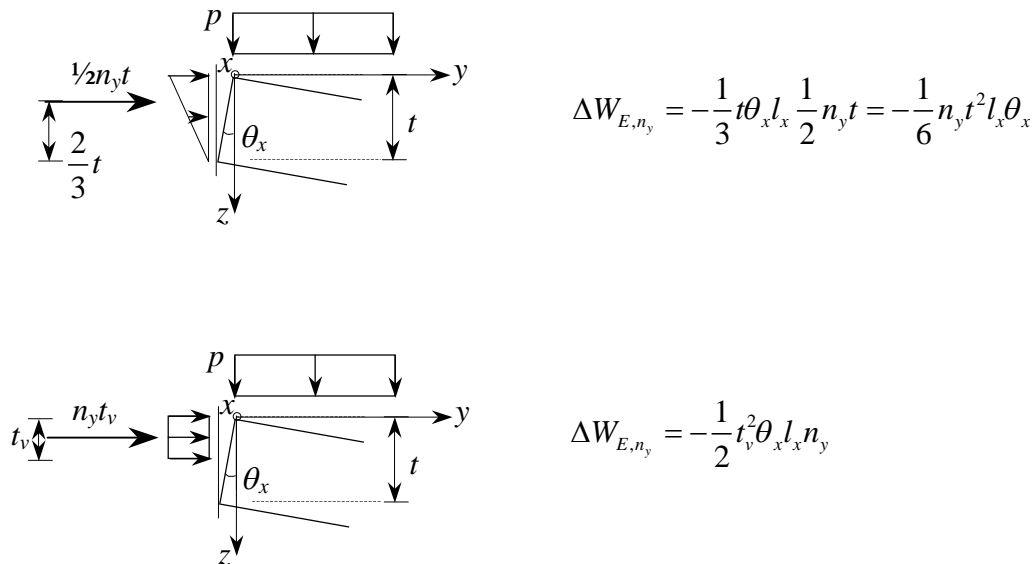


**Figure 3.3**

Similar formulas are valid for axial loads in the  $x$ -direction.

Including the normal force in the external work makes it possible to calculate the load carrying capacity of a masonry wall by the work equation.

A rectangular wall simply supported on all four edges is considered. The axial load is in the  $y$ -direction. Three different load positions of the axial load are treated. From Figure 3.4, it is seen that the load carrying capacity of the lateral load is increased as the axial load is applied further away from the surface where the lateral load is applied as pressure. In the calculations the parameter  $\mu$  has been calculated using formula (2.12) with the data listed in Table 2.1.

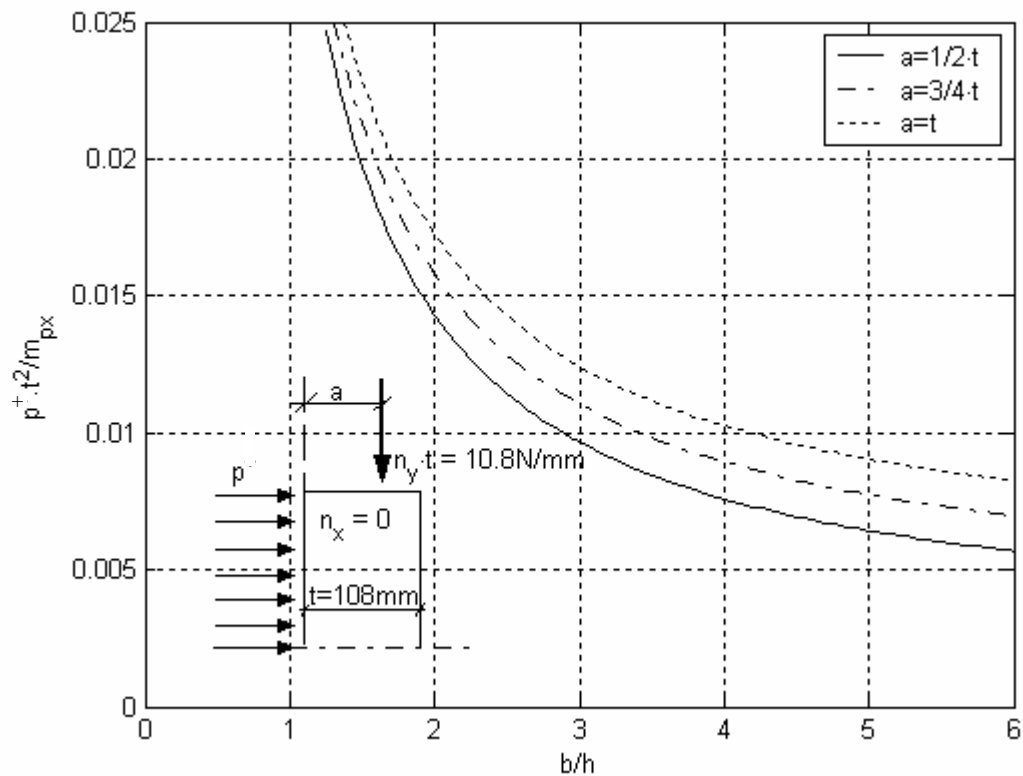


Figure 3.4 Effect of the position of the axial load

## 3.2.2 Illustrative examples

In this section the method described will be illustrated through a couple of examples.

### 3.2.2.1 Example 1. Calculation of a wall

In this example the masonry wall considered in section 2.2.4.1 will be considered once again. This time the wall is loaded with axial loads in two perpendicular directions as well as a transverse pressure,  $p$ , as shown in Figure 3.5. The axial loads are uniform pressures. The general method described in section 2.1.2 is used, i.e. the angle  $\beta$  is related to  $\theta$  according to Figure 2.2.

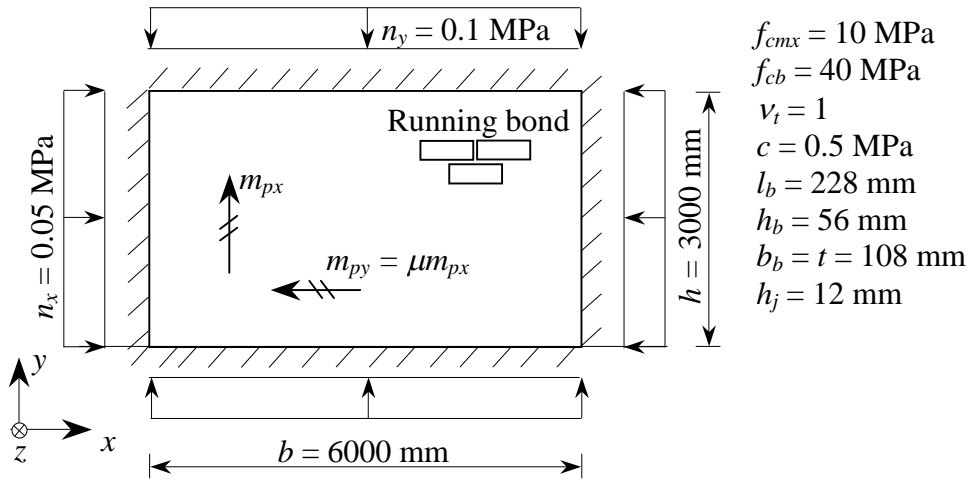


Figure 3.5 Data for wall

The yield line pattern is shown in Figure 3.6. The angle  $\theta$  is chosen as the free parameter.

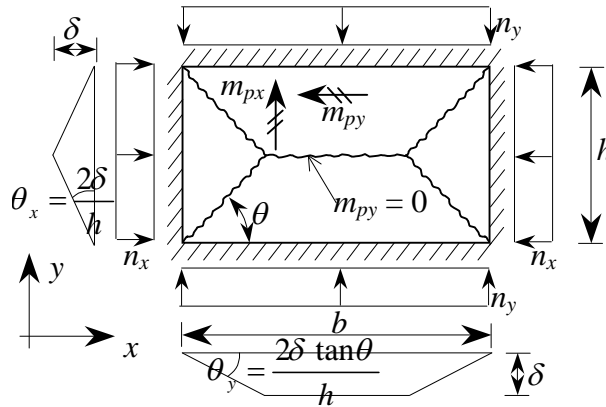


Figure 3.6 Yield line pattern

The internal work becomes

$$W_I = 2m_{px}\theta_y h + 4m_{py}\theta_x \frac{h}{2 \tan \theta} \quad (3.2)$$

The rotations  $\theta_x$  and  $\theta_y$  are given in Figure 3.6. The bending yield moments becomes, formula (2.4),

$$m_{px} = \frac{1}{8} t^2 f_{ci} \frac{1 - \sin(90^\circ - \theta)}{\cos(90^\circ - \theta)} \frac{(l_b + h_j)}{h_b + h_j} \quad (3.3)$$

$$m_{py} = \frac{1}{2} t^2 f_{ci} \frac{1 - \sin(\theta)}{\cos(\theta)} \frac{h_b + h_j}{(l_b + h_j)}$$

The external work becomes

$$W_E = p^+ \delta \left( \frac{1}{2} bh - \frac{1}{6} \frac{h^2}{\tan \theta} \right) - t^2 (n_y b \theta_x + n_x h \theta_y) \quad (3.4)$$

From the work equation the minimum value of  $p^+$  may be calculated. In Figure 3.7  $p^+$  as a function of  $\theta$  may be seen.

It appears that the minimum solution for  $p$  is obtained for  $\theta = 40.5^\circ$ , which is in the interval of angles giving valid solutions ( $\varphi \leq \theta \leq 90^\circ - \varphi$ , where  $\varphi = 30^\circ$ ).

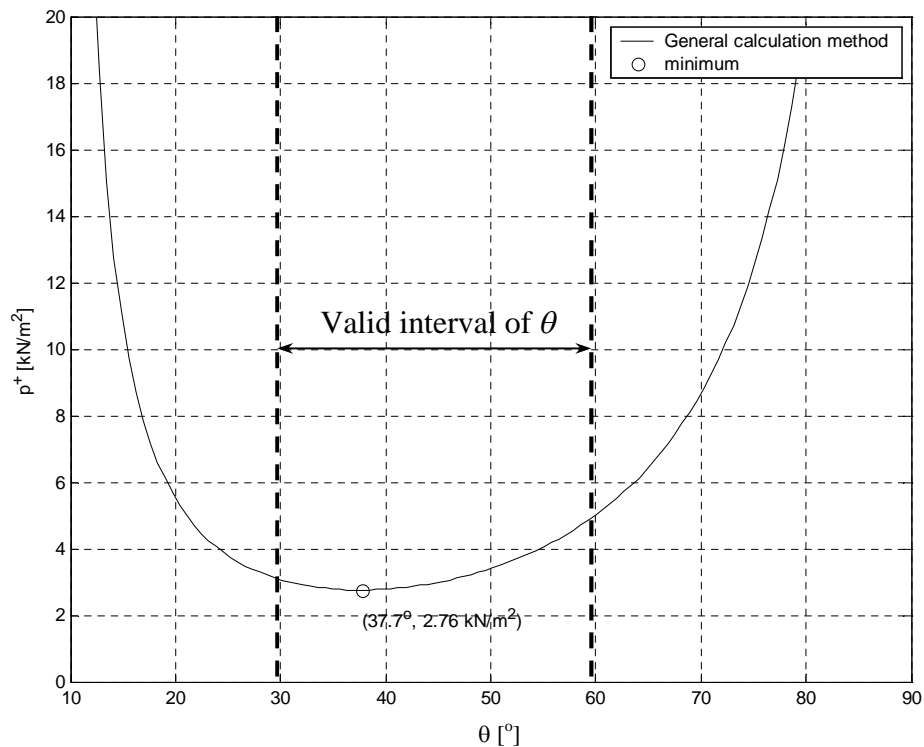


**Figure 3.7 Load carrying capacity as a function of  $\theta$**

The ratio between the bending yield moments,  $\mu$ , changes with  $\theta$  as shown in Figure 3.8. It is seen that for  $\theta = 37.7^\circ$   $\mu = 0.41$ .

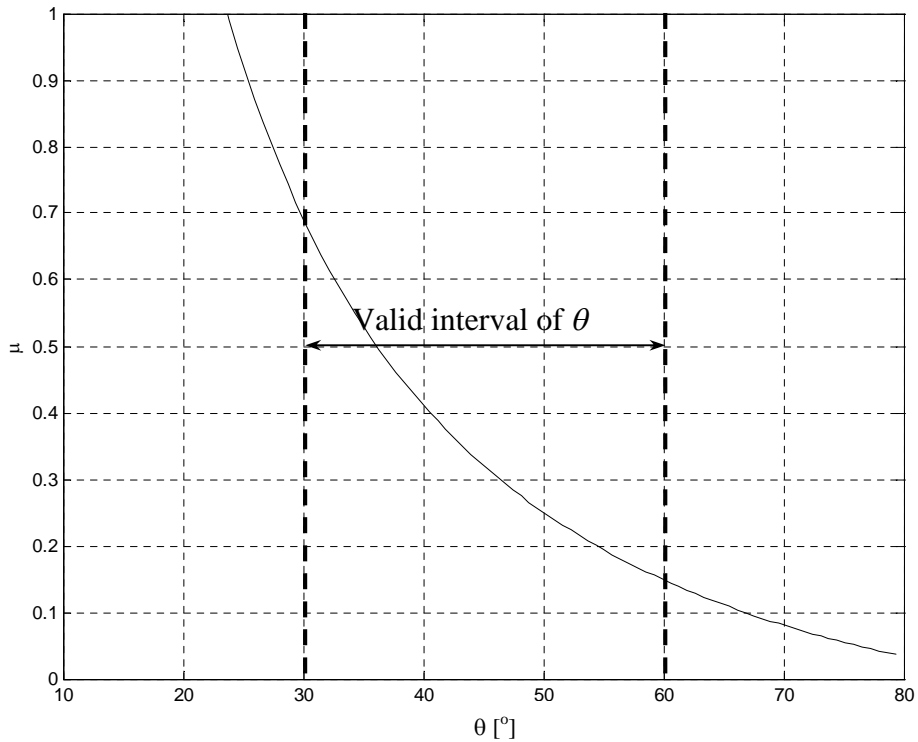


Figure 3.8  $\mu$  as a function of  $\theta$

### 3.2.2.2 Example 2. Simplified calculation of a masonry wall

In this example a masonry wall simply supported on four edges and loaded with a transverse pressure  $p$  (kN/m<sup>2</sup>) and axial loads in two perpendicular directions will be considered. The axial loads are uniform pressures. The properties of the wall are listed in Figure 3.9. They are identical to the data of Example 1. The purpose of this example is to evaluate the simplified calculation procedure proposed in the case of transversely loaded walls and to illustrate the influence of the axial load. It is remembered that in this case the calculation of the bending yield moments is based on  $\beta = 45^\circ$ .

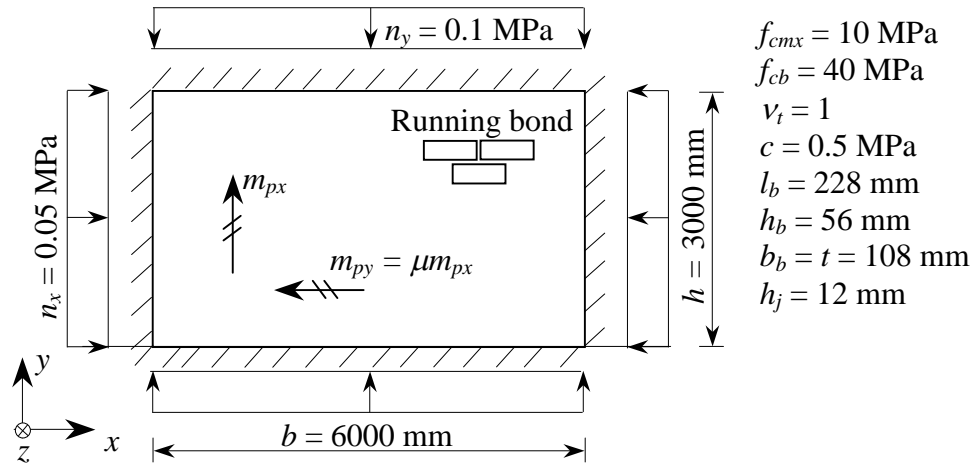


Figure 3.9 Data for wall

The moment capacity in the head joint is determined as in Example 1, section 2.2.4.1 for  $\beta = 45^\circ$ . The tensile strength  $p_x^+$  becomes

$$p_x^+ = \frac{\frac{1}{2}(l_b + h_j)}{h_b + h_j} \left( c \frac{\cos \varphi}{\cos 45^\circ} \frac{1 - \sin 45^\circ}{1 - \sin \varphi} \right) = 0.63 \text{ MPa}$$

The tensile strength is calculated by equation (2.10), when  $f_{ci} = 2c \cdot \cos \varphi / (1 - \sin \varphi)$ . The maximum tensile strength is calculated by (2.20), with  $f_{tb} = 1/20 f_{cb}$ , see Appendix 1.

$$p_{x,\max}^+ = \frac{h_b}{2(h_b + h_j)} f_{tb} \Rightarrow$$

$$p_{x,\max}^+ = \frac{56}{2(56 + 12)} \frac{1}{20} 40 = 0.82 \text{ MPa}$$

The yield moment  $m_{px}$  is determined from equation (2.13).

$$m_{px} = \frac{1}{2} t^2 p_x^+ \Rightarrow$$

$$m_{px} = \frac{1}{2} 108^2 \cdot 0.63 = 3.69 \frac{\text{kNm}}{\text{m}}$$

The yield moment in the bed joint is determined in the same way.

$$p_y^+ = \frac{h_b + h_j}{\frac{1}{2}(l_b + h_j)} \left( c \frac{\cos \varphi}{\cos 45^\circ} \frac{1 - \sin 45^\circ}{1 - \sin \varphi} \right) \Rightarrow p_y^+ = 0.2 \text{ MPa}$$

$$m_{py} = \frac{1}{2} t^2 p_y^+ \Rightarrow m_{py} = 1.19 \frac{\text{kNm}}{\text{m}}$$

Using the simplified method, the bending yield moments become independent of the yield line pattern and optimization may be carried out more easily.

The load carrying capacity is calculated from the yield line pattern shown in Figure 3.10.

The moment capacity in the horizontal yield line is zero because of the rotation axis being at the top face of the wall and because the tensile strength of the bed joint is assumed equal to zero.

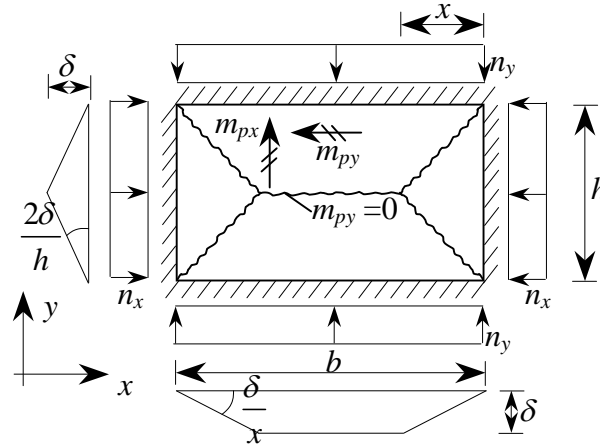


Figure 3.10 Yield line pattern

The internal work becomes:

$$W_I = 2m_{px} \left( 4 \frac{m_{py}}{m_{px}} \frac{x}{h} + \frac{h}{x} \right) \delta$$

The external work becomes, when  $n_x$  and  $n_y$  are uniform pressures.

$$W_E = p^+ \delta \left( \frac{1}{2}bh - \frac{1}{3}hx \right) - 2 \frac{1}{2}n_y t^2 b \frac{2\delta}{h} - 2 \frac{1}{2}n_x t^2 h \frac{\delta}{x}$$

The work equation provides the load carrying capacity

$$p^+ = \frac{2m_{px} \left( 4 \frac{m_{py}}{m_{px}} \frac{x}{h} + \frac{h}{x} \right) + 2t^2 \left( n_y \frac{b}{h} + \frac{1}{2}n_x \frac{h}{x} \right)}{\frac{1}{2}bh - \frac{1}{3}hx}$$

The optimal solution of  $x$  is found from  $dp^+/dx = 0$ :

$$\frac{x}{h} = \frac{-2m_{px}h - t^2n_xh \pm \sqrt{h^2(m_{px} + t^2n_x)(t^2n_xh^2 + 3t^2n_yb^2 + 2h^2m_{px} + 18m_{py}b^2)}}{2b(6m_{py} + t^2n_y)}$$

The load carrying capacity of the wall becomes:

$$p^+ = 2.80 \frac{\text{kN}}{\text{m}^2}$$

The solution is illustrated in Figure 3.11.

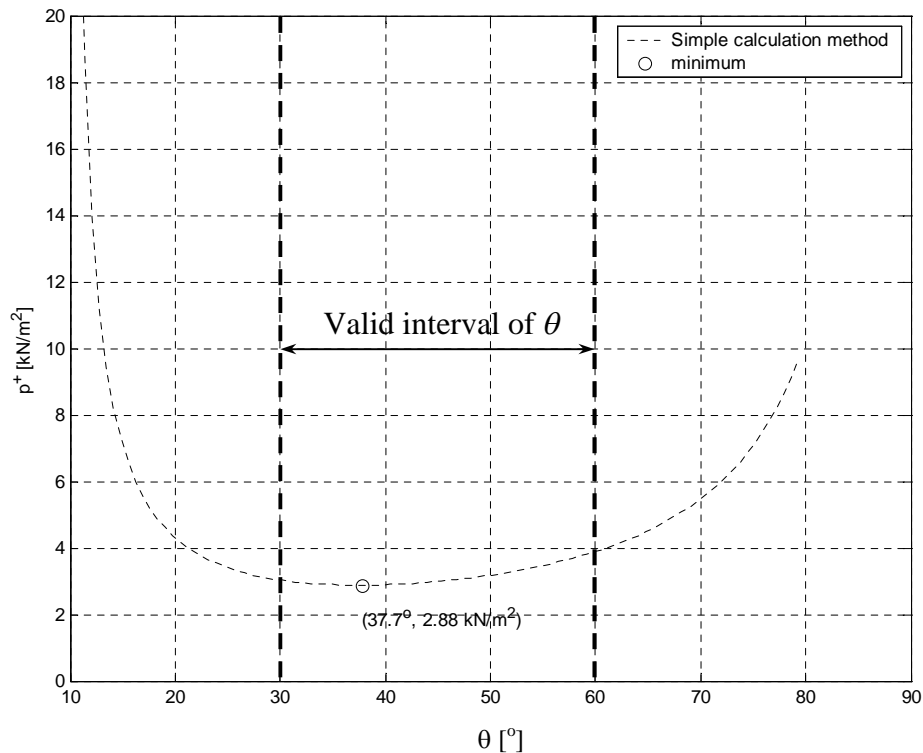


**Figure 3.11 Result of calculations**

It is seen that the yield line pattern is geometrically possible since  $\varphi \leq \theta \leq 90^\circ - \varphi$  ( $\varphi = 30^\circ$ ).

The simplified calculation method is compared with the method used in section 3.2.2.1 in Figure 3.12. The calculations show that the two methods provide almost identical results around the optimised solution. However, the general approach provides a slightly smaller load carrying capacity.

The results also show that the load carrying capacity is increased by the in-plane loads from  $2.36 \text{ kN/m}^2$  to  $2.88 \text{ kN/m}^2$  when comparing with the result obtained in section 2.2.4.1. This is an increase in load carrying capacity of almost 22%. Considering the small axial loads this is a considerable increase.

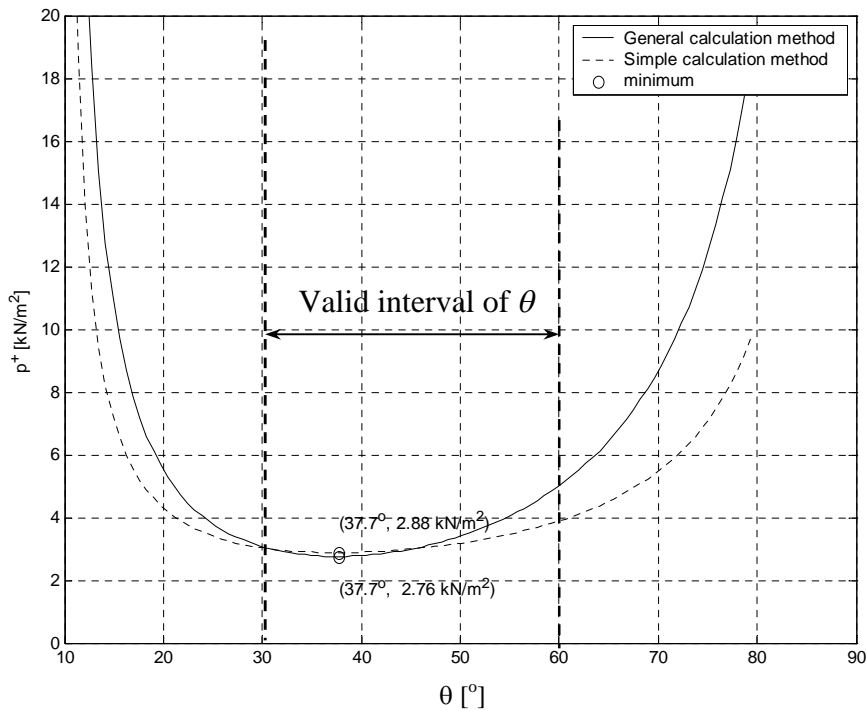


Figure 3.12 Comparison with the method of section 3.2.2.1

### 3.2.2.3 Example 3. The influence of axial load

This example illustrates further the influence of the axial load, see Figure 3.13. In the calculations  $c = 0.5$  MPa is assumed.

The axial load is a compressive stress 0.05 MPa, which is equivalent to the weight of a wall with height  $h = 2500$  mm, thickness  $t = 108$  mm and a density of  $2000 \text{ kg/m}^3$  applied to the top of the wall in the  $y$  direction. In the  $x$  direction the load is equivalent to a uniform load causing yielding at the support of a steel beam rigidly supported at one end and free in the other one and having a cross section of a HEB140-profile. The yield stress is assumed to be 235 MPa.

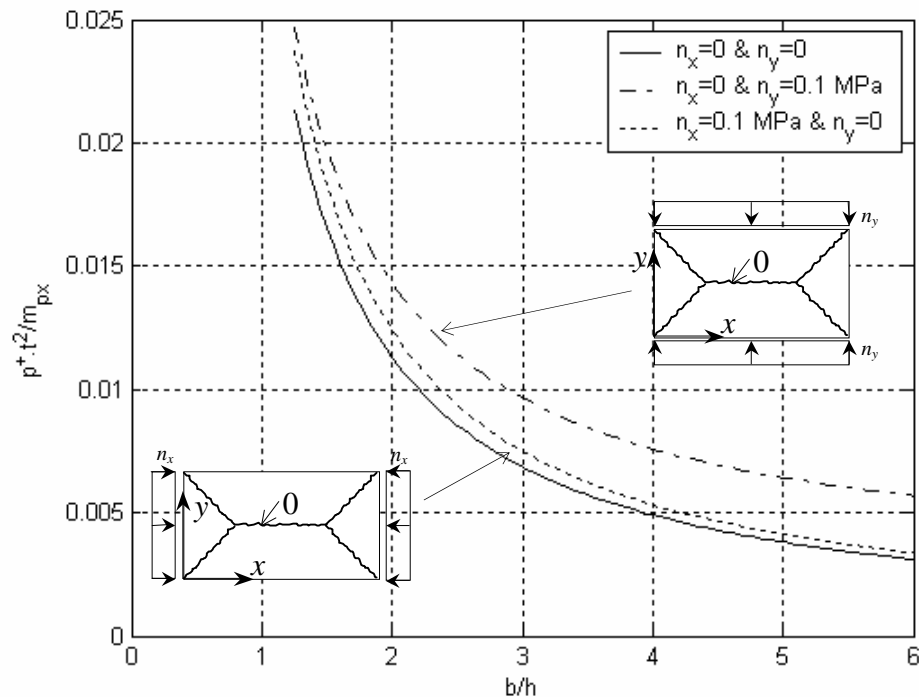


Figure 3.13 Influence of axial loads

It is seen that the load carrying capacity is increased a great deal for only a small axial loads.

### 3.3 Comparison with experiments

In this section, the experimental investigations made on masonry walls with small axial loads will be presented. Only a few experiments cover the problem. The only full scale walls were tested by Hendry, A. W. et. al.

#### 3.3.1 Investigations

*Hendry, A. W., Sinha, B. P. and Maurenbrecher, A. H. P. 1973 [17]*

The experimental investigation made by Hendry, A. W. et. al. consisted of tests on 18 walls. Six walls were without returns (returns are explained in Figure 3.14), eight walls had one return and four walls were built with two returns.

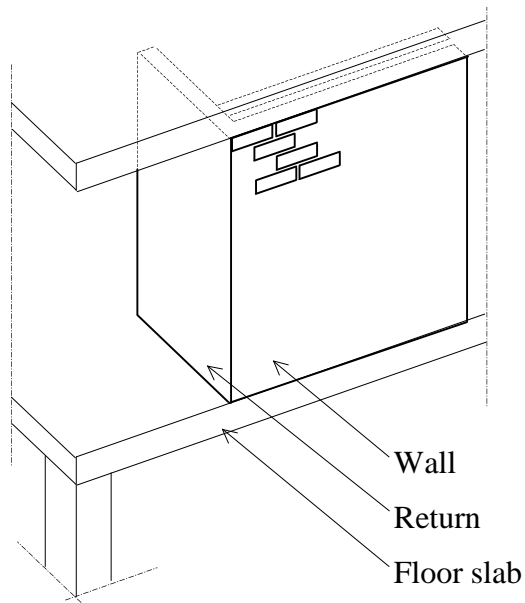


**Figure 3.14 Returns**

So-called Deep Frog Fletton bricks were used in all walls with returns. The average compressive strength of the bricks was 26.13 MPa. A 1:¼:3 rapid hardening Portland cement: lime: sand mix was used (amounts measured by volume). In all cavity walls the halves were held together by metal ties.

The rig used to test the walls was made in an existing structure rendering boundary conditions closely related to practice. The test set-up is explained in [17], see also Figure 3.15.

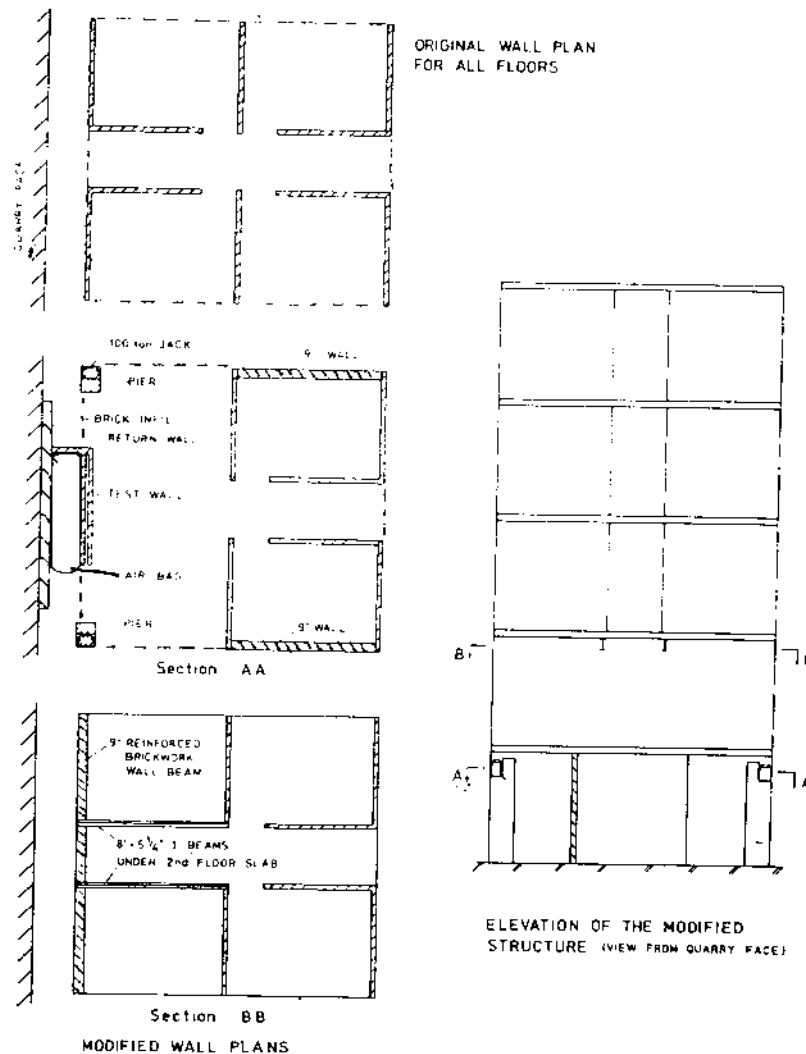


Figure 3.15 Building where the tests were carried out

The transverse load was applied by an air bag. The precompression was applied by jacks and the load was measured by load cells on the top of the wall. In the paper the moment capacity in the head joint is not reported. The bending yield moment is calculated using the theory in section 2.1.2.1. The relevant data are listed in section 7.2.1

### 3.3.2 Comparison with experiments

The method used to calculate the walls is the one explained in section 3.2.1 where  $\beta = 45^\circ$ . The yield line pattern used to calculate the load carrying capacity is in the case of one return given in Figure 3.16a and in the case of two returns in Figure 3.16b.

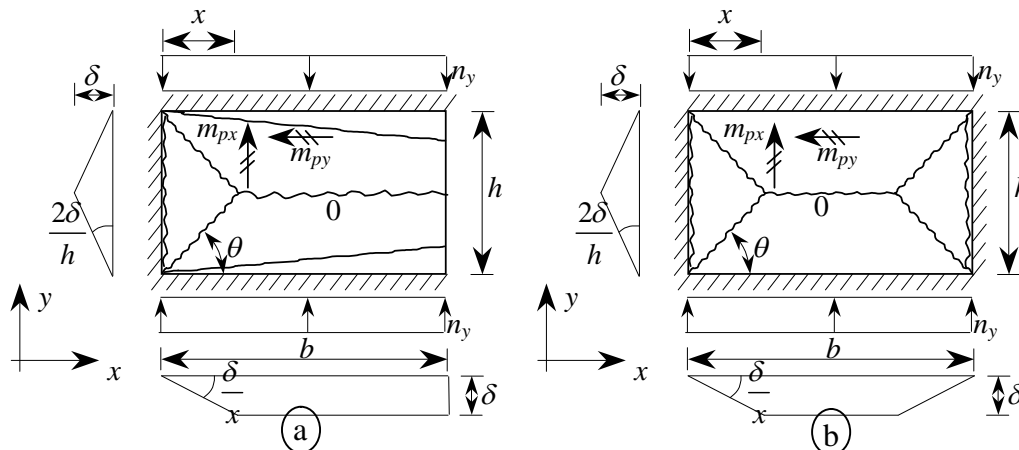


Figure 3.16 Yield patterns used in the comparison with the test.

The calculation of the bending moments is made as in Example 2, section 3.2.2.2, with  $\beta = 45^\circ$ .

In [33] the compressive strength of the mortar is measured together with the age of testing. Based on the compressive strength of the mortar it is possible to calculate the water/cement ratio ( $v/c$ ) using Bolomey's formula:

$$f_{cm} = K \left( \frac{c}{v} - 0.5 \right) \quad (3.5)$$

where  $K$  is a factor dependent, among other things, on the degree of hydration of the mortar.  $K$  is calculated by linear interpolation from the basic values  $K = 27$  MPa at 28 days, as shown in Figure 3.17.

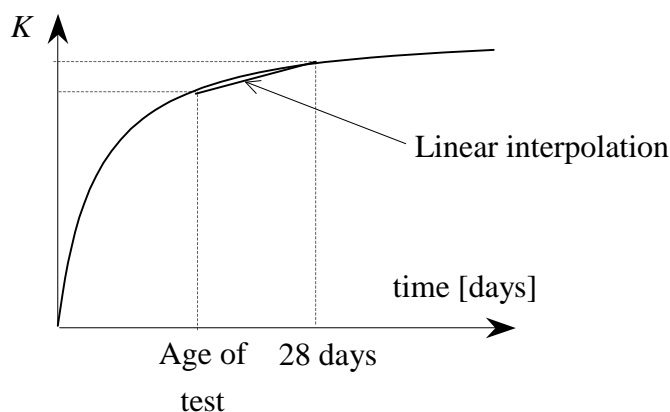


Figure 3.17

The water/lime ratio ( $v/k$ ) may then be determined as one fourth of the water/cement ratio since the mortar is a 1: 1/4 :3 mortar (cement:lime:sand), it is assumed that the amounts are measured by weights.

Using equation (2.43) to calculate the cohesion and using an effectiveness factor determined from equation (2.44) assuming that the bricks are solid with an IRA of 2.45 kg/m<sup>2</sup>/min, the bending yield moment,  $m_{px}$ , may be calculated.

The results of the calculation may be seen in Figure 3.18 and Figure 3.19.

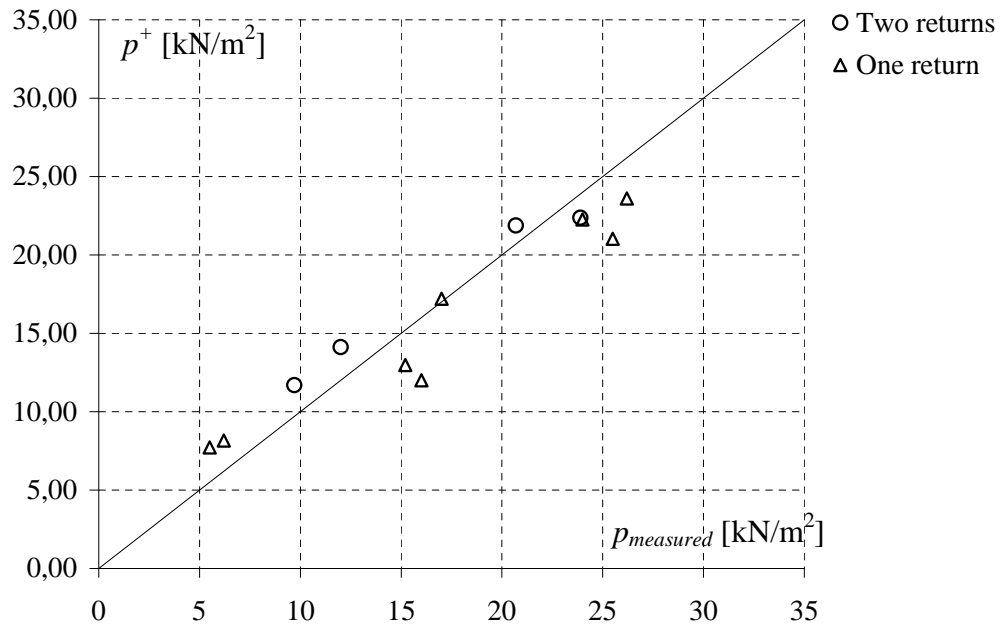


Figure 3.18 Experiments compared with theory for walls with one and two returns

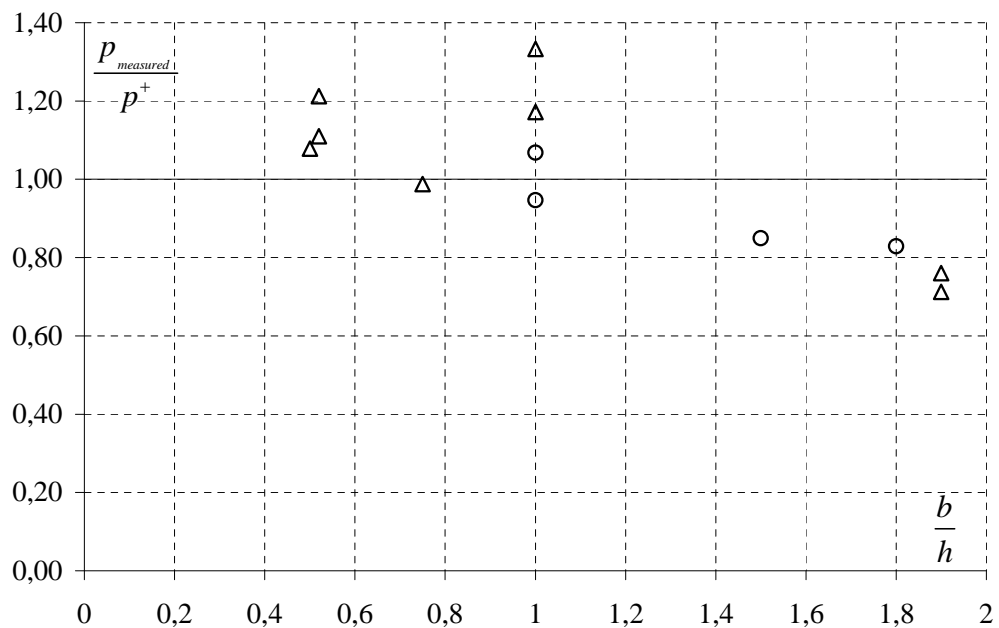


Figure 3.19 Results as a function of  $b/h$

The mean value and standard deviation of all the tests are found to be:

$$\mu = 1,01 \text{ and } s = 0.19 \quad (3.6)$$

It is seen that the correlation between the theory and the experiments is good.

## 4 Conclusion

The present report covers calculations of the load carrying capacity of laterally loaded masonry walls without axial loads and with small axial loads.

The load carrying capacity has in both cases been calculated using the yield line theory developed by Å. Ingerslev and K. W. Johansen to calculate the load carrying capacity of orthotropic concrete slabs.

For both load conditions, equations for the bending yield moments have been established. The bending yield moments have been calculated by an upper bound solution, assuming that failure takes place in the interface between the mortar and the brick. The failure is assumed to be a sliding failure following Coulombs modified failure hypothesis unless the tensile strength of the bricks is decisive. The tensile strength of the interface has been neglected.

When using the yield line theory it has been assumed that the rotation axes are placed at the face where the lateral load is applied as a pressure. This together with the assumption of no tensile strength mean that the moment capacity in a horizontal yield line becomes equal to zero.

In the case of laterally loaded masonry walls it has been observed in experiments that initial cracking takes place in the bed joint before failure, which indicates that the horizontal yield line has no moment capacity at failure.

The yield line theory in the case of small axial loads has been adjusted to the usual theory by introducing the axial load in the external work.

The yield line theory has in both cases been compared with experiments on full size walls. The comparisons showed that the theory is normally in good agreement with experiments. The tests used have been taken from the literature.

## 5 Literature

### General literature

- [1] TIMOSHENKO. S. P. and GERE. J. M.: Theory of Elastic Stability, *International student edition, McGraw-Hill, 1961.*
- [2] NIELSEN. M. P.: Limit analysis of reinforced concrete slabs, *Civil Engineering and Building Construction, Series No. 26, Copenhagen 1964.*
- [3] NIELSEN. M. P.: Om jernbetonskivers styrke, *Polyteknisk Forlag 1969.*
- [4] NIELSEN. M. P. and RATHKJEN. A.: Mekanik 2.1. Plane spændings og deformationstilstande, *Den Private Ingeniørfond, 1979.*
- [5] NIELSEN. M. P. and RATHKJEN. A.: Mekanik 5.1 del 1 og 2. Skiver og plader, *Den Private Ingeniørfond, 1981.*
- [6] JÖNSSON. J.: Continuum Mechanics of Beam and Plate Flexure, *Aalborg University, July 1995.*
- [7] NIELSEN. M. P.: Limit Analysis and Concrete Plasticity, *Second Edition, CRC Press, 1998*
- [8] NIELSEN. M. P.: Beton 2 del 1. Bjælke- og rammekonstruktioner. Skæv bøjning, *Danmarks Tekniske Universitet Institut for Bærende Konstruktioner og Materialer Lyngby, 1. Udgave, 2001.*
- [9] NIELSEN. M. P., HANSEN. L. P. and RATHKJEN. A.: Mekanik 2.2 del 1. Rumlige spændings og deformationstilstande, *Danmarks Tekniske Universitet Institut for Bærende Konstruktioner og Materialer København/Aalborg, 2001.*
- [10] NIELSEN. M. P., HANSEN. L. P. and RATHKJEN. A.: Mekanik 2.2 del 2. Rumlige spændings og deformationstilstande, *Danmarks Tekniske Universitet Institut for Bærende Konstruktioner og Materialer København/Aalborg, 2001.*

## Literature on masonry

- 
- [11] PAULSON. G. et. al.: Murværk og Jernbeton, *Egmont H. Petersons Kgl. Hof Bogtrykkeri, 1938*
- [12] HALLQUIST. Å.: Lateral loads on masonry walls (Fasthetsegenskaper for horisontalbelastet murverk), *Report 56, NBI, 1968*
- [13] HALLQUIST. Å.: Mekaniske fasthetsegenskaper for ikke-bærende murvegger belastet horisontalt, *Byggmästern 4, 1969*
- [14] LOSBERG. A. and JOHANSSON. S.: Sidotryk på murverksvægger av tegel, *Tegel 2, 1969*
- [15] SAHLIN. S.: Structural Masonry, *Prentice-Hall, 1971*
- [16] MONDORF. P. E.: Murværkskonstruktioner, *Polyteknisk Forlag, 1972*
- [17] HENDRY. A. W., SINHA, B. P. and MAURENBRECHER, A. H. P.: Full Scale Tests on the Lateral Strength of Brick Cavity Walls with Precompression, *Proc. Br. Ceram. Soc., 21, pp 165-180, 1973*
- [18] KHEIR, A. M. A.: Brickwork Panels under Lateral Loading, *M. phil. Thesis, University of Edinburgh, 1975*
- [19] BAKER, L. R.: Flexural Strength of Brickwork Panels, *Proceedings of the Third International Brick Masonry Conference (Essen) 1973, eds L. Foertig and K. Gobel (Bundesverband der Deutschen Ziegelindustrie, Bonn, 1975), pp. 378-83*
- [20] WEST, H. W. H., HODGKINSON, H. R. and WEBB, W. F.: Lateral Loading Tests on Walls with Different Boundary Conditions, *Proceedings of the Third International Brick Masonry Conference (Essen) 1973, eds L. Foertig and K. Gobel (Bundesverband der Deutschen Ziegelindustrie, Bonn, 1975), pp. 180-6*
- [21] WEST, H. W. H and HODGKINSON, H. R.: The Lateral Load Resistance of Brickwork without Precompression, *Proc. Br. Ceramic. Soc., 24, 1975, pp. 101-13.*
- [22] WEST, H. W. H., HODGKINSON, H. R. and HASELTINE, B. A.: The Resistance of Brickwork to Lateral Loading, Part 1, Experimental Methods and Results of Tests on Small Specimens and Full Sized Walls, *Struct. Engr., 55, 1977, pp. 411-21*
- [23] HASELTINE, B. A.. WEST, H. W. H and TUTT, J. N.: The Resistance of Brickwork to Lateral Loading. Part 1. Design of Walls to Resist Lateral Loading, *Struct. Engr., 55, 1977, pp. 422-30.*
- [24] BRINCKER, R.: Murede vægges tværbæreevne, en undersøgelse af murværks fysiske egenskaber, *Afdelingen for Bærende Konstruktioner, DTU, Rapport nr. R 111, 1979.*
- [25] Kalk- og Teglværkslaboratoriet: Murstens træk-, bøjningstræk- og spaltningsstyrke, *1980*
-

- [26] KRISTENSEN, O.: Tværbelastet murværk, *Kalk og Teglværkslaboratoriet*.
- [27] CAJDERT, A.: Laterally Loaded Masonry Walls, *Chalmers University of Technology, Publication 80:5, Göteborg 1980*.
- [28] PAGE, A. W.: An experimental investigation of the biaxial strength of brick masonry, *Proceedings of the sixth International Brick Masonry Conference, Andil, Rome pp 3-15 1982*
- [29] LAWRENCE, S. J.: "Behaviour of brick masonry walls under lateral loading", *Vol. 1-2, Ph.D. thesis, University of New South Wales, Australia 1983*.
- [30] EXNER, H.: Plasticitetsteori for Coulomb-materialer, *Afdelingen for Bærende Konstruktioner, DTH, Serie R, No. 176, 1983*.
- [31] BUHELT, M.: Tværbelastede murværk, *SBI-Rapport 1458, Statens Byggeforskningsinstitut, 1984*
- [32] PAGE, A. W. and BROOKS, D. S.: The Design of Masonry Walls for Vertical Loading – A Review of the Provisions of the SAA Masonry Code, *Civil Engineering Transactions, 1988*
- [33] HENDRY, A. W.: Structural Masonry, *MacMillan, 1990*.
- [34] HENDRY, A. W.: Reinforced & Prestressed Masonry, *Longmann Scientific & Technical, 1991*.
- [35] GOTTFREDSEN, F. R.: Laterally loaded masonry, Properties and Behaviour, *SBI-report 289, Danish Building Research Institute, 1997*
- [36] SINHA, B. P., NG, C. L. and PEDRESCHI, R. F.: Failure Criterion and Behavior of Brickwork in Biaxial Bending, *Journal of Materials in Civil Engineering, Vol. 9, No. 2, May 1997, pp. 70-75*.
- [37] HANSEN, K. F.: Bending and Shear Tests with Masonry, *SBI- Bulletin 123, Danish Building Research Institute, 1999*
- [38] VAN DER PLUIJM, R.: Out-of-Plane Bending of Masonry Behaviour and Strength, *Dr. Thesis, Eindhoven 1999*.
- [39] HAGSTEN, L.G.: Plasticitetsteori for murværk Del 1: Trykstyrke, *Department of Structural Engineering and Materials, DTU, Series R, No. 72, 2000*.
- [40] HAGSTEN, L.G.: Plasticitetsteori for murværk Del 2: Trækstyrke parallelt med liggefugerne, *Department of Structural Engineering and Materials, DTU, Series R, No. 73, 2000*.
- [41] HAGSTEN, L.G.: Plasticitetsteori for murværk Del 3: Koncentreret last, *Department of Structural Engineering and Materials, DTU, Series R, No. 74, 2000*.
- [42] HAGSTEN, L.G.: Plasticitetsteori for murværk Del 4: Teglbjælkers forskydningskapacitet, *Department of Structural Engineering and Materials, DTU, Series R, No. 75, 2000*.

- [43] HAGSTEN, L.G.: Plasticitetsteori for murværk Del 5: Tværbelastet murværk, *Department of Structural Engineering and Materials, DTU, Series R, No. 76, 2000.*
- [44] HAGSTEN, L.G, and NIELSEN, M. P.: Murværk. Lærebog for ingeniører. Første foreløbige udgave, *Department of Structural Engineering and Materials, DTU, December 2000.*
- [45] HANSEN, L. Z. & GUDMAND-HØYER, T.: Strength effects from the initial rate of absorption on masonry, *Bygningsstatistiske Meddelelser, Vol. LXVIII, Nos 2-3, pp. 35-113*
- [46] HANSEN, L. Z.: Stability of Masonry Columns, *BYG.DTU, R-055, 2003*

## 6 Appendix

### 6.1 Appendix 1. Tensile strength and flexural modulus of clay bricks

The bending yield moment in a diagonal yield line has an upper limit determined by the tensile strength of the brick. In this appendix some empirical equations for the tensile strength and the flexural modulus will be established. The main experimental investigations used are the one made at Kalk- og Teglværkslaboratoriet [25] and the one made by R. van der Pluijm [38].

The investigation made at Kalk- og Teglværkslaboratoriet consists of 60 tensile and flexural tests with 6 different types of bricks. Each series consists of 10 tests. The tensile tests were carried out using a specimen with metal plates glued to the ends of the bricks. The specimen is illustrated in Figure 6.1.

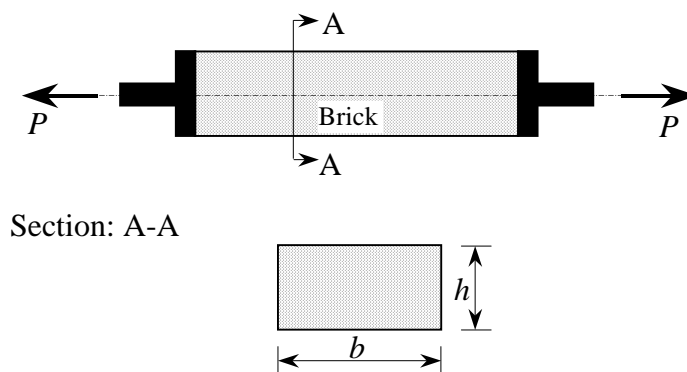


**Figure 6.1 Tensile strength**

The tensile strength is calculated as

$$f_{tb} = \frac{P_u}{bh} \quad (6.1)$$

$P_u$  being the failure load.

Equation (6.1) is used in the case of solid as well of perforated bricks in [25].

In the same investigation the flexural modulus of similar brick types was measured. The test set-up is shown in Figure 6.2 where  $l = 210$  mm

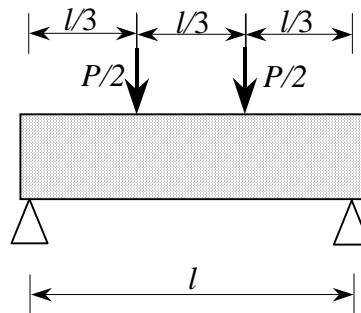


**Figure 6.2 Flexural modulus**

The cross-section was rectangular and no account was taken of the holes when evaluating the results. The flexural modulus is calculated as:

$$f_{tfb} = \frac{M}{W} = \frac{\frac{1}{6} P_u l}{\frac{1}{6} b h^2} \quad (6.2)$$

The results of the tests are listed in Table 6.1

Type		$f_{cb}$	$f_{ib}$	$f_{tfb}$	Comments
		[MPa]	[MPa]	[MPa]	
1*	<i>u</i>	10	0.74	1.46	Massive brick
	<i>s</i>	1.46	0.2	0.22	
2*	<i>u</i>	23.3	0.45	0.91	Perforated brick
	<i>s</i>	2.94	0.19	0.17	
3*	<i>u</i>	55.8	1.98	3	Perforated brick
	<i>s</i>	9.08	0.49	0.36	
4**	<i>u</i>	27.2	0.68	1.31	Perforated brick
	<i>s</i>	4.67	0.18	0.34	
5**	<i>u</i>	42.3	0.56	2.17	Perforated brick
	<i>s</i>	7.56	0.47	0.76	
6**	<i>u</i>	53.5	2.75	3.14	Perforated brick
	<i>s</i>	2.89	0.29	0.46	

\*) Normal size brick  $b = 108$  mm  
 \*\*) Brick with a width  $b = 168$  mm

**Table 6.1 Tests results taken from [25]**

The results of the tensile tests are plotted in Figure 6.3 versus the compressive strength of the brick. The results framed in a circle are the results for solid bricks.

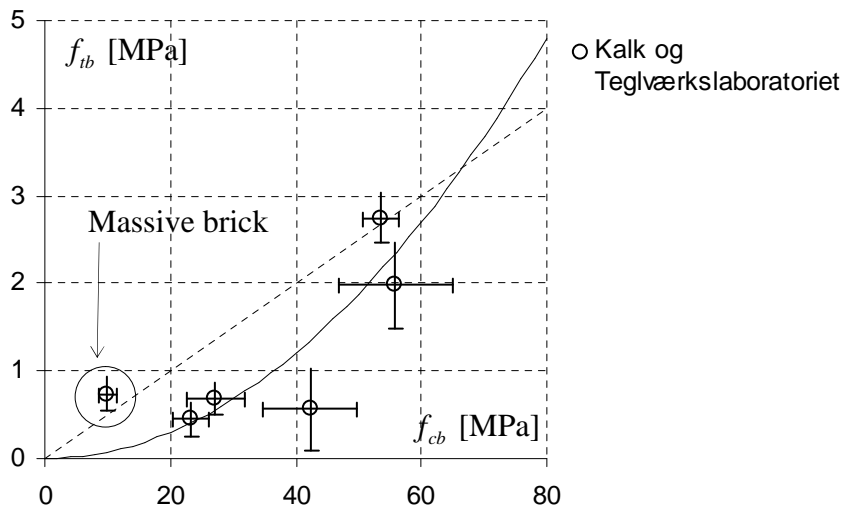


**Figure 6.3 Tensile strength versus the compressive strength of the bricks**

The solid line is given by:

$$f_{tb} = 0.0075 f_{cb}^2 \quad (f_{tb} \text{ and } f_{cb} \text{ in MPa}) \quad (6.3)$$

The broken line is given by:

$$f_{tb} = \frac{1}{20} f_{cb} \quad (6.4)$$

The flexural modulus is plotted versus the compressive strength in Figure 6.4. The solid line is given by:

$$f_{tb} = \frac{1}{20} f_{cb} \quad (6.5)$$

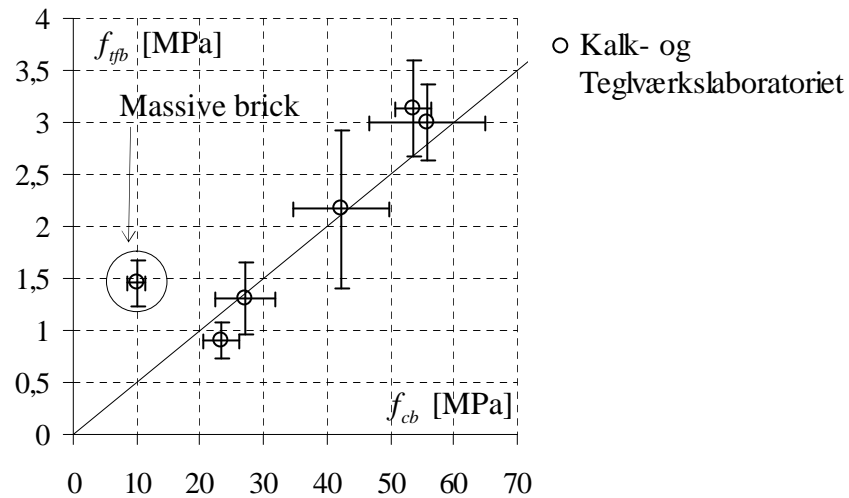


**Figure 6.4 Flexural modulus versus the compressive strength of the bricks**

In Figure 6.5 the tensile strength is plotted as a function of the flexural modulus. A relation given by equation (6.6) fit the measured values reasonably well.

$$f_{tfb} = 1.8 f_{tb}^{0.6} \quad (f_{tfb} \text{ and } f_{tb} \text{ in MPa}) \quad (6.6)$$

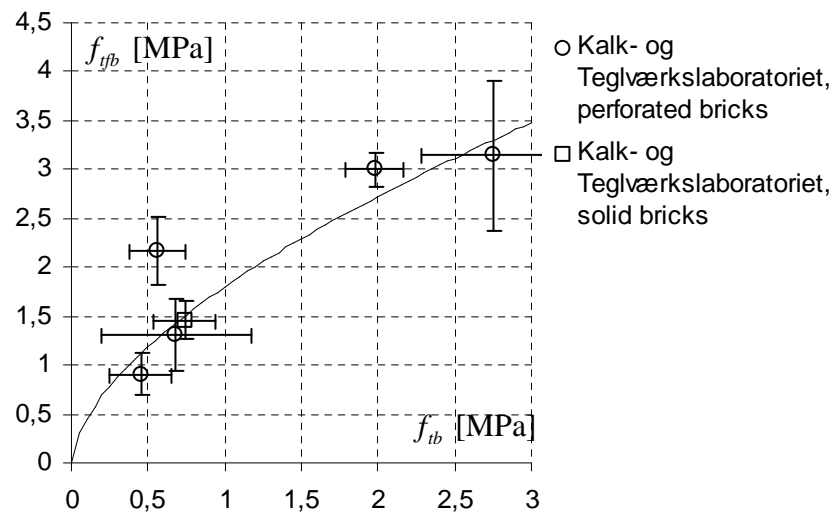


**Figure 6.5 Tensile strength as a function of the flexural modulus**

From the investigation carried out by Rob van der Pluijm 6 tests made on cylinders of clay bricks are selected. The test set-up and specimens are shown in Figure 6.6. Two different bricks are used. The bricks were solid wire cut bricks. Notice that the tensile specimens were notched. The results are shown in Table 6.2.

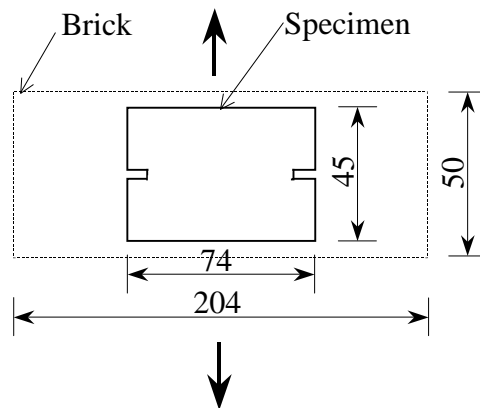


Figure 6.6 Specimen used by Rob van der Pluijm to measure the tensile strength of bricks

Type	$f_{cb}$	$f_{tb}$
	[MPa]	[MPa]
wc-jo	66	3.51
sm-ve	33	1.5

Table 6.2 Test results taken from [38]

The results for the solid bricks tested at Kalk- og Teglværkslaboratoriet are now used together with the results of Rob van der Pluijm and they are plotted versus the compressive strength of the bricks in Figure 6.7. It may be seen that the tensile strength may be calculated from the compressive strength of the brick as

$$f_{tb} = \frac{1}{20} f_{cb} \quad (6.7)$$

in the case of solid bricks.

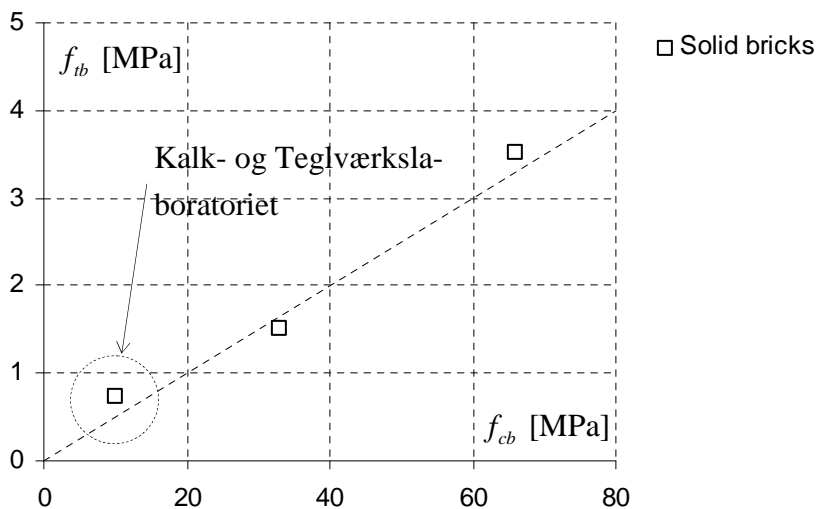


Figure 6.7 Tensile strength of solid bricks, [25] and [38]

## 6.2 Appendix 2. Deflection of laterally loaded masonry walls

In this appendix the deflection of masonry walls loaded with only lateral load will be investigated. The procedure is to determine the bending stiffnesses and postulate a simple relation between the bending stiffnesses and the torsional stiffness. The stiffnesses will be used to determine the deflection of walls. The bending stiffnesses parallel and perpendicular to the bed joint are very different and the initial stiffness of masonry in compression is believed to have little to do with the bending stiffnesses. The bending stiffness is believed to be far more influenced by the bricks than by the mortar.

The investigation begins with a preliminary experimental justification of the bending stiffnesses and the torsional stiffness. It has not been possible to find similar bending and torsion tests, so a simple relation connecting the torsional stiffness to the bending stiffnesses has been adopted and justified by an example where calculations on a wall are compared with measured deflections.

The stiffnesses of masonry bent about the head or bed joint are investigated experimentally in [26].

In [26] two different types of mortar are used together with four types of bricks. The author has limited this investigation to deal only with two types of bricks, although in [26] four types of bricks are treated. The bricks used are solid clay bricks (soft stroked). The data are listed in Table 6.3.

Brick type	Dimension			Strength	Suction
	$H$	$b$	$L$	$f_{cb}$	$IRA$
	[mm]	[mm]	[mm]	[Mpa]	[kg/m <sup>2</sup> /min]
10	55	109	229	9.8	3.2
20A	55	107	229	23.0	3.0

**Table 6.3 Properties of the bricks**

The most important properties of the mortars used in the investigation are listed in Table 6.4.

	$f_{cm}$ [MPa]
KC 60/40/850	3.5
KC 35/65/650	11.5

**Table 6.4 Mortar properties**

The test set-up used in the investigation is the standard wallette test. This test set-up is used for both bending about the head and the bed joint as shown in Figure 6.8. In the same figure the method used to monitor the rotations may be seen.

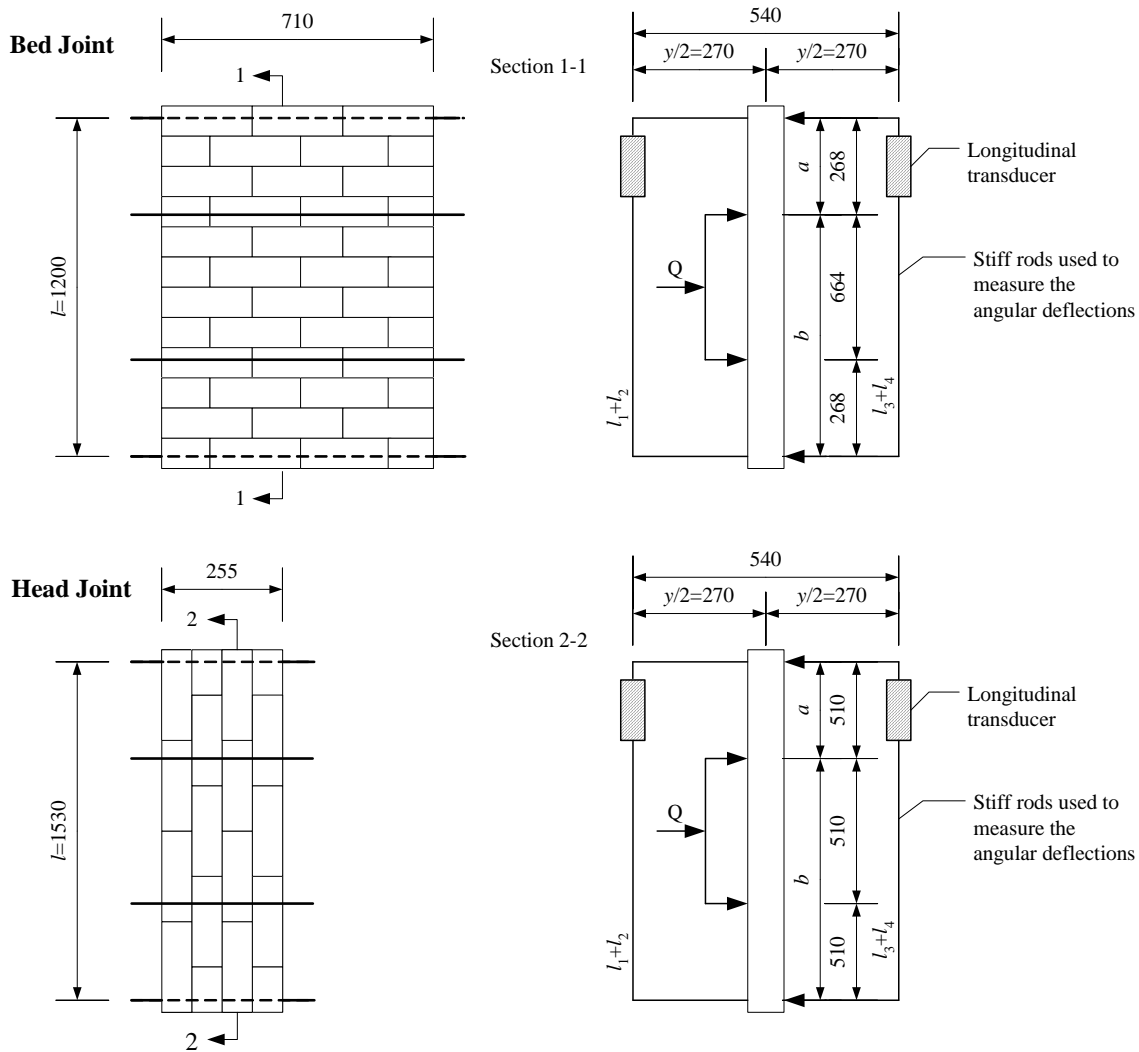


**Figure 6.8 Test set-up**

The angular deflection at the supports is determined by

$$\alpha = \frac{\Delta l_1 + \Delta l_2 + \Delta l_3 + \Delta l_4}{4 \cdot 2 \frac{y}{2}} \quad (6.8)$$

In both cases the stiffness is determined by using linear elastic theory for beams in four-point bending. This is a standard case for which we have:

$$\alpha = \frac{Qla}{12EI} \left( 1 - \left( \frac{a}{l} \right)^2 \right) + \frac{Qlb}{12EI} \left( 1 - \left( \frac{b}{l} \right)^2 \right) \quad (6.9)$$

$E$  is the Young's modulus and  $I$  is the sectional second order moment. The length  $l = a+b$ . Other parameters may be seen in Figure 6.8.  $E$  has to be substituted by either  $E_{0x}$  or  $E_{0y}$ , where  $x$  refer to bending about the head joint and  $y$  to bending about the bed joint. Thus when  $\alpha$  is known from the test, the stiffnesses may be calculated.

Each combination of brick and mortar were used in three similar tests. The moment-curvature relations obtained in each test are plotted in Figure 6.9.

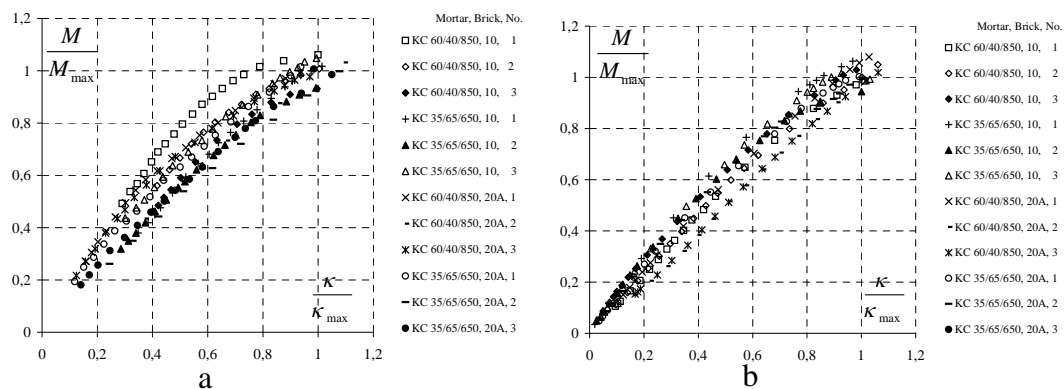


**Figure 6.9** Measurements of the moment-curvature relation, bending about the head joint (a) and bending about the bed joint (b)

Figure 6.9a shows the measured moment-curvature relation for bending about the head joint and Figure 6.9b for the bed joint.

From Figure 6.9 it may be seen that the shape of the curves are different for bending about the head joint and bending about the bed joint. Bending about the bed joint leads to a more linear behaviour than bending about the head joint, for which the moment-curvature relation has more the shape of a parabola.

The non-linear behaviour for bending about the head joint is more pronounced for weak mortars than for stronger mortars.

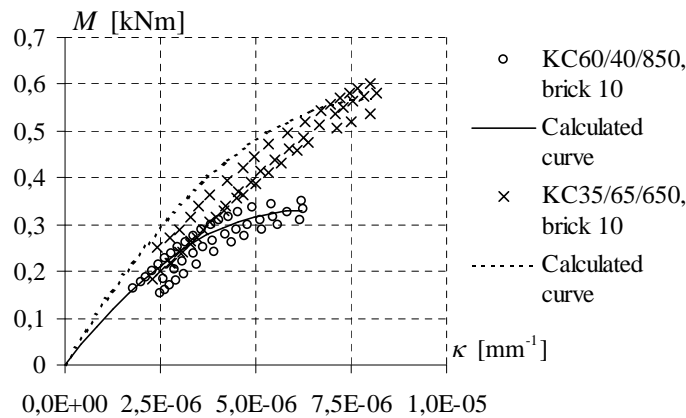


**Figure 6.10 Bending about the head joint in the case of a weak and a strong mortar, respectively**

In Figure 6.10 the measured moment-curvature relation is plotted for a weak and a strong mortar, respectively. In the same plot two curves are shown, which are calculated using equation (6.10).

$$M = M_{\max} \frac{\kappa}{\kappa_{\max}} \left( 2 - \frac{\kappa}{\kappa_{\max}} \right) \quad (6.10)$$

It is seen that the behaviour of the weak mortar may be predicted by equation (6.10), whereas the curves for the stronger mortar are more linear if  $\kappa_{\max}$  in (6.10) is identified with the curvature at failure. This may be explained by the properties of the bricks. The suction is at a level, which provides a good bond in the case of the strong mortar. Thus failure of the brick instead of failure in the interface occurs and thus a more brittle and linear moment-curvature relation may be expected.

Anyway the initial stiffness may be determined from the test results in Figure 6.9 by fitting a parabolic function to the points. The functions have the property of going through origo. The initial stiffness is determined as the value of  $dM/d\kappa$  for  $(\kappa.M) = (0.0)$ . The curvature at failure is defined as the point for which  $dM/d\kappa = 0$ .

The results may be seen in Table 6.5 where also the ratios between the stiffnesses and the maximum curvatures are listed.

Brick	Mortar	Bending about the bed joint		Bending about the head joint		$\kappa_{x,max}$	$E_{0y}$
		$\kappa_{y,max}$	$E_{0y}$	$\kappa_{x,max}$	$E_{0x}$	$\kappa_{y,max}$	$E_{0x}$
		[mm <sup>-1</sup> ]	[MPa]	[mm <sup>-1</sup> ]	[MPa]	[ ]	[ ]
10	KC60/40850	4.59E-06	1774.5	6.21E-06	3476.5	1.35	0.51
10	KC35/65/650	6.79E-06	1794.2	8.05E-06	3721.0	1.19	0.48
20A	KC60/40850	2.74E-06	2512.6	5.02E-06	5002.2	1.83	0.50
20A	KC35/65/650	8.27E-06	2945.8	5.94E-06	5185.7	0.72	0.57

**Table 6.5 Bending stiffnesses and maximum curvatures obtained from the tests**

Table 6.5 shows that the initial stiffness about the head joint ( $E_{0x}$ ) is about two times larger than the stiffness about the bed joint ( $E_{0y}$ ). The table also shows that the deformation capacity is larger for bending about the head joint than for bending about the bed joint. This is especially clear in the case of a weak mortar (KC 60/40/850), where failure is believed to take place in the interface as mentioned above.

Empirical equations for the initial stiffnesses may be established based on the results listed. The equations have to include properties of the bricks as well as the mortar. From the results listed in Appendix 1 it may be shown that the flexural modulus of massive bricks may be calculated as:

$$f_{tfb} = \frac{1}{7} f_{cb} \quad (6.11)$$

Then empirical equations for the stiffnesses  $E_{0x}$  and  $E_{0y}$ , respectively, may be established. They become:

$$\begin{aligned} E_{0x} &= 2894.5 f_{tfb}^{0.41} f_{cm}^{0.04} \\ E_{0y} &= 1487.9 f_{tfb}^{0.41} f_{cm}^{0.04} \end{aligned} \quad (6.12)$$

where  $f_{cm}$  is the compressive strength of the mortar. Units are MPa.

Using these equations the mean value of the ratios  $E_{0x,(6.12)} / E_{0x,measured}$  and  $E_{0y,(6.12)} / E_{0y,measured}$  are found to be 0.99 and 1, respectively. The standard deviations become 0.008 and 0.05, respectively. The calculated values may be seen in Table 6.6

$f_{cb}$	$f_{cm}$	$f_{tfb}$	$E_{0x}$	$E_{0y}$
[MPa]	[MPa]	[MPa]	[MPa]	[MPa]
9.8	3.5	1.4	3504.5	1801.9
9.8	11.5	1.4	3690.2	1897.3
23.0	3.5	3.3	4958.7	2551.0
23.0	11.5	3.3	5221.4	2686.1

**Table 6.6 Calculated values of the bending stiffness**

**Example 1. Calculation of wall deflections**

In this example, the load deflection curve of a wall tested in [11] will be calculated by using the results obtained above. The procedure will be to estimate a simple analytical form of the deflection. When the deflection corresponding to maximum curvature about the bed joint is achieved, this stiffness will be set at zero and the wall only has bending stiffness about the head joint. The wall calculated is shown in Figure 6.11.

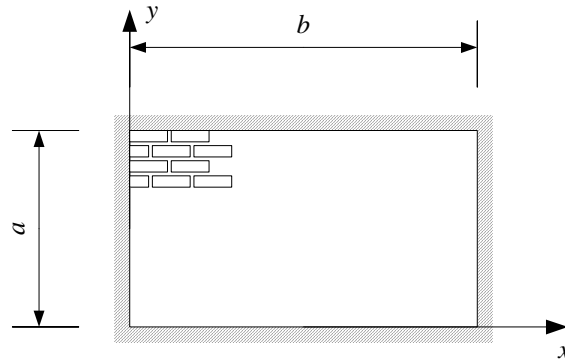


**Figure 6.11 Wall for deflection analysis**

The data used in the calculations may be seen in Table 6.7. From the table the dimensions of the wall are indicated together with the initial stiffnesses. Furthermore the maximum curvatures in the  $x$  and  $y$  direction are listed. These values are estimated since in [11] no information has been given on this matter. Here the initial stiffnesses are taken from the Norwegian code which is based on the work of Hallquist [11].

$a$	2300	mm	
$b$	4500	mm	
$t$	310	mm	
$E_{0x}$	5500	MPa	for $\kappa_x = \frac{\partial^2 w_z}{\partial x^2} < 2.0 \cdot 10^{-6}$ else zero
$E_{0y}$	3667	MPa	for $\kappa_y = \frac{\partial^2 w_z}{\partial y^2} < 0.4 \cdot 10^{-6}$ else zero

**Table 6.7 Data used in the calculations**

The bending stiffnesses and the torsional stiffness are calculated as:

$$\begin{aligned}
 D_x &= E_{0x} \frac{1}{12} t^3 \\
 D_y &= E_{0y} \frac{1}{12} t^3 \\
 D_{xy} &= \sqrt{D_x D_y}
 \end{aligned}
 \tag{6.13}$$

The deflection of the wall is estimated by equation (6.14),  $w_m$  being the midpoint deflection,

$$w_z = w_m \sin\left(\frac{\pi x}{b}\right) \sin\left(\frac{\pi y}{a}\right) \quad (6.14)$$

The load for a given deflection may be obtained by considering the elastic energy. The internal work may be calculated as:

$$A_i = \frac{1}{2} \int_0^a \int_0^b \left( D_x \left( \frac{\partial^2 w_z}{\partial x^2} \right)^2 + D_y \left( \frac{\partial^2 w_z}{\partial y^2} \right)^2 + 2D_{xy} \left( \frac{\partial^2 w_z}{\partial x \partial y} \right)^2 \right) dx dy \quad (6.15)$$

Inserting (6.14) into (6.15) the internal work may be calculated as

$$A_i = \frac{1}{8} \pi^4 w_m^2 ab \left( \frac{D_x}{b^4} + \frac{D_y}{a^4} + 2 \frac{D_{xy}}{a^2 b^2} \right) \quad (6.16)$$

The external work becomes:

$$A_y = \frac{1}{2} \int_0^a \int_0^b q w_z dx dy = 2 \frac{ab}{\pi^2} w_m q \quad (6.17)$$

Thereby the load at a given midpoint deflection may be calculated by:

$$q = w_m \pi^4 \left( \frac{D_x}{b^4} + 2 \frac{D_{xy}}{b^2 a^2} + \frac{D_y}{a^4} \right) \quad (6.18)$$

The load-deflection curve obtained is shown in Figure 6.12. In the same figure, measurements by Hållquist [11] are plotted. It may be seen that the calculations fit the tests results well, except for very small deflections.

The example gives a preliminary support for calculating the torsional stiffness by equation (6.13).

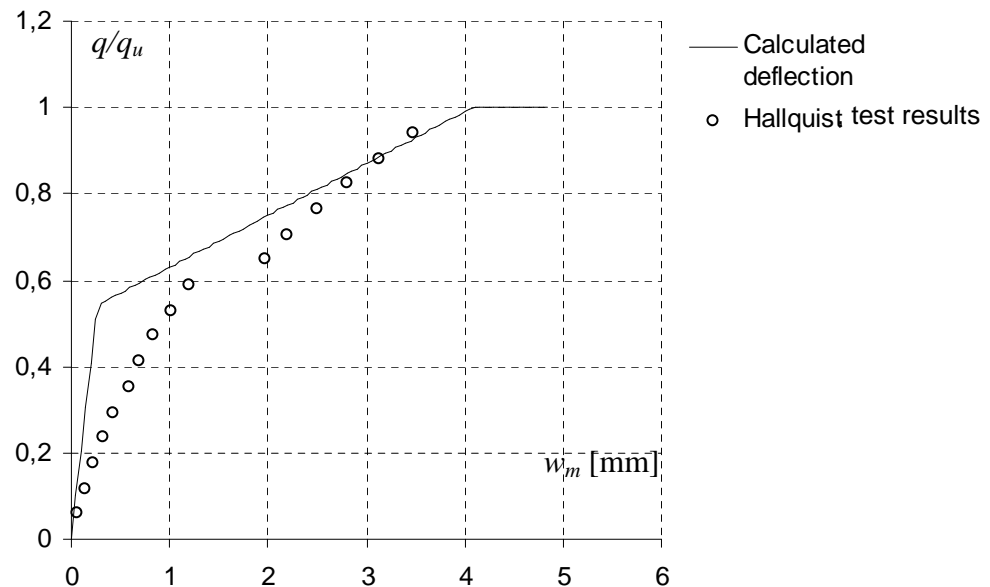
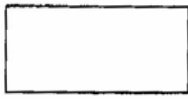
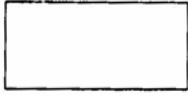
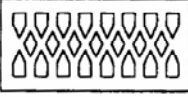
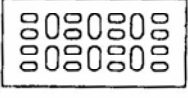
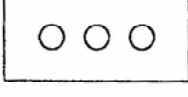


Figure 6.12 Load-deflection curve

From the above example it is clear that the maximum curvature is an important factor. Rob van der Pluijm arrives at similar conclusions in [38].

The behaviour of masonry in bending has also been investigated by Klavs Feilberg [37]. In this investigation bending about the head and bed joint is undertaken. Five types of bricks are used together with two types of mortars. The tests were deformation controlled, making it possible to obtain the maximum deflection from the reported curves, which may be used to calculate the maximum curvature.

In the case of bending about the head joint, the specimens tested were made with one mortar together with two types of bricks. The data for the bricks and the mortar used may be seen in Table 6.8 and Table 6.9.

Brick type	Mean compressive strength N/mm <sup>2</sup>	Suction rate Kg/m <sup>2</sup> /mm	Geometry
Solid S	26	2.8	
Solid O	26	3.2	
Perforated P	46	2.9	
Perforated Y	47	2.0	
Perforated G	66	2.5	

All the bricks are of Standard Danish size 228 × 108 × 55 mm.

**Table 6.8 Properties of the bricks in [37]**

Type	A	B
Composition		
<i>Cement</i>	40 kg	65 kg
<i>Lime</i>	60 kg	35 kg
<i>Sand</i>	850 kg	650 kg
Compressive strength	3.8 N/mm <sup>2</sup>	11.5 N/mm <sup>2</sup>
Tensile flexural strength	1.51 N/mm <sup>2</sup>	3.65 N/mm <sup>2</sup>

**Table 6.9 Properties of the mortar in [37]**

Only tests with bricks in running bond with half a brick overlap are used for determination of the maximum curvature.

In the case of two different bricks laid with mortar B, the influence of the width of the specimen was investigated. The results may be seen in Table 6.10, which only covers bending about the head joint.

No	Brick	$f_{cb}$	Mortar	b	$w_z$	$l_x$	$\kappa_{x,max}$	$b/l_x$	Failure
		[MPa]		[mm]	[mm]	[mm]	[mm <sup>-1</sup> ]		
1	P	46	B	872	1.3	1498	6E-06	0.58	Brick
3	P	46	B	600	1.7	1498	8E-06	0.40	Interface/brick
5	P	46	B	328	2.2	1498	1E-05	0.22	Interface/brick
7	P	46	B	260	2	1258	1E-05	0.21	Interface/brick
9	S	26	B	872	2	1498	9E-06	0.58	Interface/brick
11	S	26	B	600	1.6	1498	7E-06	0.40	Interface/brick
13	S	26	B	328	0.7	1498	3E-06	0.22	Brick
15	S	26	B	260	2.15	1258	1E-05	0.21	Interface/brick
18	G	66	B	600	1.4	1498	6E-06	0.40	Brick

**Table 6.10 Results taken from [37]**

If the maximum curvature is plotted versus  $b/l$  a variation as shown in Figure 6.13 is obtained. The point in a dotted circle has to be disregarded since the test produced unexpected low results. It may be seen that the maximum curvature declines with increasing ratio,  $b/l$ . The solid line is calculated as:

$$\kappa_{x,max} = 0.36 \cdot 10^{-5} \left( \frac{b}{l} \right)^{-0.77} \quad (6.19)$$

However a constant level of  $\kappa_{x,max}$  is used in the further calculations. Formula (6.16) is quoted only to illustrate the importance of a standard specimen for the determination of  $\kappa_{x,max}$ .

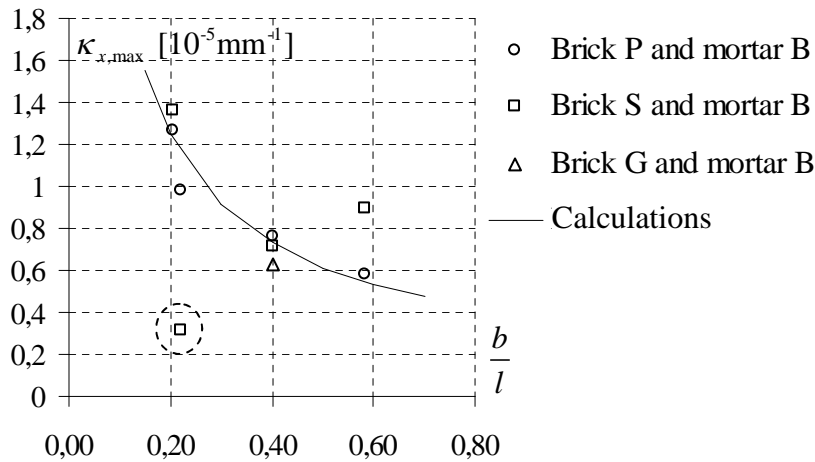


Figure 6.13 Maximum curvature as a function of the ratio width/length

Furthermore, bending tests with specimens of a constant width, 600 mm, were carried out using one mortar together with different bricks. Both bending tests about the head and bed joint were carried out. The results of the tests may be seen in Table 6.11.

Brick	$f_{cb}$	Mortar	Head joint				Bed joint				$\kappa_{y,max}$
			$b$	$w_z$	$l_x$	$\kappa_{x,max}$	$b$	$w_z$	$l_y$	$\kappa_{y,max}$	
	[MPa]		[mm]	[mm]	[mm]	[mm <sup>-1</sup> ]	[mm]	[mm]	[mm]	[mm <sup>-1</sup> ]	$\kappa_{x,max}$
S	26	A	600	1	1498	4.5E-06	468	0.1	668	2.2E-06	0.50
P	46	A	600	1.2	1498	5.3E-06	468	0.1	668	2.2E-06	0.42
G	66	A	600	1.4	1498	6.2E-06	468	0.1	668	2.2E-06	0.36
Y	47	A	600	1.3	1498	5.8E-06	468	0.1	668	2.2E-06	0.39
O	26	A	600	1	1498	4.5E-06	468	0.12	668	2.7E-06	0.60

Table 6.11 Results taken from [37]

From Table 6.11 it appears that a ratio of 0.5 between the maximum curvatures is a reasonable estimate. This is the same as the ratio between the initial stiffnesses. It may be seen that the initial rate of absorption has no influence on the value of the initial stiffnesses.

The maximum curvature may be calculated in the case of bending about the head joint using the secant stiffness at origo. If  $M(\kappa)$  is given by (6.10) the secant stiffness is half the initial stiffness  $E_{0x}$ . The curvature is calculated assuming linear elastic material behaviour with a maximum stress equal the flexural modulus for bending about the head joint, see Figure 6.14.

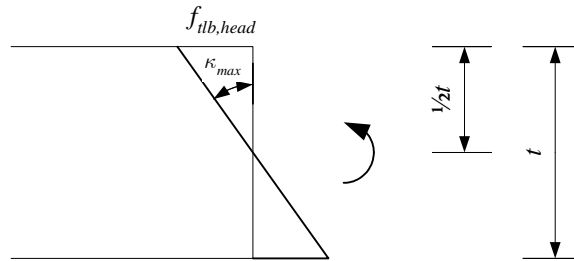


**Figure 6.14 Determination of  $\kappa_{max}$**

$$\kappa_{max} = \frac{2f_{tlb,head}}{E_{0x}t} \quad (6.20)$$

To illustrate the procedure of the calculations, an example with Danish brickwork is outlined.

**Example 2. Load-deflection curve**

A simply supported wall as shown in Figure 6.15 is considered. The wall is built with G bricks and an A mortar (data taken from the text above). The moment capacity is measured in [37] to be 2.3 kNm/m. By means of the yield line theory, see Chapter 2, the load carrying capacity of the wall shown in Figure 6.15 is found to be 2.6 kN/m<sup>2</sup>.

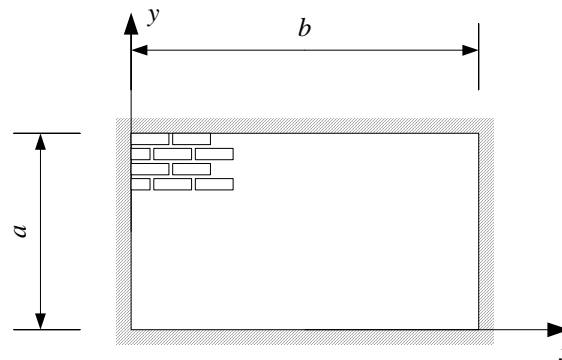


**Figure 6.15 Wall for deflection analysis**

The data necessary to carry out the calculations are shown in Table 6.12. The maximum curvatures are taken from Table 6.11. The maximum curvature in the x-direction is reduced so that a ratio of 1/2 between the maximum curvatures is achieved.

$a$	2500mm	
$b$	4500mm	
$t$	108mm	
$E_{0x}$	5000 MPa	for $\kappa_x = \frac{\partial^2 w_z}{\partial x^2} < 6.2 \cdot 10^{-6}$ else zero
$E_{0y}$	2500 MPa	for $\kappa_y = \frac{\partial^2 w_z}{\partial y^2} < 3.1 \cdot 10^{-6}$ else zero

**Table 6.12 Data used in the calculations**

By the same procedure as outlined in Example 1 the result becomes as shown in Figure 6.16.

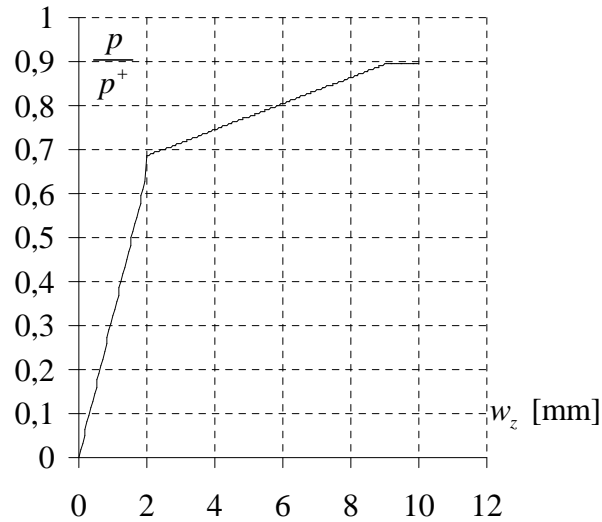


Figure 6.16 Load deflection curve

It appears from Figure 6.16 that the ultimate load found by deflection calculation is almost the same as the load obtained by the yield line theory ( $p^+$ ). The shape of the load deflection curve is believed to be correct since a test made by Rob van der Pluijm, [38] given in Figure 6.17 shows similar behaviour.

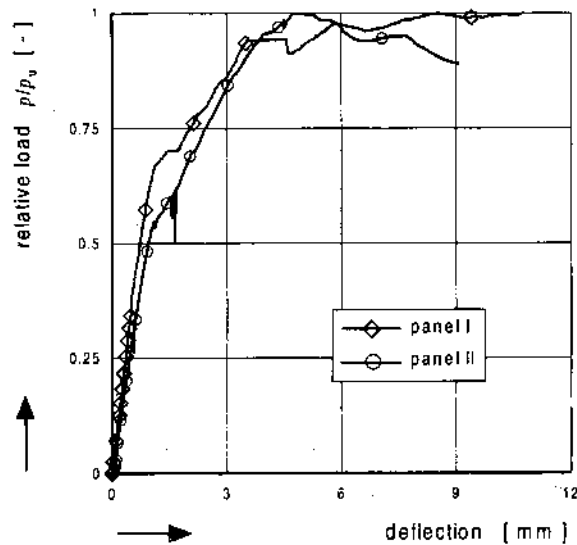


Figure 6.17 Measured load-deflection curve, taken from[38]

Figure 6.17 was obtained for a wall with the height 1740 mm and the width 3950 mm.

This appendix has demonstrated how to calculate deflections of a masonry wall. Different bending stiffnesses about the head and the bed joint have to be introduced together with a simple equation for the torsional stiffness and maximum values of the curvatures in each direction. This provides the bilinear behaviour shown in Figure 6.16. Thereby it is possible to get estimates of the deflection and furthermore a value of the load carrying capacity.

### 6.3 Appendix 3. Inclination of a diagonal yield line

The inclination of a diagonal yield line running in the interface, depends on the bond in which the masonry wall is built. In Denmark different types of bonds are used. In this Appendix a short survey of diagonal yield lines and the mean inclination will be presented.

The inclination is calculated as, see Figure 2.14 for the notation  $x_0$  and  $y_0$ ,

$$\theta = \text{Arc tan} \left( \frac{x_0}{y_0} \right) \quad (6.21)$$

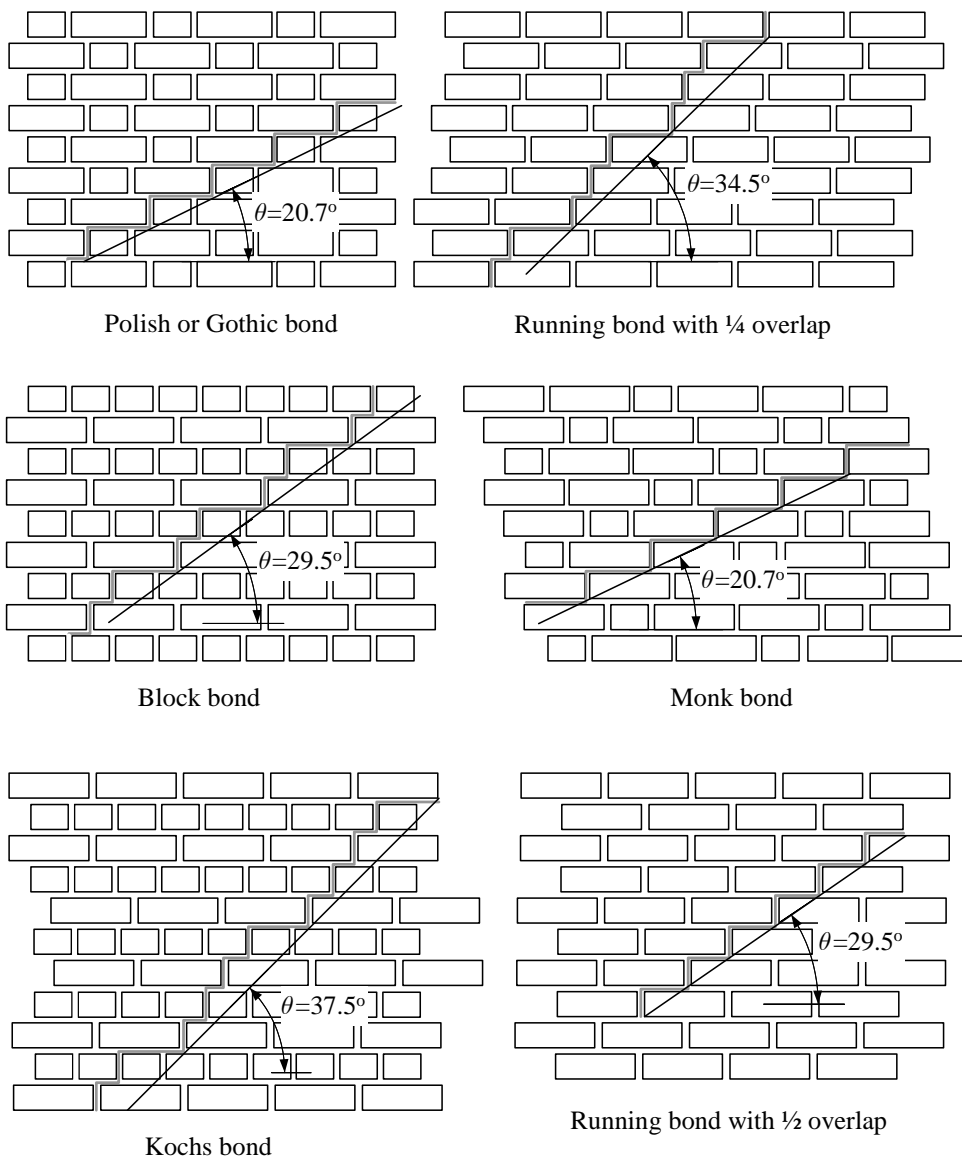


**Figure 6.18** Survey of diagonal yield lines

In the case of Polish or Gothic bond:  $x_0 = \frac{3}{4}(l_b + h_j)$  and  $y_0 = h_b + h_j$ , which for a normal size Danish brick with a joint thickness of 12 mm gives  $\theta = 20.7^\circ$ . Other bonds may be found in [11].

## 7 Supplements

### 7.1 Laterally loaded walls

#### 7.1.1 Kheir, A. M. A. 1975

no.	Brick	Supports	$b$	$h$	$p_{meas}$	$m_{px}$	$p^+_{min}$	$p_{meas}$	$\frac{b}{h}$
	Mortar		[mm]	[mm]	[kN/m <sup>2</sup> ]	[kNm/m]	[kN/m <sup>2</sup> ]	$p^+$	
A1	-	3	190	380	8.4	0.08	7.6	1.1	0.5
A2	-	3	190	380	5.8	0.07	7.0	0.8	0.5
A3	-	3	190	380	6.3	0.08	7.3	0.9	0.5
A5	-	3	190	380	9.3	0.09	9.1	1.0	0.5
A6	-	3	190	380	10	0.10	9.4	1.1	0.5
B1	-	3	380	380	3.1	0.07	3.3	0.9	1.0
B7	-	3	380	380	4.7	0.09	4.0	1.2	1.0
B8	-	3	380	380	4.6	0.09	4.1	1.1	1.0
C3	-	3	760	380	2.35	0.08	1.5	1.6	2.0
C4	-	3	760	380	2.9	0.09	1.8	1.7	2.0
C5	-	3	760	380	2.8	0.08	1.6	1.8	2.0
G1	-	4	400	200	18.2	0.10	16.8	1.1	2.0
G2	-	4	400	200	19	0.10	17.2	1.1	2.0
G3	-	4	400	200	18	0.09	14.4	1.2	2.0
F1	-	4	400	400	8.4	0.08	8.5	1.0	1.0
F2	-	4	400	400	10.5	0.09	9.3	1.1	1.0
F3	-	4	400	400	10	0.10	10.7	0.9	1.0
H1	-	4	400	800	5.6	0.09	6.5	0.9	0.5
H2	-	4	400	800	7	0.09	6.8	1.0	0.5

Table 7.1  $\mu = 0,4$

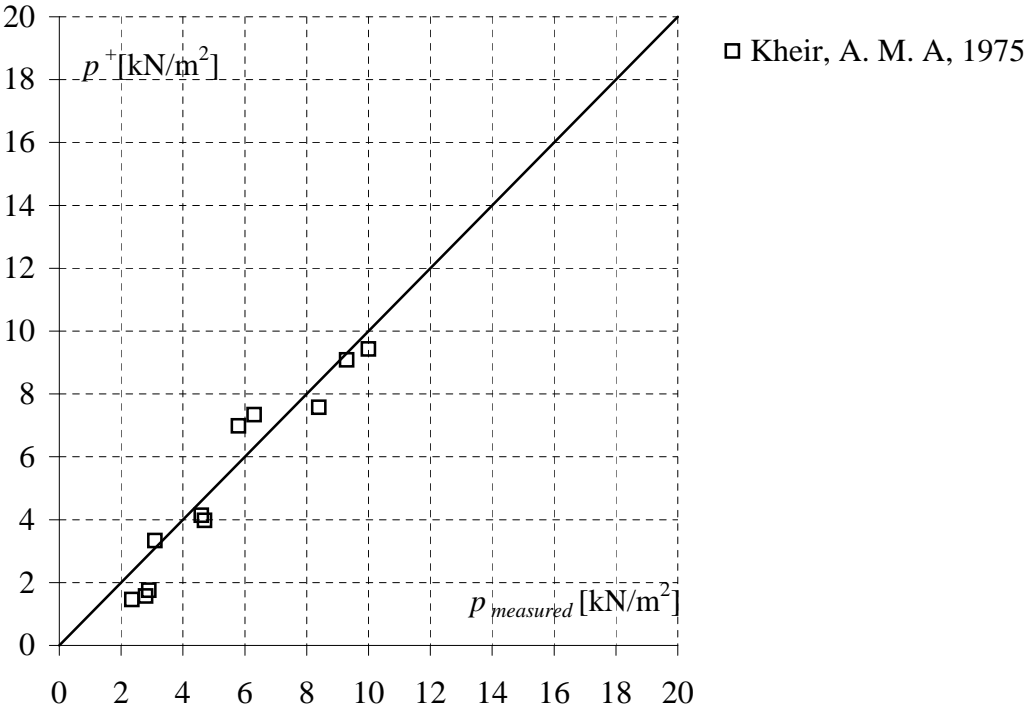


Figure 7.1

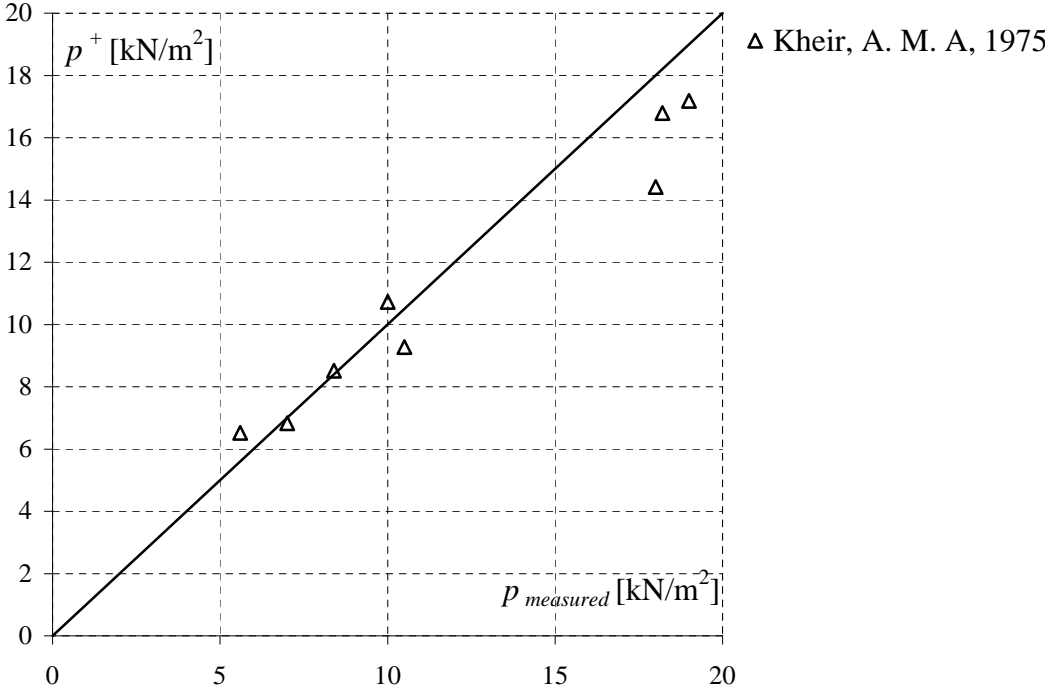


Figure 7.2

## 7.1.2 West, H. W.H et. al. 1977

no.	Brick	Supports	$b$	$h$	$p_{meas}$	$m_{90}$	$p^+_{min}$	$p_{meas}$	$b$
	Mortar		[mm]	[mm]	[kN/m <sup>2</sup> ]	[kNm/m]	[kN/m <sup>2</sup> ]	$p^+$	$h$
Brick A, 1:1/4:3 Mortar, IRA = 0.84 kg/m <sup>2</sup> /min									
757	AX	3	5500	2600	2.9	4.90	2.9	1.0	2.1
795	AX	3	5500	2600	3.45	4.90	2.9	1.2	2.1
825	AX	3	5500	2600	3.1	4.90	2.9	1.1	2.1
826	AX	3	5500	2600	3.52	4.90	2.9	1.2	2.1
844	AX	3	5500	2600	2.83	4.90	2.9	1.0	2.1
845	AX	3	5500	2600	2.96	4.90	2.9	1.0	2.1
852	AX	3	5500	2600	3.21	4.90	2.9	1.1	2.1
869	AX	3	5500	2600	3.45	4.90	2.9	1.2	2.1
782	AX	3	5500	2600	3.79	4.90	2.9	1.3	2.1
827	AX	3	5500	2600	4.38	4.90	2.9	1.5	2.1
835	AX	3	4570	2600	3.79	4.90	3.6	1.0	1.8
841	AX	3	4570	2600	4.21	4.90	3.6	1.2	1.8
892	AX	3	4570	2600	4.72	4.90	3.6	1.3	1.8
821	AX	3	3660	2600	5.45	4.90	5.0	1.1	1.4
836	AX	3	3660	2600	3.1	4.90	5.0	0.6	1.4
842	AX	3	3660	2600	4	4.90	5.0	0.8	1.4
850	AX	3	3660	2600	5.38	4.90	5.0	1.1	1.4
893	AX	3	3660	2600	5.58	4.90	5.0	1.1	1.4
809	AX	3	3050	2600	5.03	4.90	6.6	0.8	1.2
834	AX	3	3050	2600	5.79	4.90	6.6	0.9	1.2
840	AX	3	3050	2600	5.1	4.90	6.6	0.8	1.2
822	AX	3	2440	2600	5.1	4.90	9.4	0.5	0.9
829	AX	3	2440	2600	6.69	4.90	9.4	0.7	0.9
830	AX	3	2440	2600	6.83	4.90	9.4	0.7	0.9
919	AX	3	2440	2600	5.1	4.90	9.4	0.5	0.9
1078	AX	3	2440	2600	7.65	4.90	9.4	0.8	0.9
1079	AX	3	2440	2600	8.25	4.90	9.4	0.9	0.9
932	AX	3	1520	2600	15.51	4.90	21.2	0.7	0.6
Brick B, 1:1/4:3 Mortar, IRA = 2.5 kg/m <sup>2</sup> /min									
787	BX	3	5500	2600	2.76	3.10	1.8	1.5	2.1
820	BX	3	5500	2600	2.76	3.10	1.8	1.5	2.1
838	BX	3	5500	2600	2.62	3.10	1.8	1.4	2.1
839	BX	3	5500	2600	2.48	3.10	1.8	1.4	2.1
846	BX	3	5500	2600	2.83	3.10	1.8	1.6	2.1
847	BX	3	5500	2600	2.45	3.10	1.8	1.4	2.1
896	BX	3	5500	2600	2.65	3.10	1.8	1.5	2.1
897	BX	3	5500	2600	2.76	3.10	1.8	1.5	2.1
899	BX	3	5500	2600	3.03	3.10	1.8	1.7	2.1
851	BX	3	3660	2600	2.89	3.10	3.2	0.9	1.4

903	BX	3	3660	2600	4.83	3.10	3.2	1.5	1.4
898	BX	3	2440	2600	6.58	3.10	6.0	1.1	0.9
920	BX	3	2440	2600	4.96	3.10	6.0	0.8	0.9
1075	BX	3	2440	2600	3.2	3.10	6.0	0.5	0.9
1076	BX	3	2440	2600	5.2	3.10	6.0	0.9	0.9
904	BX	3	1520	2600	12.06	3.10	13.4	0.9	0.6
Brick A, 1:1:6 Mortar, IRA = 0.84 kg/m <sup>2</sup> /min									
786	AY	3	5500	2600	2.14	4.10	2.4	0.9	2.1
907	AY	3	5500	2600	2.55	4.10	2.4	1.1	2.1
912	AY	3	5500	2600	2.48	4.10	2.4	1.0	2.1
913	AY	3	5500	2600	2.31	4.10	2.4	1.0	2.1
910	AY	3	2440	2600	5.45	4.10	7.9	0.7	0.9
895	AY	3	1520	2600	12.41	4.10	17.8	0.7	0.6
908	AY	3	1520	2600	14.82	4.10	17.8	0.8	0.6
Brick B, 1:1:6 Mortar, IRA = 2.5 kg/m <sup>2</sup> /min									
789	BY	3	5500	2600	2.21	2.60	1.5	1.5	2.1
902	BY	3	5500	2600	2.21	2.60	1.5	1.5	2.1
918	BY	3	5500	2600	1.65	2.60	1.5	1.1	2.1
922	BY	3	3660	2600	2.28	2.60	2.7	0.9	1.4
901	BY	3	2440	2600	6.55	2.60	5.0	1.3	0.9
911	BY	3	2440	2600	6	2.60	5.0	1.2	0.9
921	BY	3	1520	2600	9.38	2.60	11.3	0.8	0.6
Brick W2, 1:1/4:3 Mortar, IRA=3.20 kg/m <sup>2</sup> /min									
928	W2X	3	5500	2600	2.14	3.51	2.1	1.0	2.1
960	W2X	3	5500	2600	3.03	3.51	2.1	1.5	2.1
973	W2X	3	3660	2600	3.03	3.51	3.6	0.8	1.4
926	W2X	3	2440	2600	4.14	3.51	6.8	0.6	0.9
974	W2X	3	2440	2600	5.38	3.51	6.8	0.8	0.9
Brick W2, 1:1:6 Mortar, IRA=3.20 kg/m <sup>2</sup> /min									
924	W2Y	3	5500	2600	1.72	2.84	1.7	1.0	2.1
956	W2Y	3	5500	2600	2.76	2.84	1.7	1.7	2.1
954	W2Y	3	3660	2600	3.45	2.84	2.9	1.2	1.4
944	W2Y	3	2440	2600	5.79	2.84	5.5	1.1	0.9
Brick W8, 1:1/4:3 Mortar, IRA=0.10 kg/m <sup>2</sup> /min									
923	W8X	3	5500	2600	2.07	2.84	1.7	1.2	2.1
931	W8X	3	3660	2600	4.62	2.84	2.9	1.6	1.4
927	W8X	3	2440	2600	9.93	2.84	5.5	1.8	0.9
1080	W8X	3	2440	2600	7.1	2.84	5.5	1.3	0.9
1081	W8X	3	2440	2600	7.5	2.84	5.5	1.4	0.9

$$\text{Table 7.2 } \mu = \left( \frac{65+10}{\frac{1}{2}(215+10)} \right)^2 = 0.44$$

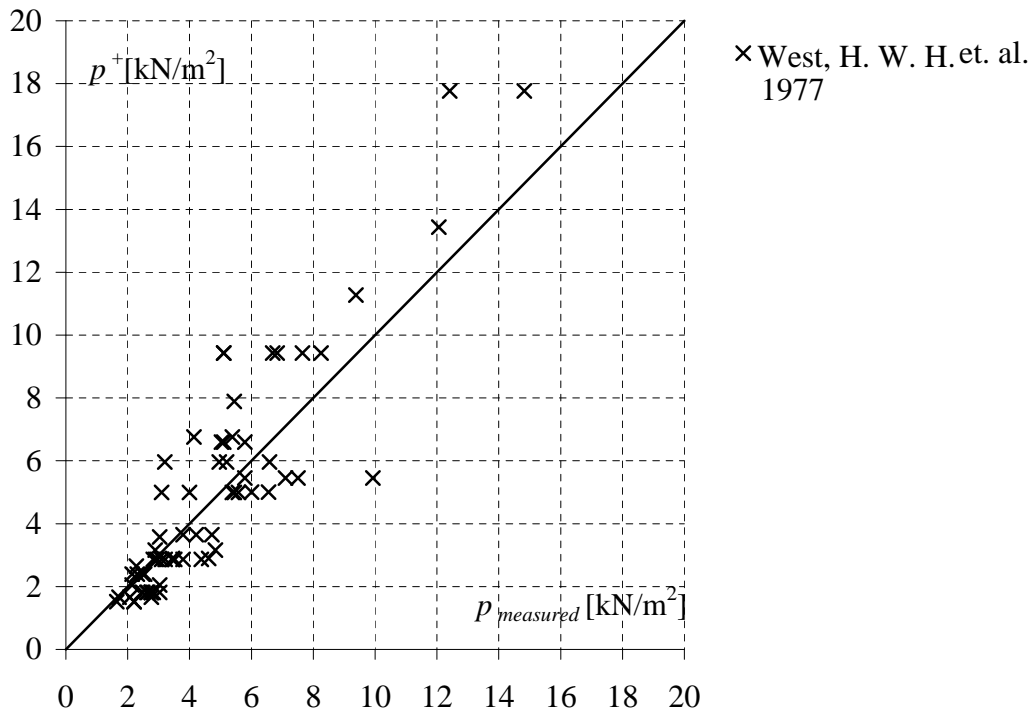


Figure 7.3

### 7.1.3 Cajdert, A. 1980

no.	Brick	Supports	$b$	$h$	$p_{meas}$	$m_{px}$	$p^+_{min}$	$p_{meas}$	$\frac{b}{h}$
	Mortar		[mm]	[mm]	[kN/m <sup>2</sup> ]	[kNm/m]	[kN/m <sup>2</sup> ]	$p^+$	
51	1B	4	3400	1900	8.6	4.25	7.9	1.1	1.8
56	2A	4	3400	1900	9.6	4.25	7.9	1.2	1.8
58	3B	4	3400	1900	9.8	4.25	7.9	1.2	1.8
60	4B	3	3400	1950	6.2	4.25	3.1	2.0	1.7
61	5B	3	3400	1130	11.5	4.25	5.0	2.3	3.0
66	6B	3	3400	1450	8.7	4.25	3.9	2.2	2.3

Table 7.3  $\mu = 0,28$

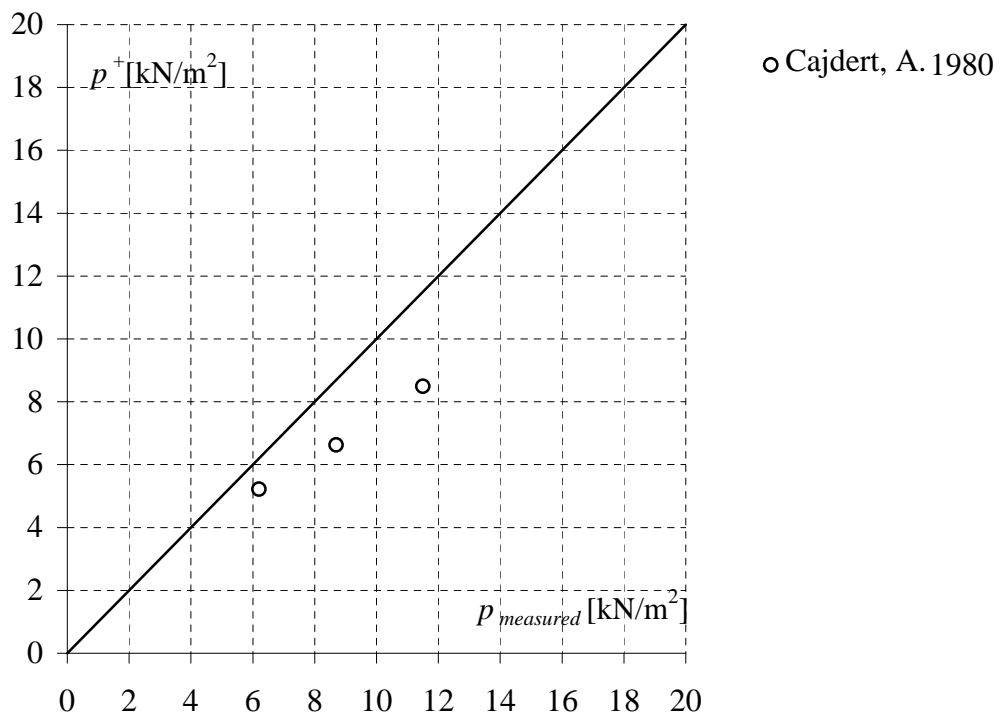


Figure 7.4

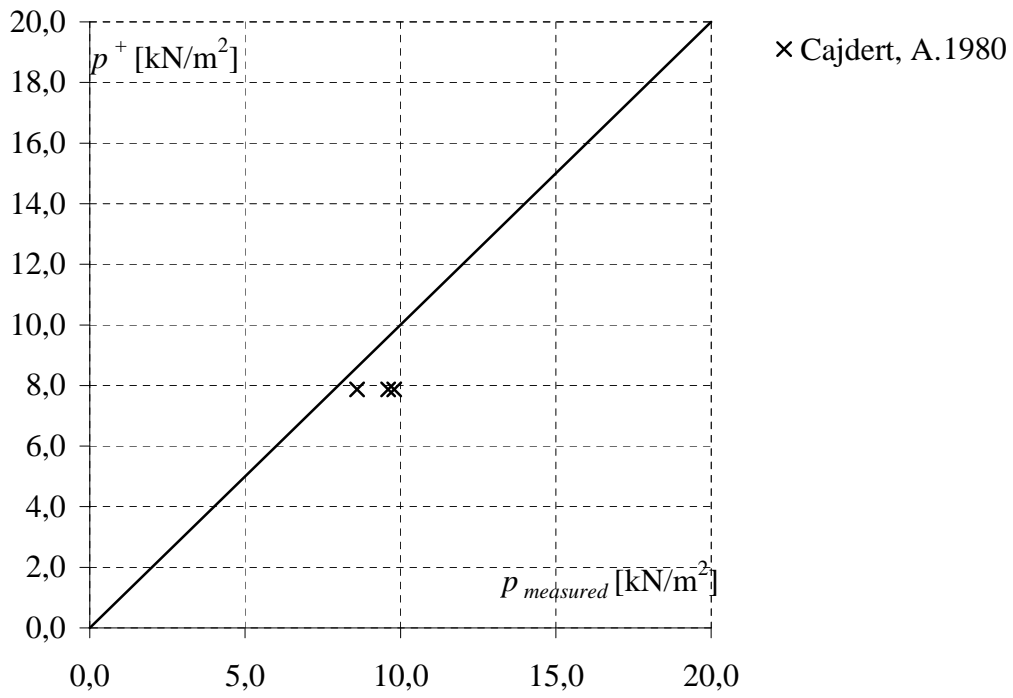
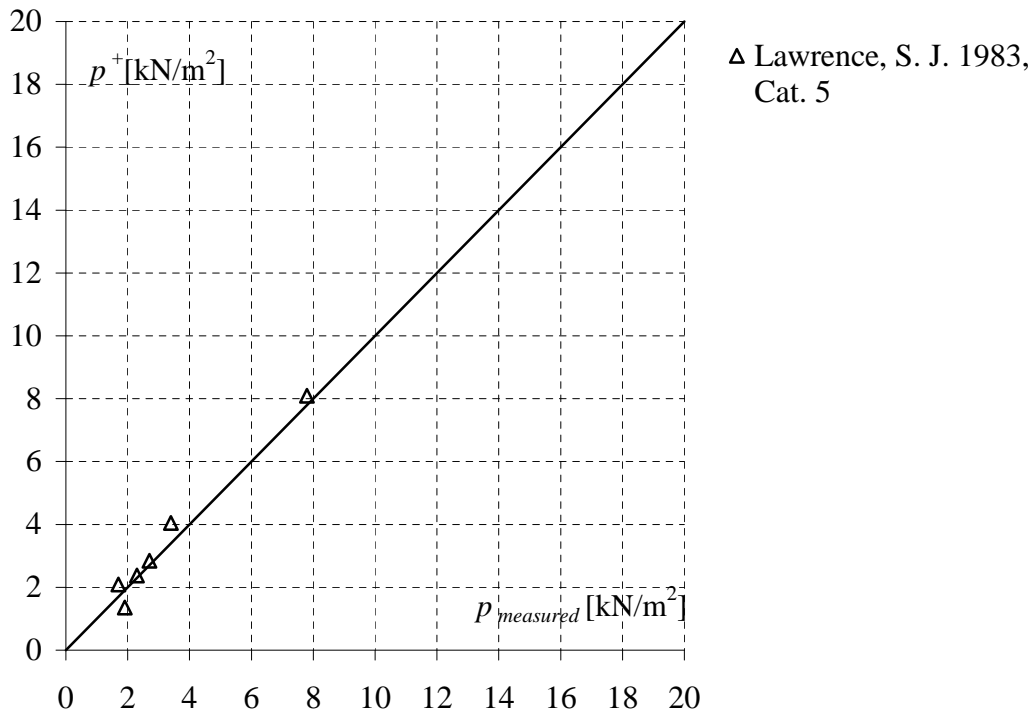


Figure 7.5

### 7.1.4 Lawrence, S. J. 1983

no.	Brick	Supports	$b$	$h$	$p_{meas}$	$m_{px}$	$p^+_{min}$	$p_{meas}$	$\frac{b}{h}$
	Mortar		[mm]	[mm]	[kN/m <sup>2</sup> ]	[kNm/m]	[kN/m <sup>2</sup> ]	$p^+$	
Category 1									
12	0	4	2500	2500	8.6	3.89	10.9	0.8	1.0
18	0	4	3750	2500	4.9	4.15	6.6	0.7	1.5
22	0	4	5000	2500	4.7	3.99	4.4	1.1	2.0
27	0	4	6000	2500	3.1	3.89	3.5	0.9	2.4
8	0	4	6000	3000	3	3.95	3.0	1.0	2.0
32	0	4	6000	3000	3.5	4.70	3.6	1.0	2.0
Category 2									
13	0	4	2500	2500	9.1	4.19	18.1	0.5	1.0
37	0	4	2500	2500	10.7	2.40	10.3	1.0	1.0
20	0	4	3750	2500	5.2	3.83	9.1	0.6	1.5
23	0	4	5000	2500	5.5	4.48	7.2	0.8	2.0
31	0	4	6000	2500	4.2	4.44	5.6	0.7	2.4
6	0	4	6000	3000	4.4	3.83	4.3	1.0	2.0
7	0	4	6000	3000	4.4	3.89	4.3	1.0	2.0
33	0	4	6000	3000	3.3	3.77	4.2	0.8	2.0
Category 3									
14	0	4	2500	2500	11.3	4.15	17.8	0.6	1.0
38	0	4	2500	2500	9	2.76	11.8	0.8	1.0
19	0	4	3750	2500	4.8	3.55	8.4	0.6	1.5
24	0	4	5000	2500	5	5.16	8.2	0.6	2.0
30	0	4	6000	2500	4.7	4.70	5.9	0.8	2.4
9	0	4	6000	3000	2.5	4.68	5.2	0.5	2.0
34	0	4	6000	3000	3	3.57	3.9	0.8	2.0
Category 4									
16	0	3	2500	2500	8	4.38	8.3	1.0	1.0
21	0	3	3750	2500	3.9	2.76	2.8	1.4	1.5
25	0	3	5000	2500	2.6	4.21	2.9	0.9	2.0
29	0	3	6000	2500	2.4	4.28	2.4	1.0	2.4
35	0	3	6000	3000	1.7	3.61	1.7	1.0	2.0
Category 5									
15	0	3	2500	2500	7.8	4.21	4.7	1.7	1.0
17	0	3	3750	2500	3.4	3.89	2.5	1.4	1.5
26	0	3	5000	2500	2.7	4.01	1.9	1.5	2.0
28	0	3	6000	2500	2.3	4.15	1.6	1.4	2.4
10	0	3	6000	3000	1.7	4.24	1.4	1.3	2.0
36	0	3	6000	3000	1.9	2.74	0.9	2.2	2.0

**Table 7.4**  $\mu = \left( \frac{75+10}{\frac{1}{2}(230+10)} \right)^2 = 0.5$



**Figure 7.6**

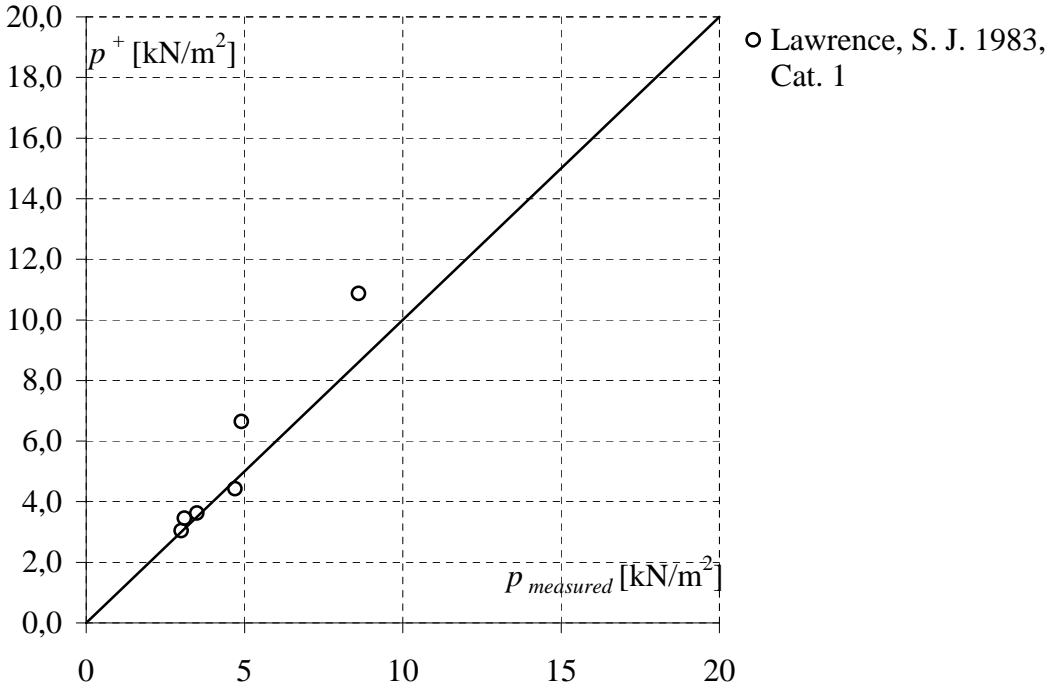


Figure 7.7

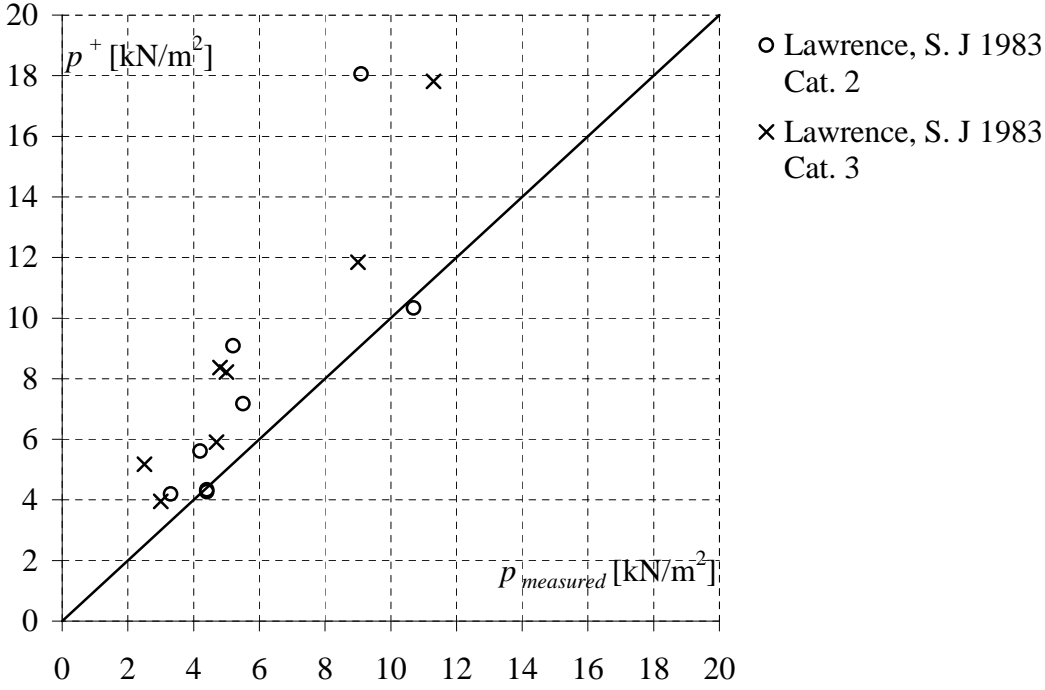


Figure 7.8

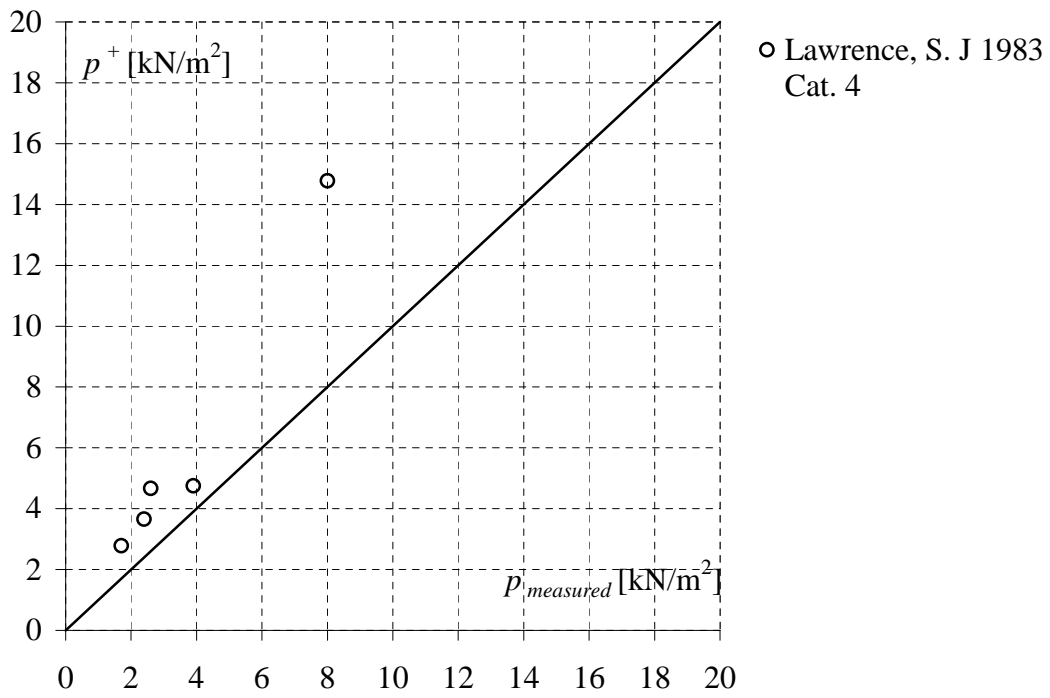


Figure 7.9

### 7.1.5 Buhelt, M. 1984

no.	Brick	Supports	$b$	$h$	$p_{meas}$	$m_{px}$	$p^+_{min}$	$p_{meas}$	$\frac{b}{h}$
	Mortar		[mm]	[mm]	[kN/m <sup>2</sup> ]	[kNm/m]	[kN/m <sup>2</sup> ]	$p^+$	
S121	2	2	1430	1470	2.41	2.83	2.2	1.1	1.0
S122	2	2	1430	1470	2.73	2.83	2.2	1.2	1.0
S123	2	2	1430	1470	1.69	2.83	2.2	0.8	1.0
S221	2	2	2390	1470	1.66	2.83	1.4	1.2	1.6
S222	2	2	2390	1470	1.55	2.83	1.4	1.1	1.6
S223	2	2	2390	1470	1.65	2.83	1.4	1.1	1.6

$$\text{Table 7.5 } \mu = \left( \frac{55+12}{0,75(228+12)} \right)^2 = 0.14$$

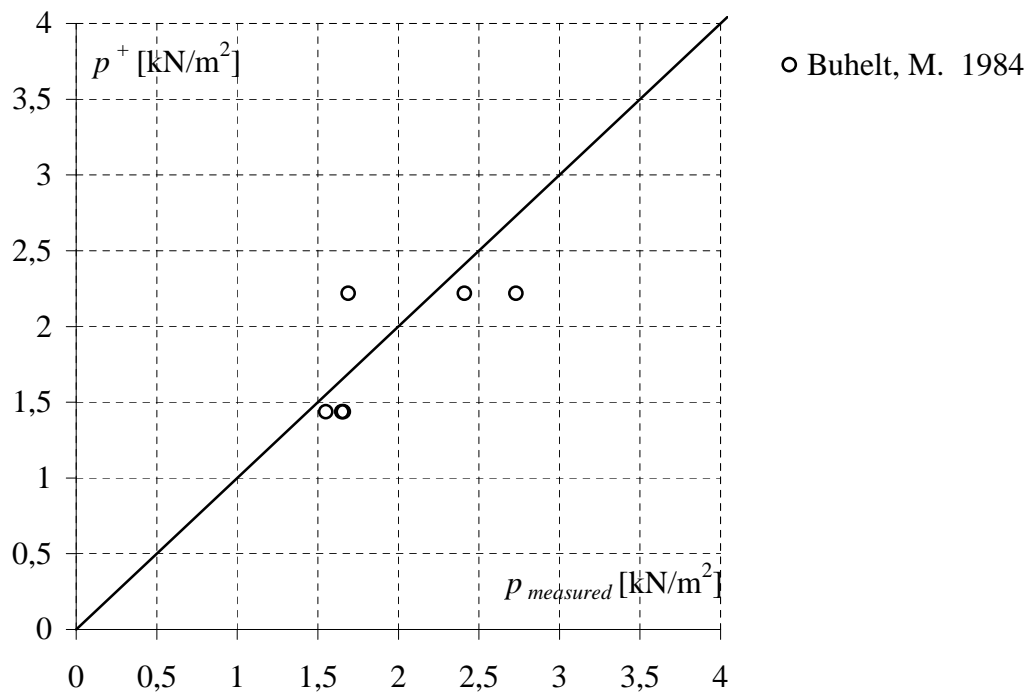


Figure 7.10

## 7.2 Laterally loaded walls with small axial loads

### 7.2.1 Hendry, A. W., Sinha, B. P. and Maurenbrecher, A. H. P. 1973

no.	Returns	$b$	$h$	$f_{cm}$	$p_{meas}$	$n_y$	$m_{px}$	$p_{min}^+$	$p_{meas}$	$\frac{b}{h}$
		[mm]	[mm]	[MPa]	[kN/m <sup>2</sup> ]	[MPa]	[kNm/m]	[kN/m <sup>2</sup> ]	$p^+$	
5	1	1370.00	2634.62	14.4	26.20	1.14	4.66	23.61	1.03	0.52
6	1	1370.00	2634.62	8.5	25.50	0.96	4.28	21.03	1.06	0.52
15	1	1320.00	2640.00	14.7	24.00	1.00	4.39	22.25	0.95	0.50
16	1	1880.00	2506.67	14.1	17.00	0.73	4.54	17.20	0.97	0.75
9	1	2590.00	2590.00	9.05	15.20	0.65	4.56	12.97	1.19	1.00
10	1	2590.00	2590.00	13.15	16.00	0.51	4.67	12.00	1.37	1.00
13	1	4670.00	2457.89	17.9	5.50	0.48	4.43	7.72	0.84	1.90
14	1	4730.00	2489.47	15.35	6.20	0.55	4.52	8.15	0.90	1.90
11	2	2720.00	2720.00	9.76	20.70	0.48	4.39	21.87	1.28	1.00
12	2	2720.00	2720.00	14.5	23.90	0.54	4.38	22.38	1.43	1.00
17	2	3890.00	2593.33	17.1	12.00	0.38	4.46	14.12	1.14	1.50
18	2	4570.00	2538.89	22.5	9.70	0.36	4.31	11.70	1.07	1.80

Table 7.6

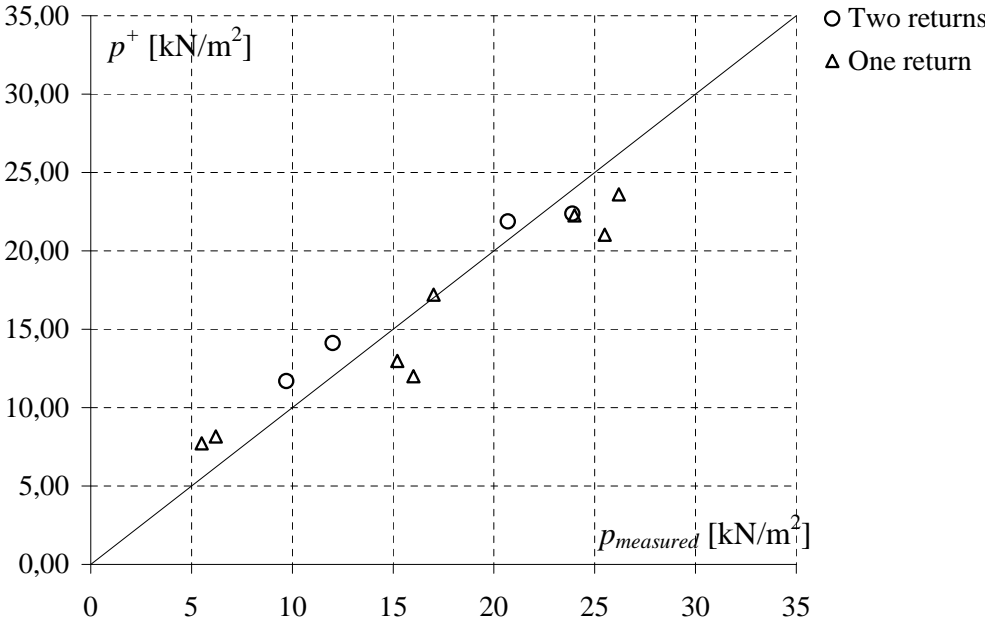


Figure 7.11



Report no R-117  
ISSN 1601-2917  
ISBN 87-7877-185-4